

**APPENDIX M**

**SCOTT KING THESIS**

**THE EFFECTIVE DISCHARGE CONCEPT  
IN GRAVEL-BED STREAM RESTORATION:  
THE TWELVE MILE REACH OF THE SALMON RIVER AT CHALLIS, IDAHO**

**A Thesis**

**Submitted in Partial Fulfillment of the requirements for the**

**Degree of Master of Science**

**with a**

**Major in Civil Engineering**

**in the**

**College of Graduate Studies**

**University of Idaho**

**by**

**Scott N. King**

**December, 2002**

**Major Professor: Peter Goodwin, Ph.D.**

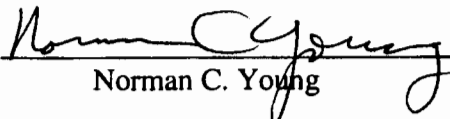
### Authorization to Submit Thesis

---

The thesis of Scott N. King, submitted for the degree of Master of Science with a major in Civil Engineering and titled "The Effective Discharge Concept in Gravel-Bed Stream Restoration: The Twelve Mile Reach of the Salmon River at Challis, Idaho" has been reviewed in final form. Permission, as indicated by the signatures and dates given below, is now granted to submit final copies to the College of Graduate Studies for approval.

Major Professor  Date 12/8/02  
Peter Goodwin

Committee Members  Date 17 Dec 02  
James Milligan

 Date 12/8/02  
Norman C. Young

Department Administrator  Date 12/18/02  
Sunil Sharma

College Dean  Date 12/18/02  
David E. Thompson

Final Approval and Acceptance by the College of Graduate Studies

 Date 12/30/02  
Charles R. Hatch

## Abstract

---

The Twelve Mile Reach of the Salmon River supports important fisheries habitat. However, the reach is degraded and suffers from encroachment. Fisheries managers are proceeding with plans to restore important habitat areas. This study characterizes the hydrologic and geomorphic characteristics and investigates utilizing effective discharge as a reference for restoration assessment and as a design parameter. Over the past 100 years, meanders in the reach have undergone a thirty percent decrease in wavelength, amplitude, and radius of curvature. Sinuosity has decreased from 1.18 to 1.12, and stream length has been reduced by 3.7 percent. Effective discharge is determined based on streamflow records and bedload measurements. It corresponds closely to bankfull discharge indicating that the reach is near equilibrium and is neither incised nor aggraded. Effective discharge is a useful parameter for designing specific restoration measures.

## Acknowledgements

---

This thesis is the result of several years of research that would not have been possible without the technical, financial, and emotional support from a number of individuals. First, I wish to acknowledge my major professor, Dr. Peter Goodwin, for his guidance on this project, and for his insight into the importance of aquatic restoration worldwide. Also, thanks to my other committee members, James Milligan and Norman Young, for their direction with this research and review of this document.

This research was funded by Bonneville Power Administration, Contract No. 99B120612, Project No. 99-19-01, *Aquatic Ecosystem Review: Twelve Mile Reach of Salmon River*. Additional financial support has been provided by the DeVlieg Foundation through the DeVlieg Graduate Student Fellowship.

I also wish to express my gratitude to the Custer Soil and Water Conservation District, and especially to Karma Bragg, for continued support and assistance with this project. The U.S. Army Corps of Engineers provided detailed topographic mapping of the floodplain. The Idaho Department of Water Resources was a source of significant data, and has also supported my interest in this project.

A number of individuals deserve mentioning for their interest and support, including: Allyn Meuleman, Janet Pope, David Tuthill, Wendell Greenwald, Mike Larkin, Tom Curet, Mark Olsen, Erik Ryan, and Tom Coates.

Finally, but most important, I want to express my deepest gratitude to Cyndi, Cassandra, and Michael for their endless hours of patience and support.

## Table of Contents

---

Title Page .....	i
Authorization to Submit Thesis .....	ii
Abstract .....	iii
Acknowledgements .....	iv
Table of Contents .....	v
List of Tables .....	vii
List of Figures .....	viii
1 Introduction.....	1
1.1 Background .....	1
1.2 Restoration Project Goals .....	2
1.3 Purpose of Study .....	3
1.4 Definition of Effective Discharge .....	3
1.5 Study Outline .....	4
2 Site Description .....	7
2.1 Geographic Location.....	7
2.2 Physical Characteristics .....	8
3 Geomorphic Characteristics.....	14
3.1 General Description .....	14
3.2 Available Data .....	15
3.3 Slope .....	20
3.4 Channel Braiding .....	22
3.5 Channel Width to Depth Ratio.....	24
3.6 Channel Width .....	25
3.7 Meanders.....	26
4 Hydrologic Conditions.....	42
4.1 Mean Daily Discharge .....	42
4.2 Peak Annual Discharge.....	43
4.3 Flood Frequency Analysis .....	47
4.4 Bankfull Discharge .....	49

4.5	Sediment Transport.....	51
4.6	Effective Discharge.....	56
5	Chinook Salmon .....	63
5.1	Spawning.....	63
5.2	Rearing.....	65
6	River Model .....	69
6.1	Description.....	69
6.2	Calibration.....	69
6.3	Model .....	71
6.4	Results.....	72
7	Conclusions and Recommendations .....	74
7.1	Conclusions.....	74
7.2	Recommendations for Further Research.....	75
	References.....	77
	List of Symbols .....	79
	Metric to English Units Conversion Chart.....	80
	Appendix A. Profiles and Photographs of Selected Cross-Sections.....	81
	Appendix B. Survey Descriptors .....	102
	Appendix C. The Hydrodynamic Model .....	104

**List of Tables**

---

Table 3.1. Channel width-to-depth ratio at selected cross-sections.....	25
Table 3.2. Channel width at selected cross-sections.....	26
Table 3.3. Number of meander features determined by sub-reach.....	34
Table 3.4. Meander wavelength by reach.....	36
Table 3.5. Meander amplitude by reach.....	37
Table 3.6. Meander radius of curvature by reach.....	38
Table 3.7. Meander sinuosity by reach.....	39
Table 3.8. Reach-level sinuosity.....	40
Table 3.9. Channel centerline length.....	40
Table 4.1. Recent peak annual discharge at Salmon and near Challis.....	47
Table 4.2. Exceedance Probability and Return Interval.....	48
Table 4.3. Simulated discharge for selected cross-sections.....	51
Table 4.4. Bedload transport capacity at cross-section 10 based on Bagnold (1966).....	55
Table 4.5. Bedload transport capacity at cross-section 10 based on Bathurst (1987).....	55
Table 4.6. Shear stress and critical particle size at bankfull flow.....	57
Table 5.1. Idaho Department of Fish and Game aerial counts of Chinook redds.....	63
Table 6.1. Roughness values used for simulated conditions.....	70
Table B.1. Cadastral Survey descriptors.....	103

## List of Figures

---

Figure 1.1. The Twelve Mile Reach of the Salmon River, 1992 aerial photography .....	6
Figure 2.1. Twelve Mile Reach Salmon River and regional location map .....	7
Figure 2.2. Major tributaries of the upper Salmon River basin .....	8
Figure 2.3. One Mile Island area depicting braided nature of the Twelve Mile Reach .....	9
Figure 2.4. Topographic map of Challis and vicinity .....	10
Figure 2.5. Salmon River profile from East Fork Salmon River to Bruno Bridge .....	11
Figure 2.6. Significant tributaries within the Twelve Mile Reach .....	12
Figure 2.7. Common land uses and scenery in the Twelve Mile Reach area .....	13
Figure 3.1. Historic channel alignment .....	15
Figure 3.2. 1947 aerial photography of the Twelve Mile Reach .....	17
Figure 3.3. 1957 aerial photography of the Twelve Mile Reach .....	18
Figure 3.4. 1999-2000 cross-section survey points .....	19
Figure 3.5. Twelve Mile Reach surveyed cross-sections, numbered .....	20
Figure 3.6. Channel profile of the Twelve Mile Reach .....	21
Figure 3.7. Channel and water surface profile of upper 15 km .....	21
Figure 3.8. Channel and water surface profile of lower 14 km .....	22
Figure 3.9. Relation of discharge to slope and a line which separates meandering and braided channels .....	23
Figure 3.10. Relation of discharge and slope and several threshold boundaries distinguishing braided from non-braided channels .....	24
Figure 3.11. Channel alignments for upper third of the Twelve Mile Reach .....	27
Figure 3.12. Channel alignments for middle third of the Twelve Mile Reach .....	28
Figure 3.13. Channel alignments for lower third of the Twelve Mile Reach .....	29
Figure 3.14. Sub-reach segments of the Twelve Mile Reach .....	30
Figure 3.15. Meander radius and sinuosity for 1893 channel alignment .....	32
Figure 3.16. Meander inflection points, wavelength and amplitude .....	33
Figure 3.17. Meander wavelength by reach .....	35
Figure 3.18. Meander amplitude by reach .....	36
Figure 3.19. Meander radius of curvature by reach .....	37

Figure 3.20. Meander sinuosity by reach.....	38
Figure 3.21. Reach-level sinuosity.....	39
Figure 4.1. USGS gaging station 13298500, Salmon River near Challis .....	42
Figure 4.2. Salmon River near Challis, average daily discharge, 1928 – 1972.....	43
Figure 4.3. Salmon River near Challis, annual peak discharge, 1929 – 1976 .....	43
Figure 4.4. Salmon River at Salmon, annual peak discharge, 1912 – 2001 .....	44
Figure 4.5. Salmon River at White Bird, annual peak discharge, 1894 – 2001.....	44
Figure 4.6. Salmon River peak annual discharge, 1912 – 2001 .....	45
Figure 4.7. Relation between peak annual discharge of the Salmon River near Challis and the peak discharge at Salmon less Pahsimeroi River.....	46
Figure 4.8. Salmon River near Challis, Log Pearson III fit .....	47
Figure 4.9. Salmon River Flood Frequency.....	48
Figure 4.10. Total sediment transport ( $Q_{ST}$ ), Salmon River below Yankee Fork.....	52
Figure 4.11. Suspended sediment transport ( $Q_{SS}$ ), Salmon River below Yankee Fork.....	52
Figure 4.12. Bedload transport ( $Q_{SB}$ ), Salmon River below Yankee Fork .....	53
Figure 4.13. Instantaneous bedload transport rate, flow frequency, total bedload transport, and a curve fitted to the total bedload transport data.....	59
Figure 4.14. Cumulative percentage of bedload discharge as a function of stream discharge	60
Figure 4.15. Slope of the cumulative sediment discharge curve as a function of stream discharge showing the relative magnitude of effective discharge .....	61
Figure 5.1. Chinook redd locations in the Twelve Mile Reach, September 2001 .....	64
Figure 5.2. Chinook salmon and steelhead / rainbow trout densities in Hannah Slough .....	66
Figure 5.3. Chinook salmon and steelhead / rainbow trout densities in Philps Slough.....	66
Figure 5.4. Photographs of Philps Slough and a spring near Challis Hot Springs .....	67
Figure 5.5. Chinook salmon and steelhead / rainbow trout densities in Challis Hot Springs Creek.....	67
Figure 5.6. Chinook salmon densities in Capehorn Creek (no steelhead).....	68
Figure 6.1. Model Network.....	71
Figure 6.2. Extent of flooding for 10-, 25-, and 100-year flood flows .....	72
Figures A.1. to A.39. Profiles and photographs of selected cross-sections.....	82-105

## 1 Introduction

---

### 1.1 Background

In 1996, above average runoff from snowmelt in the Upper Salmon River basin caused flooding of the Twelve Mile Reach of the Salmon River near Challis, Idaho. Significant bank erosion threatened a major avulsion of the Salmon River with potential for significant property damage and loss of important Chinook salmon (*Oncorhynchus tshawytscha*) rearing habitat. Emergency actions were implemented to halt bank erosion and prevent the avulsion.

The heavy bank armoring placed to prevent river avulsion raised concerns from several agencies responsible for management of Chinook salmon under the Endangered Species Act and for habitat restoration in the Salmon River basin. Agencies are concerned about the loss of valuable habitat and the continued trend toward degrading river conditions including less frequent floodplain inundation, river channel incision, loss of geomorphic diversity, bank armoring, heavy grazing of riparian vegetation, and extreme water temperatures. Many of the private property owners adjacent to the river are also concerned about aquatic habitat and recognize the importance of healthy fish populations, and are also concerned about protecting their valuable land from flooding and erosion. Many are also keenly aware of the negative downstream effects that some bank-hardening projects bring.

Historic land use in the Salmon River Basin including mining, logging, and grazing has likely altered to some degree the amount of sediment discharged into the river. Locally, landowners along the Twelve Mile Reach have a long history of channel management practices including construction of jetties, barbs, and levees, riprapping stream banks, blocking oxbow channels, channel straightening, and removal of riparian vegetation and large woody debris. These issues have caused concern for fishery managers that the river system is out of balance and that important habitat features have been lost and are continuing to degrade. Some are concerned that the river is incised and therefore does not maintain regular healthy floodplain inundation. Others argue the opposite is true and that observed braiding indicates that the river is aggrading. In either case, managers have a desire to

understand current conditions of the reach in order to make informed decisions regarding future management and possible restorative measures.

In response to these concerns, local property owners formed the Custer County Watershed Group. This local group worked together with the Custer Soil and Water Conservation District, the Idaho Department of Fish and Game, the U. S. Army Corps of Engineers, and other state and federal agencies to prepare a plan for improving and restoring aquatic habitat in the Twelve Mile Reach. Typical action items included in the plan are fencing to reduce bank-side grazing, improvement of riparian vegetation, floodplain protection and restoration to promote more frequent inundation, lowering of dikes and riprap, improvement of irrigation diversions, and construction of barbs, riprap, and other bank hardening to reduce erosion. Funding assistance was sought from Bonneville Power Administration and the U. S. Army Corps of Engineers for implementation of the restoration plan.

## **1.2 Restoration Project Goals**

The above working groups have identified the following goals for restoration of the Twelve Mile Reach:

- Improve fish habitat for both migratory and local populations.
  - Provide appropriate and abundant rearing and spawning habitat including gravels, cover, flow, and bed forms (riffles and pools).
  - Improve temperature conditions by reducing channel width to depth ratio, establishing shading cover, and increasing pool density.
- Protect floodplain processes.
  - Decrease the erosive energy of high flood flows and capture and store fine sediments while providing appropriate livestock forage opportunities.
- Return the channel to a natural sinuosity.
  - An increased sinuosity may reduce braiding and provide additional fisheries habitat.
- Improve bank stability.

- Restore the thick riparian vegetation that once was abundant throughout the river corridor, establish and protect woody material, anticipate problem areas, and reinforce banks when necessary.
- Promote dynamic channel equilibrium.
  - Allow channel braiding, meander migration, and formation of new channels and sloughs by establishing a meander corridor where natural river functions can continue.
- Protect critical structures including existing homes, bridges, highways, and irrigation diversions.

### **1.3 Purpose of Study**

This study provides background information in understanding the Twelve Mile Reach and presents information that can be used by agencies in formulating restoration and management plans. Specifically, this study characterizes reach geomorphology, including degree of channel incision, and determines an appropriate channel size to be used for restoration design plans. Historic conditions are presented and the study examines the geomorphic evolution of the reach over the past 100 years. Effective discharge is determined and compared to current channel capacity in order to assess degree of channel incision, and implications for river restoration are investigated. A hydrodynamic river model is prepared to assist in assessing geomorphic conditions, to simulate flooding conditions, and as a platform for simulating proposed restoration measures.

### **1.4 Definition of Effective Discharge**

River channels often have a tendency to adjust to water and sediment supply and are typically shaped to accommodate bankfull discharge as a frequent discharge occurrence. In the western United States, bankfull discharge is often found to have a 1 to 2 year recurrence interval. However, return interval for bankfull discharge has also been found to vary from 1.01 to 32 years (Knighton, 1998), especially in highly degraded or manipulated river systems where significant incision or aggradation is occurring. Field identification of bankfull conditions can often be difficult as channels frequently have segments that are

oversized or undersized. This condition may be worse in montane environments where floodplains are relatively young and not well formed (Wohl, 2000).

River restoration projects frequently have the goal of creating a channel that will have a certain degree of stability yet function in dynamic equilibrium with the design discharge. A channel's current bankfull discharge may be an inappropriate criterion for restoration design.

A single channel-forming discharge may largely be responsible for channel geometry and cross-sectional capacity of self-formed alluvial channels (Wolman and Leopold, 1957). This effective, or also termed dominant, discharge performs the most work by transporting the most sediment over a long period of time (Wolman and Miller, 1960). Application of effective discharge to alluvial sand-bed streams is widespread. Researchers have found effective and bankfull discharges to be equivalent in undisturbed systems, and thus effective discharge can be a useful parameter in assessing incised conditions. It is also a useful analytical device in that the replacement of the frequency distribution of flows by a single discharge simplifies modeling problems (Knighton, 1998). The use of effective discharge is evaluated through the example of the Twelve Mile Reach where this paper examines its usefulness as an assessment tool and design parameter.

## **1.5 Study Outline**

The Twelve Mile Reach (see Figure 1.1) is introduced in Chapter 2, which provides a description of this site and its characteristics. Chapter 3 provides a detailed description of geomorphic elements. It includes an analysis of historical channel alignments dating from the late 1800's to 1992. Current channel slope, width, and width-to-depth ratio are presented based on detailed survey of river cross-sections. Meanders are characterized by reach, providing a revealing view at how they have developed over time.

The hydraulic conditions of the reach are presented in Chapter 4. Peak annual discharge is compared for several Salmon River gaging stations and a relationship is presented to approximate peak discharge at Challis based on discharge at downstream stations. An adjustment is made to the flood frequency analysis. Bankfull discharge is

estimated based on in-field observations, cross-section surveys, and hydraulic modeling. Sediment transport measurements are used in conjunction with streamflow records to determine effective discharge, a primary parameter in assessing the river's degree of incision and designing an appropriate channel size.

The impetus for this study is a concern about fishery habitat, in particular for Chinook salmon. The Twelve Mile Reach holds habitat features that have been found to be very productive for juvenile salmon and steelhead, and may also provide productive spawning areas. In order to provide support for this study and for the importance of the Twelve Mile Reach to fisheries management in the Upper Salmon River Basin, results of fish counts are provided in Chapter 5.

Chapter 6 includes a description of the hydraulic model used for this study and presents results of modeling exercises. Finally, conclusions and recommendations are presented in Chapter 7.

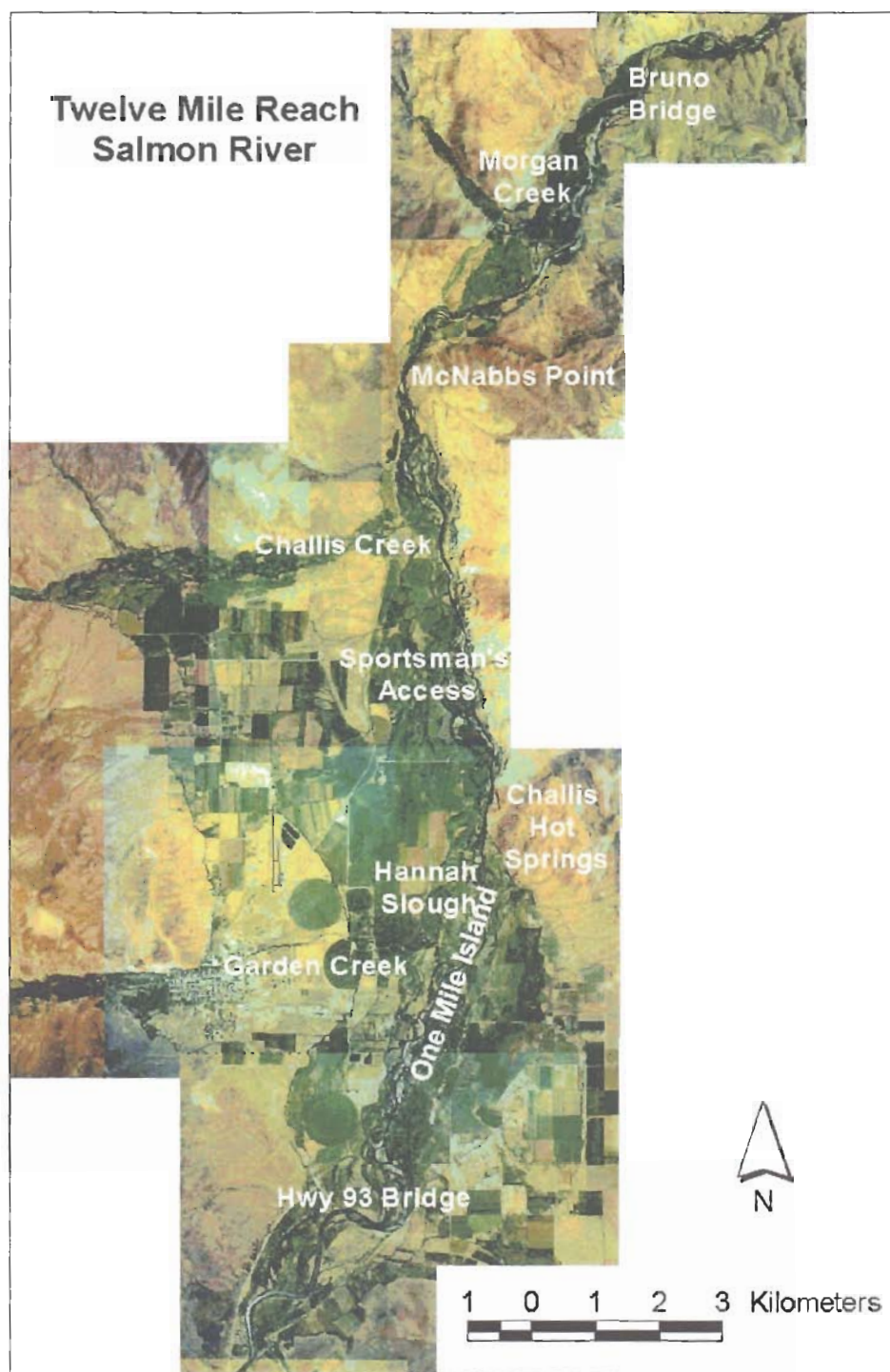


Figure 1.1. The Twelve Mile Reach of the Salmon River is bounded by the Highway 93 Bridge to the south and the Bruno Bridge to the north, 1992 aerial photography.

## 2 Site Description

### 2.1 Geographic Location

The Twelve Mile Reach of the Salmon River is located in central Idaho near the town of Challis, Idaho (elevation 1576 m, NAVD 1988). Two State Highway bridges serve as reference and provide approximate boundaries for the upper and lower ends of the reach (see Figure 2.1), which is actually 15 miles long from bridge to bridge.

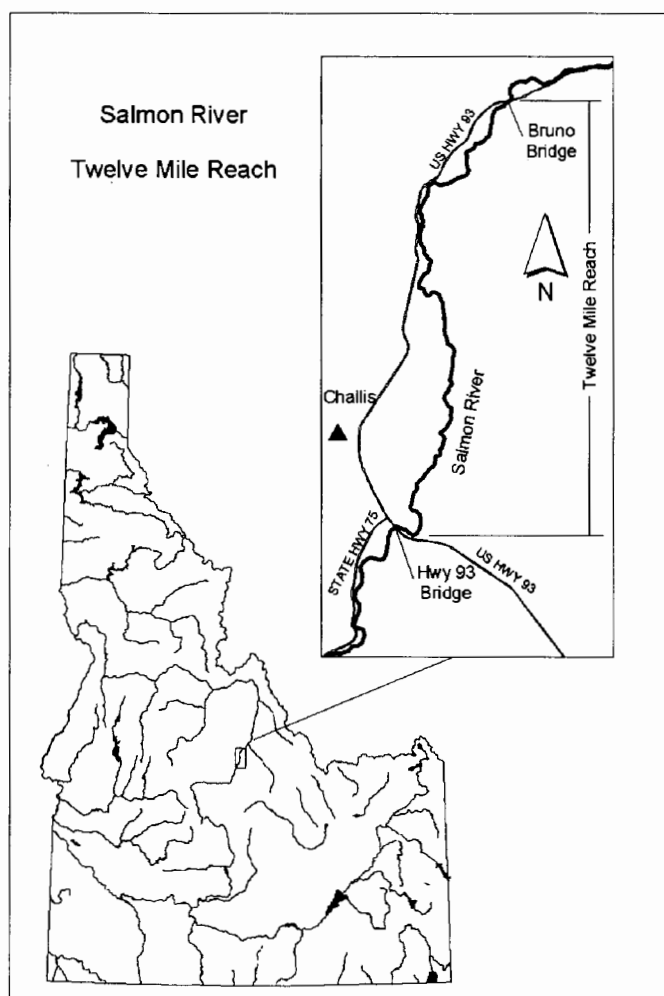


Figure 2.1. Twelve Mile Reach Salmon River (inset) and regional location map.

## 2.2 Physical Characteristics

Major tributaries upstream of the Twelve Mile Reach include East Fork Salmon River, Yankee Fork, Valley Creek and the headwaters of the Salmon River (see Figure 2.2).

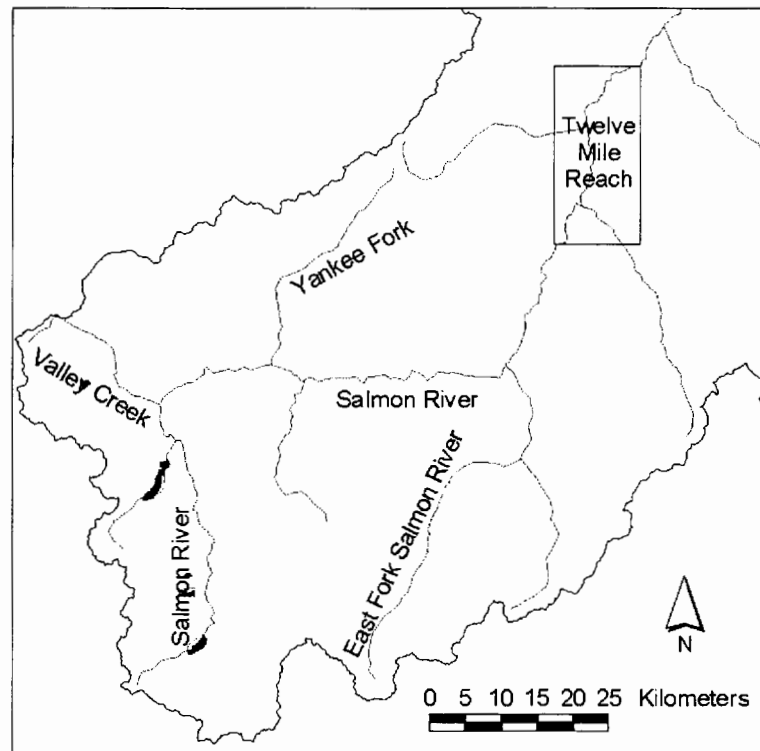


Figure 2.2. Major tributaries of the upper Salmon River basin.

The Salmon River is confined in a canyon environment from the confluence with Valley Creek down to the Twelve Mile Reach. The canyon region can be best described as a sediment transport reach where few opportunities exist for significant out of channel sediment storage or deposition. In comparison, the Twelve Mile Reach with its relatively wide floodplain and active channel characteristics is considered a response reach where sediment is deposited and eroded creating a dynamic channel pattern. Channel braiding exists although the tendency is only mild and tends to occur at limited locations through the reach. Imagery of One Mile Island (see Figure 2.3) depicts channel braiding and provides evidence of multiple historic channel alignments. Topographic maps display the difference between the upstream canyon and the relatively flat floodplain (see Figure 2.4). The Salmon River

profile from East Fork Salmon River to the Bruno Bridge at the bottom of the Twelve Mile Reach is presented in Figure 2.5.

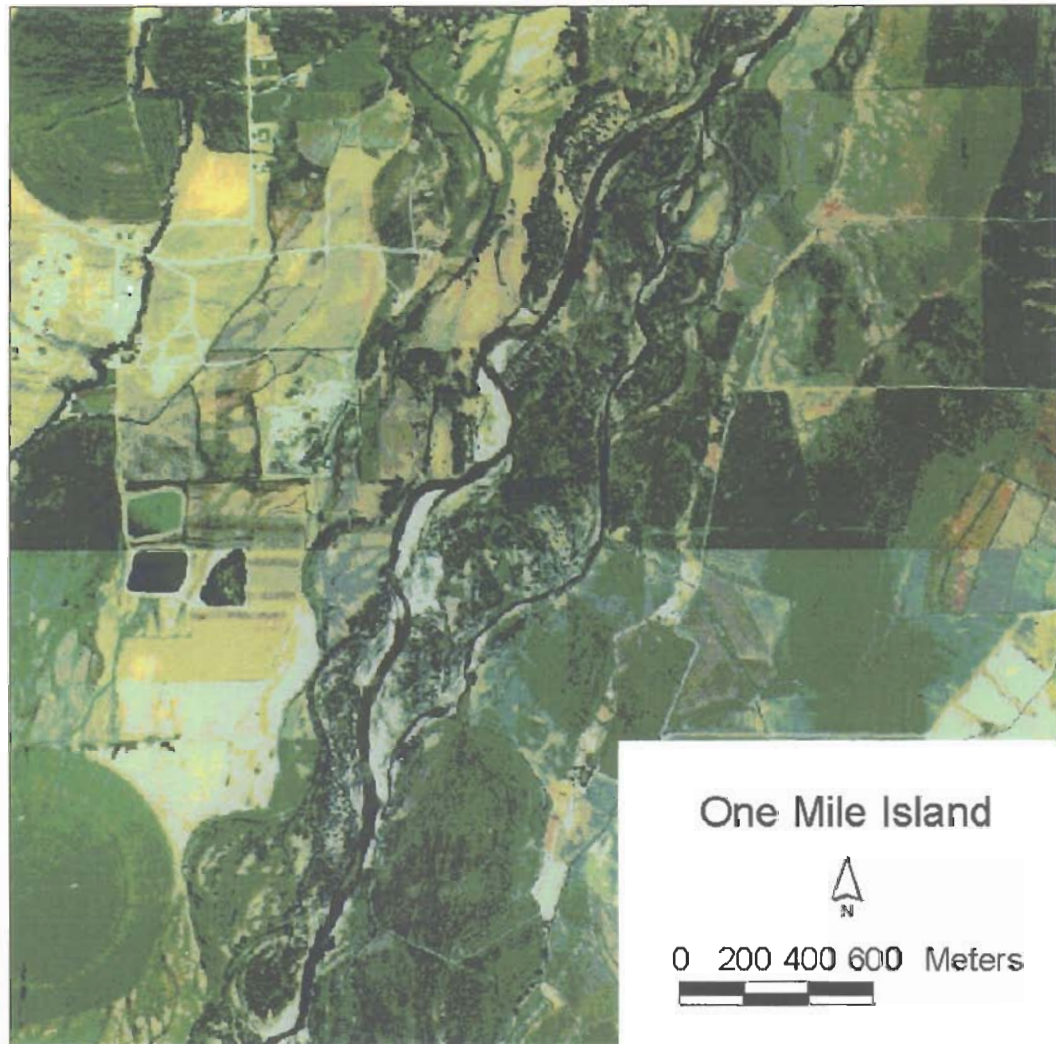


Figure 2.3. One Mile Island area depicting braided nature of the Twelve Mile Reach.

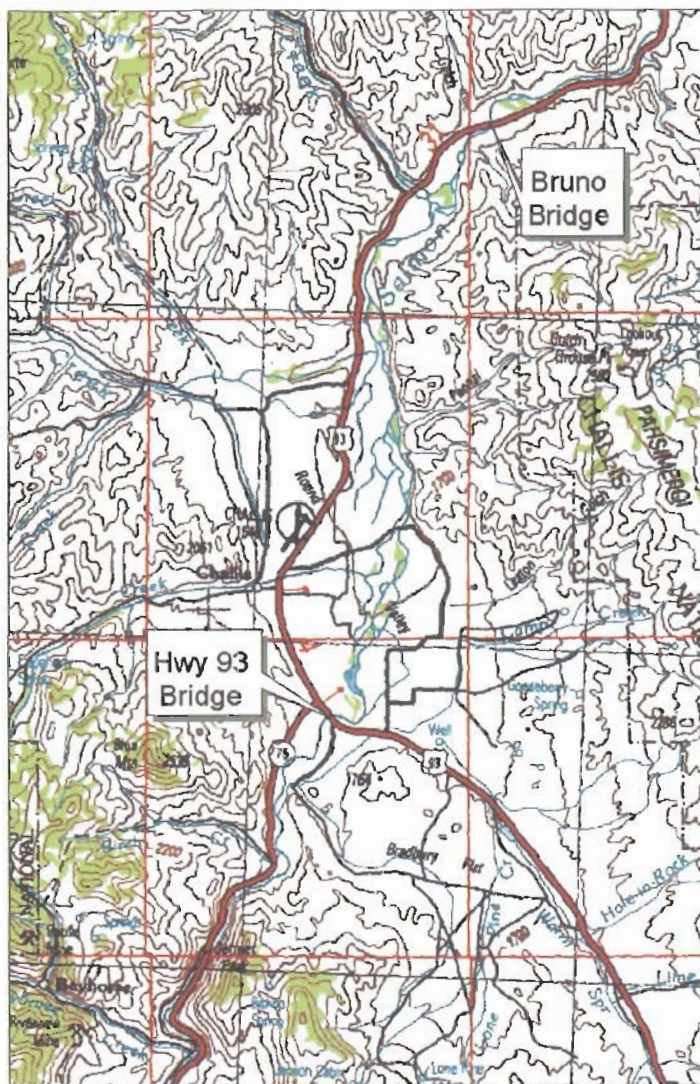


Figure 2.4. Topographic map of Challis and vicinity contrasting the upstream canyon environment in lower left with wider floodplain throughout the Twelve Mile Reach.

Elevation of the Salmon River's headwaters originating in the Idaho batholith exceeds 3000 m. River elevation through the **Twelve Mile Reach** ranges from 1525 m at the upper Highway 93 Bridge to 1440 m at the lower Bruno Bridge.

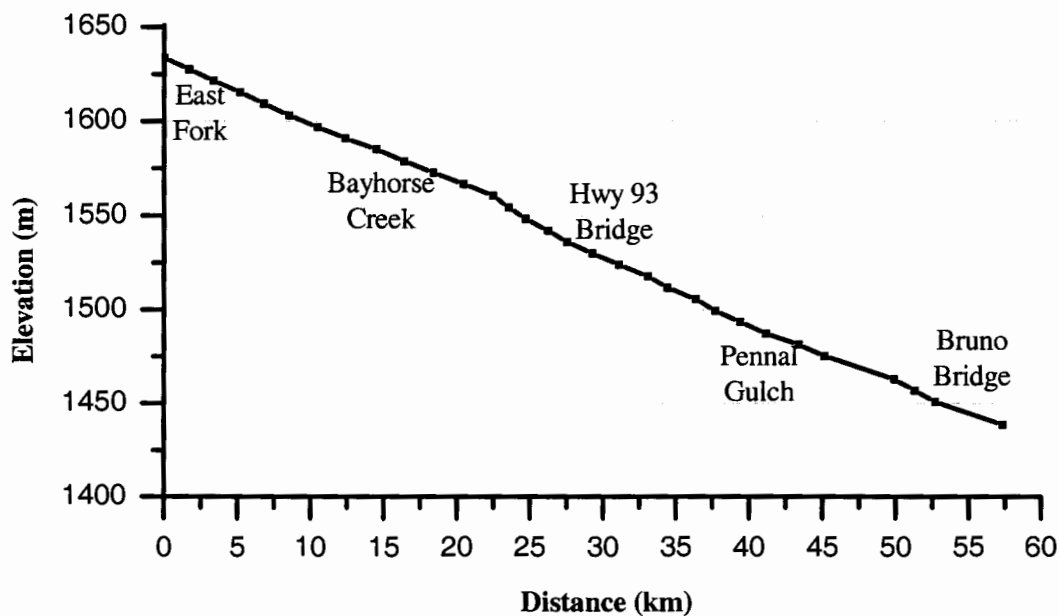


Figure 2.5. Salmon River profile from East Fork Salmon River to Bruno Bridge.

Significant tributaries within the Twelve Mile Reach include Challis Creek, Garden Creek, Morgan Creek, Warm Springs Creek, and Pennal Gulch with minor discharges from about six smaller gulches (see Figure 2.6). Flow contributions from these tributaries appears to be of only minor significance compared with the magnitude of flow in the main river. However, gaging records for these tributaries are sparse and discharge from them was not accounted for in this study. Drainage area is 4660 km<sup>2</sup> at the gaging station near Bayhorse Creek 13 km upstream of the project reach (USGS station 13298500). At the upper Highway 93 Bridge, drainage area is 4740 km<sup>2</sup>, and at the downstream Bruno Bridge, drainage area is 6160 km<sup>2</sup>.

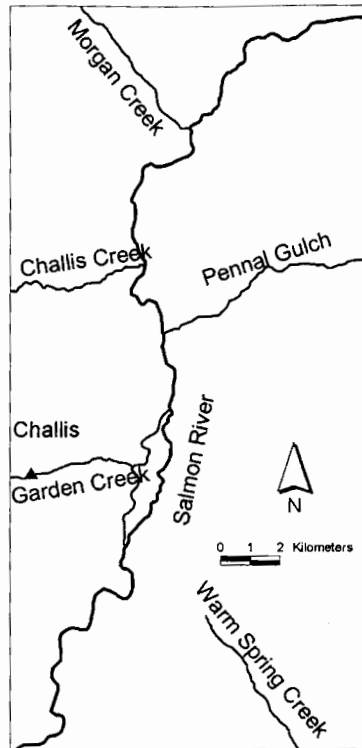


Figure 2.6. Significant tributaries within the Twelve Mile Reach.

Flow conditions at the upstream gaging station, Salmon River near Challis, range from a typical late summer low of  $23 \text{ m}^3/\text{s}$  to bankfull discharge near  $225 \text{ m}^3/\text{s}$ . The peak discharge of record is  $500 \text{ m}^3/\text{s}$ , occurring June 17, 1974. Peak discharges generally occur in May and June driven by snowmelt in the upper basin.

Lands adjacent to the river through the Twelve Mile Reach are primarily privately-owned agricultural properties utilized for ranching, grazing and farming with typical crops including pasture, hay, and small grains such as wheat. There is also a trend toward new homes and subdivisions causing encroachment on the river. Soils near the river are generally non-cohesive sandy loams and gravelly sandy loams (USDA).

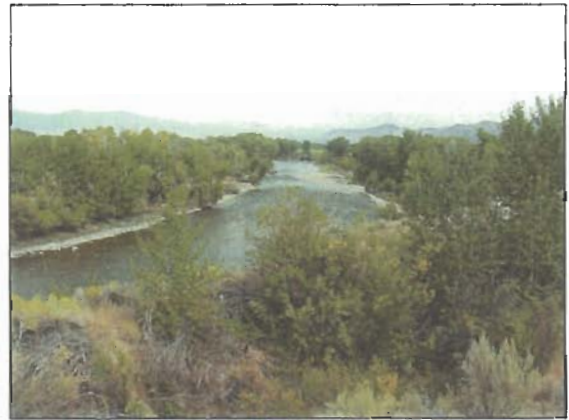


Figure 2.7. Common land uses and scenery in the Twelve Mile Reach area.

### 3 Geomorphic Characteristics

---

#### 3.1 General Description

The Twelve Mile Reach of the Salmon River may be described as a large gravel-bed reach with moderate slope and confinement. It responds to sediment input from upstream sources by meandering, braiding, and avulsing. Its relatively wide montane floodplain environment is situated below 95 km of canyon-confined transport reach where floodplains are either very narrow or nonexistent. Several large tributaries including the Yankee Fork and East Fork Salmon River discharge water and sediment into the upstream canyon where it is conveyed down to the Twelve Mile Reach with little opportunity for overbank storage. Average conditions include a channel slope of 0.0032, valley slope of 0.0038, and sinuosity of 1.18. Average bankfull width is 76 m and bankfull width-to-depth ratio is 30.

Floodplain width varies from a few tens of meters up to 1 km. Although portions of the reach are unconfined, significant segments are confined on the east side by cliffs and steep hill slopes. Several small levees protect adjacent land from inundation during smaller flood events. These levees are usually non-engineered and often constructed of gravel and cobble sized materials. At a few locations, levees are more substantial and will confine larger discharges.

The bed comprises large gravels and cobbles with  $d_{50}$  of the armor layer ranging from about 100 to 150 mm. Median size of sub-surface bar material is 10 to 50 mm (Greenwald, 2002).

Bank materials are generally non-cohesive sands and gravels with mild to moderate vegetation including perennial grass, willow, rose, and cottonwoods. Banks are often heavily grazed, subject to erosion, and frequently reinforced with rock riprap. At a number of locations riprap armoring is heavy and continuous. At others the riprap is discontinuous and installed only in short segments. Application of bank armoring is generally piecemeal and applied by individual landowners as a reaction to local erosion.

At the uppermost end of the Twelve Mile Reach where the river first exits the canyon and enters a wider valley, the stream is entrenched and can be described using the frequently cited classification system (Rosgen, 1996) as a B-type channel. It transitions to a C-type channel through most of the reach with local areas of mild to moderate D-type channel braiding. The reach would be described as alluvial plane-bed and step-pool type under the Montgomery Buffington stream classification (1997).

## 3.2 Available Data

### 3.2.1 Cadastral Surveys

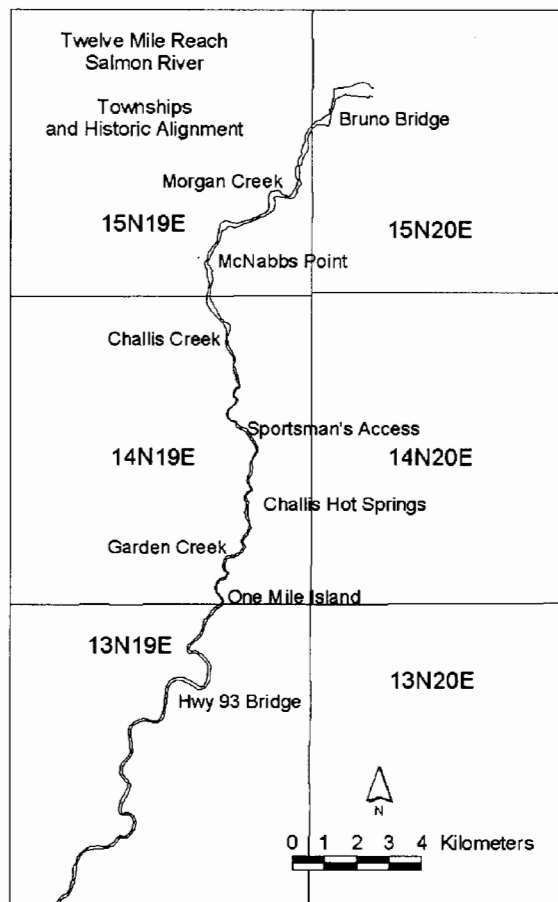


Figure 3.1. Historic channel alignment based on meander corridor surveys conducted in 1893, 1896, and 1911.

U.S. Government Cadastral Surveys were conducted through the Challis area during the late 1800s and early 1900s. In 1893, Township 14 North, Range 19 East, Boise Meridian (abbreviated to T14N R19E) was surveyed. Then in 1896, T13N R19E was surveyed, and T15N R19E was surveyed in 1911 (Figure 3.1). Surveys delineated 40-acre tracts through the township and also the meander corridor of the Salmon River. Records from these surveys provide insight to historic channel conditions. Specifically, the meander corridor survey provides channel alignment lines that are compared to current conditions. Also, survey notes provide descriptions of land use and vegetation with frequent references to “dense willow undergrowth,” “slough,” “timber,” and “cottonwood.” See Appendix B for a summary of common descriptors.

### 3.2.2 Aerial Photography

Aerial photographs from 1947 were obtained for the majority of the project (see Figure 3.2). 1957 photos were used for the southern portion of the reach (see Figure 3.3) where 1947 photos were not available. The photos were scanned and geo-referenced using Idaho Department of Water Resources’ (IDWR) 1992 imagery as a base reference so that comparisons could be made in a GIS environment.

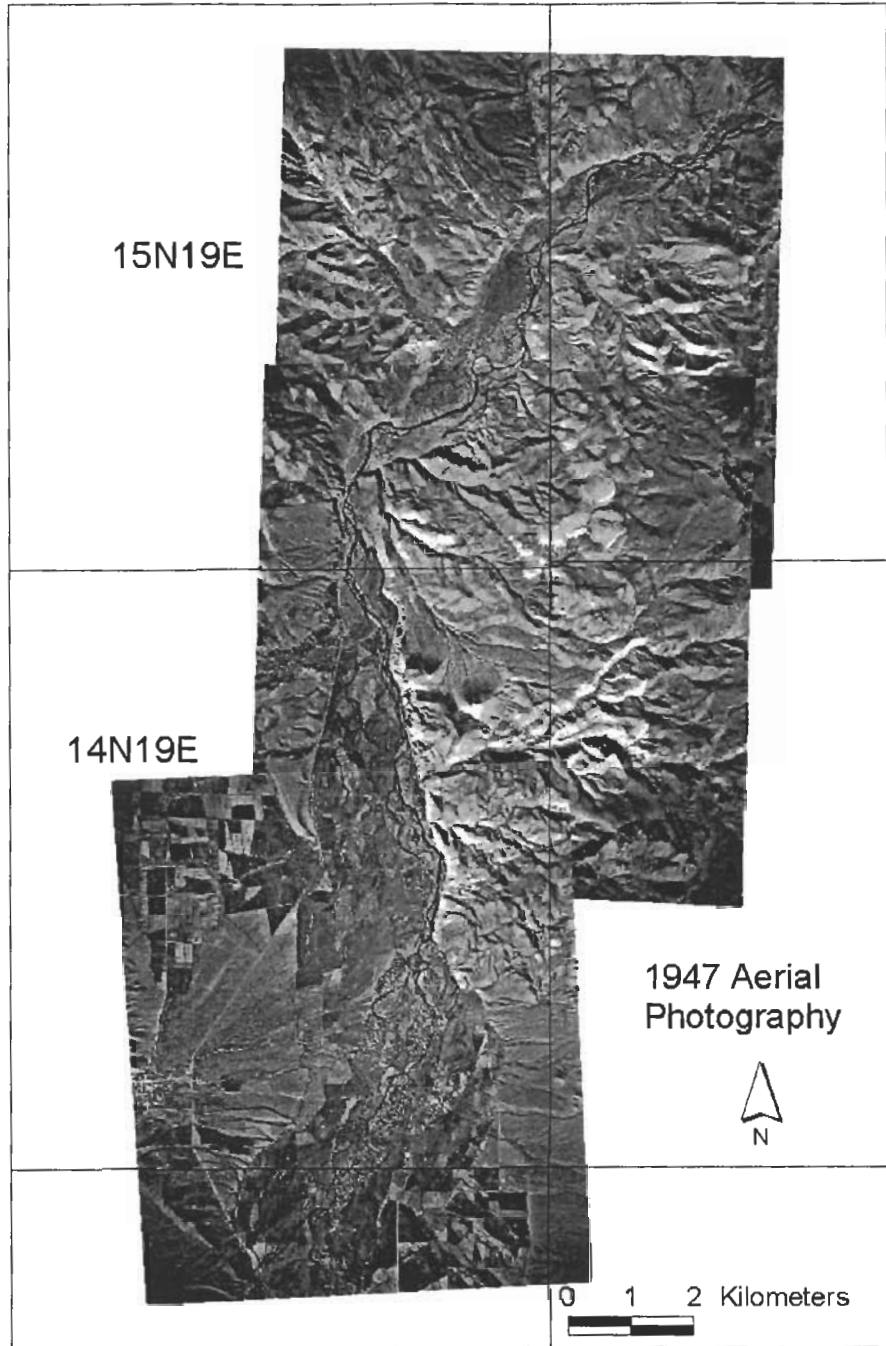


Figure 3.2. 1947 aerial photography of the Twelve Mile Reach.

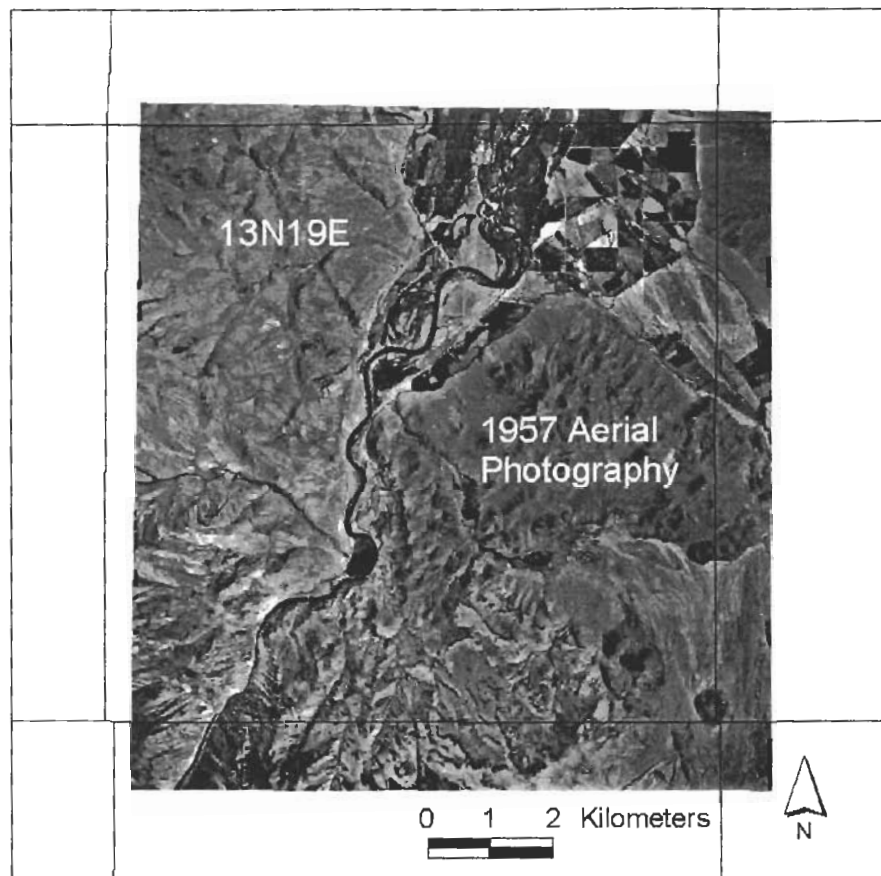


Figure 3.3. 1957 aerial photography of southern (upstream) portion of the Twelve Mile Reach.

### 3.2.3 USGS Quadrangle Maps

U.S. Geological Survey quadrangle maps are also available in digital format. In the southern reach the Bradbury Flat quad map is based on the 1957 aerial photography. The remaining quad maps including Challis, Gooseberry Creek, and Ellis are based on 1984 aerial photography. Between these multiple sets of data, channel alignment is available for at least portions of the reach for 1893, 1895, 1911, 1947, 1957, 1985, and 1992. These data sets provide a very useful tool for observing channel alignment migration patterns and changes in meander characteristics.

### 3.2.4 Channel Survey

During December 1999 and April 2000, 68 cross-sections were surveyed through the Twelve Mile Reach from above the Highway 93 Bridge to below the Bruno Bridge. The survey was conducted using real-time kinetic GPS technology at centimeter-level accuracy. Above McNabb's Point, most surveyed cross-sections extended across the 500-year floodplain; below McNabb's Point most sections included only the river channel from left top-of-bank to right top-of-bank (see Figure 3.4). Figure 3.5 displays the same survey points and includes cross-sections identified by number.

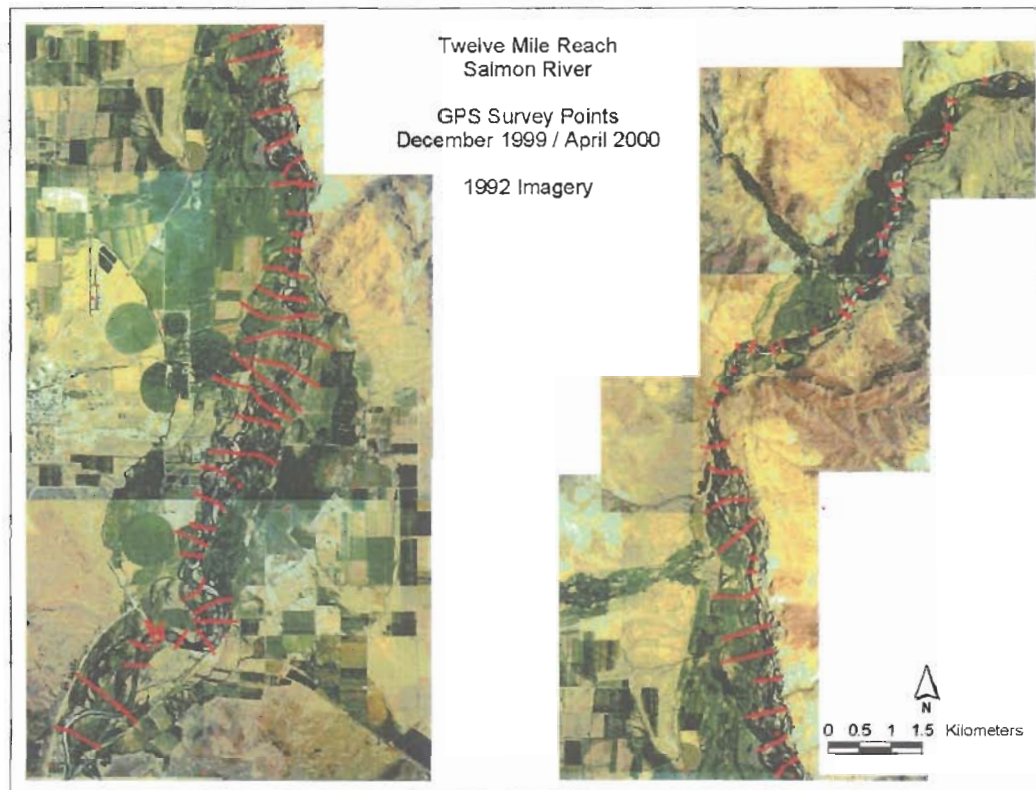


Figure 3.4. 1999-2000 cross-section survey points.

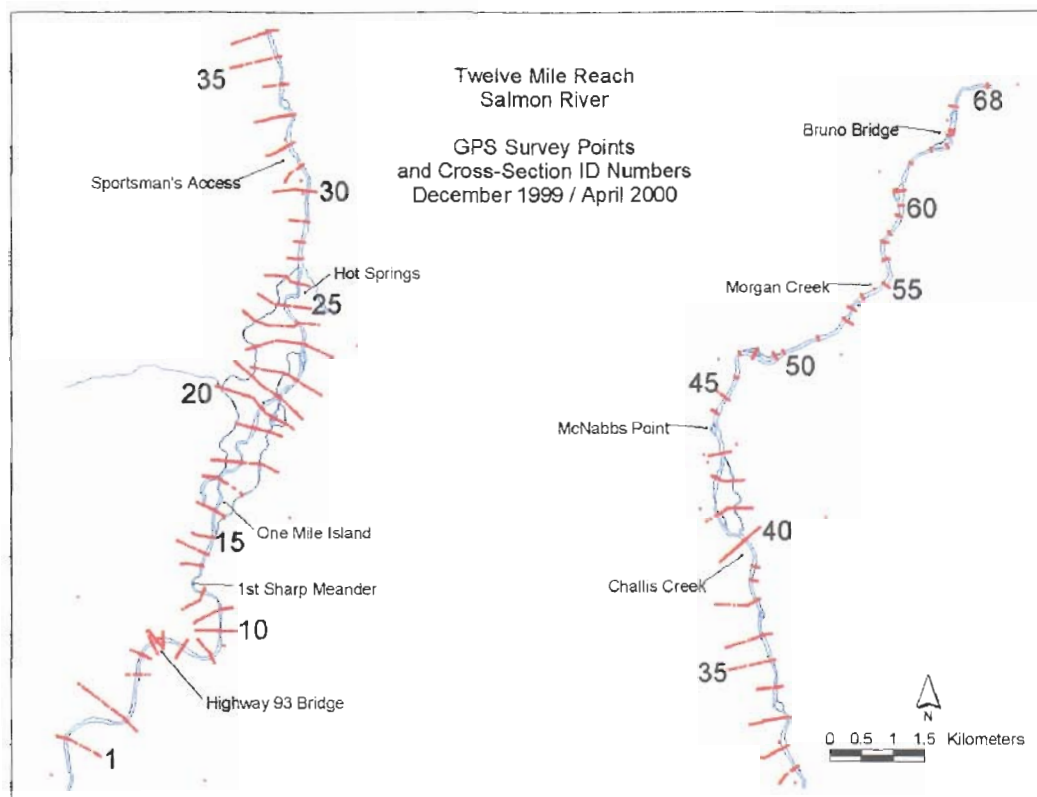


Figure 3.5. Twelve Mile Reach surveyed cross-sections plotted against 1992 channel alignment. Selected sections are numbered.

### 3.3 Slope

Figure 3.6 presents the channel profile based on surveyed sections with elevation of channel thalweg (lowest point in the channel) plotted against chainage where chainage is distance along the channel centerline from the upstream section to the downstream section. The water surface profile is added to this plot in Figures 3.7 and 3.8 where the reach is split between the two figures to show greater detail.

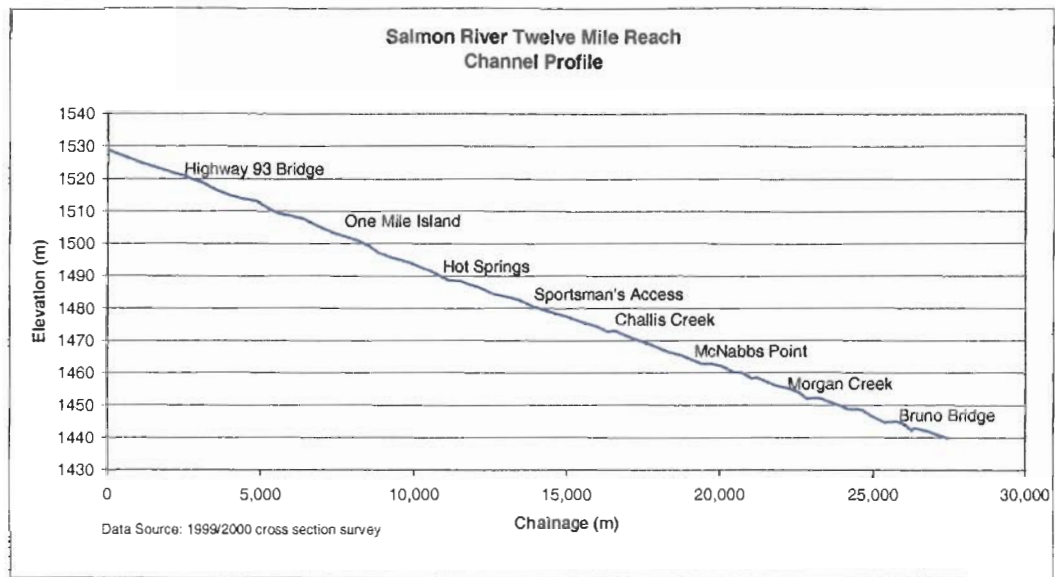


Figure 3.6. Channel profile of the Twelve Mile Reach.

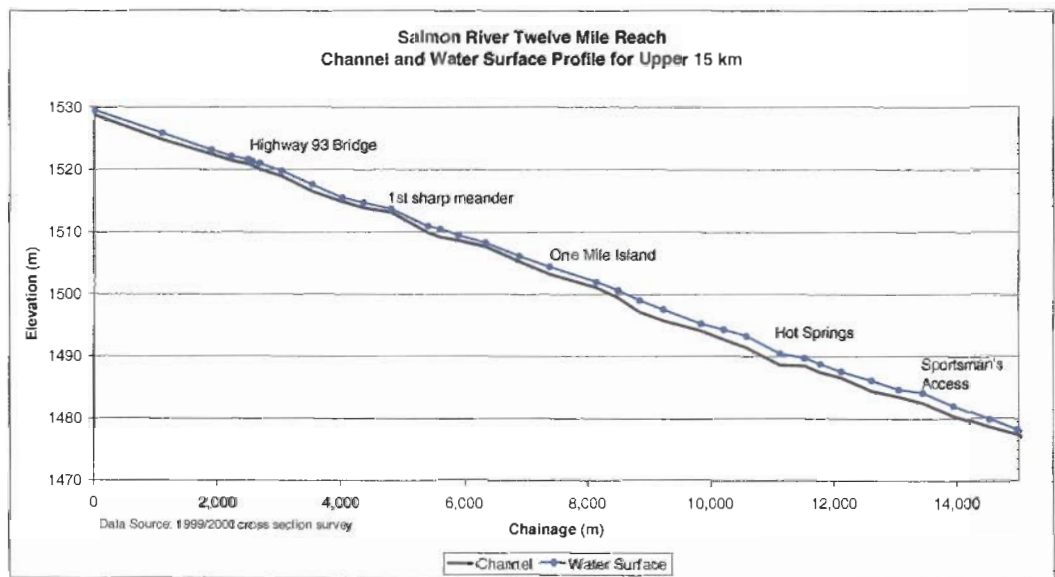


Figure 3.7. Channel and water surface profile of upper 15 km.

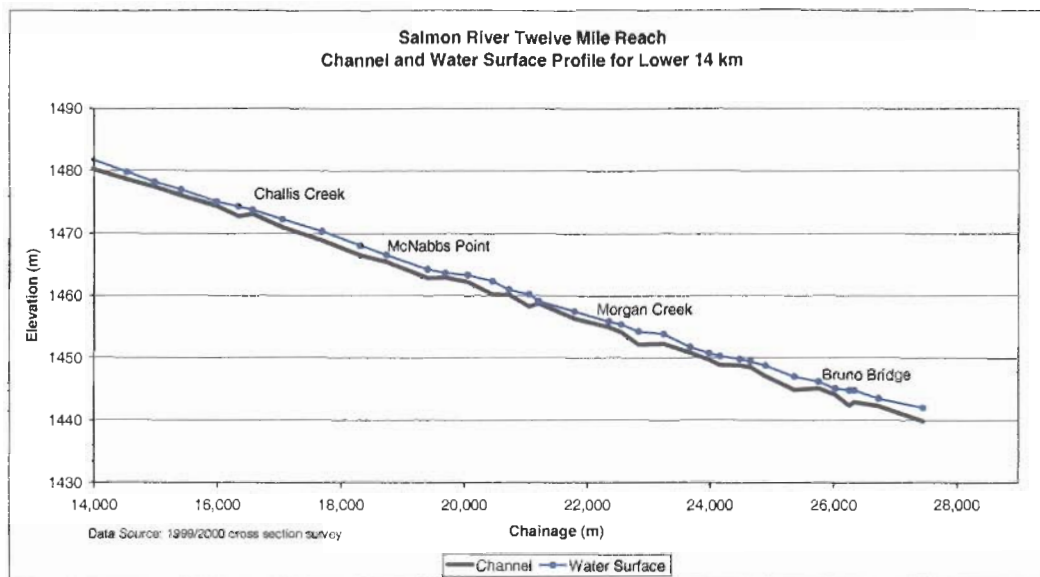


Figure 3.8. Channel and water surface profile of lower 14 km.

The reach-average bed slope is 0.0032. The range of bed slopes observed based on 68 cross-sections (67 segments) along 27.4 km ranges from  $-0.0075$  to  $0.0077$ . There does not appear to be any significant reach-level break in slope through the reach. Also, based on USGS quad maps, stream slope in the canyon reach several kilometers upstream of the Twelve Mile Reach is 0.003 indicating little change in slope between the near-upstream transport reach and this response reach (see Figure 2.5). Based on the same segments used for bed slope analysis, water surface slope varies from horizontal to 0.0072 with a reach-wide average equal to bed slope.

### 3.4 Channel Braiding

Figure 3.9 presents a relationship between bankfull discharge and slope based on field observations of many rivers. A line of slope  $S=0.06Q^{-0.44}$  is drawn separating the data between meandering and braided channels. The Twelve Mile Reach channel slope is 0.003 and bankfull discharge is in the range of  $156$  to  $225 \text{ m}^3/\text{s}$  ( $5500$  to  $7950 \text{ cfs}$ ). These values plot above the threshold line and in the territory of braided streams. Figure 3.10 is similar and presents several observed thresholds between braided and meandering channels.

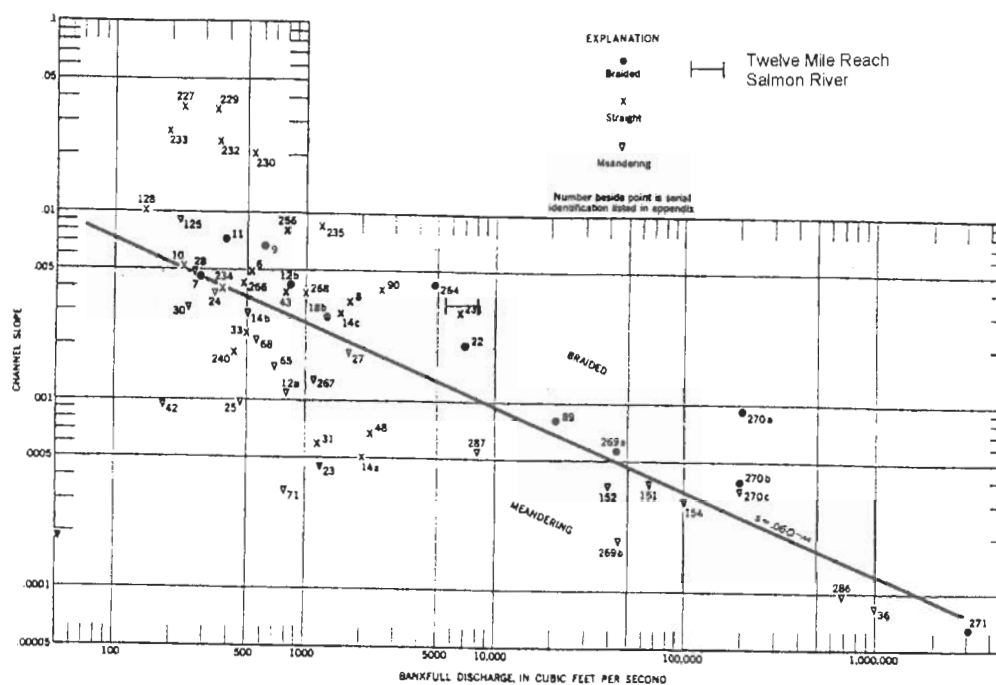


FIGURE 46.—Values of slope and bankfull discharge for various natural channels and a line defining critical values which distinguish braided from meandering channels.  
406703—57—4

Figure 3.9. Relation of discharge to slope and a line which separates meandering and braided channels (Leopold and Wolman, 1957).

Aerial photography and river surveys verify the tendency of this system to braid. Aerial photos presented elsewhere in this report (e.g. Figures 2.3 and 3.4) display numerous channels and display the nature of frequent avulsions as sediment is deposited and eroded. However, when compared to classic examples of other braided rivers, braiding through the Twelve Mile Reach is mild and usually confined to specific locations. Braiding may be an adjustment that tends to increase the ability of the channel to carry a larger amount of bedload, and may also be as close to equilibrium as are meandering rivers (Leopold et al., 1964).

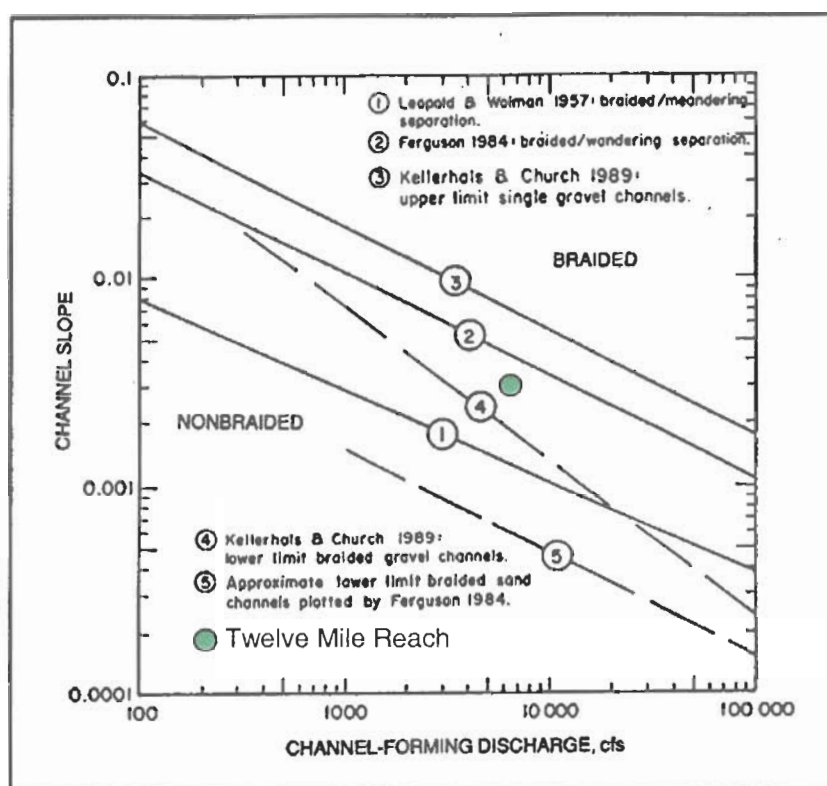


Figure 3.10. Relation of discharge and slope and several threshold boundaries distinguishing braided from non-braided channels with Twelve Mile Reach indicated between lines 2 and 4 (U.S. Army Corps of Engineers, 1994).

### 3.5 Channel Width to Depth Ratio

Width-to-depth (w:d) ratio is a common stream channel assessment indicator. The ratio is determined for the same 14 cross-sections described in section 4.4 at various water level elevations including the surveyed edge of water, high water marks, top of bar, top of bank, and at simulated flows of 156 and 212 m<sup>3</sup>/s (see Table 3.1). Depth is the distance from the lowest point in the channel (thalweg) to the elevation of the point of interest. Width is the distance across the channel at the elevation of interest and was computed by MIKE11 (see Chapter 6) based on surveyed sections. MIKE11 computations were checked for consistency and accuracy. The discharge of 156 m<sup>3</sup>/s is an earlier determination of bankfull at the gaging station 13 km upstream of the Twelve Mile Reach (Emmett, 1975). The discharge of 212 m<sup>3</sup>/s is selected as it was the preliminary determination of effective

discharge and is near to bankfull. Discharge during the December 1999 cross-section survey was approximately  $25 \text{ m}^3/\text{s}$  and during the April 2000 survey discharge was about  $41 \text{ m}^3/\text{s}$ .

Table 3.1. Channel width-to-depth ratio at selected cross-sections for various conditions.

Cross Section	Lower Bank	Width-to-Depth Ratio								
		December 1999 Edge of Water	April 2000 Edge of Water	Lower high water mark	Upper high water mark	Top of Left Bank	Top of Right Bank	Top of Bar	156 $\text{m}^3/\text{s}$ (simulated)	212 $\text{m}^3/\text{s}$ (simulated)
10	Right	39		44	31	43	29		33	30
13	Left	33	30	27		28	29	36	30	27
15	Right	66	58	38	36	33	34	38	38	37
18	Left	37	34	28	24	22	21		23	21
21	Left	22		27		31	32		29	30
23	Right	43	39	30		31	28		28	27
25	Left	23	27	32		37	37	39	38	37
28	Left	48	40	32		21	19		29	26
32	Left		45	28		27			29	26
37	Left		60			41			44	47
43	Left		44			34		45	38	34
50	Left		33			27		37	28	26
54	Right		25	23	23		22		21	23
57	Right		46	45		39	48	48	42	47
Average:		39	40	32	28	32	30	40	32	31

The bankfull stage (selected as the lower of the right or left bank) w:d ratio ranges from 21 to 48 with an average of 30. These values are considered high with some being very high and typical of a mildly braiding system (Rosgen, 1996).

### 3.6 Channel Width

Channel width at selected cross-sections is presented in Table 3.2. These values represent the width of the water surface at conditions described in the prior section. Also as previously described, the values were determined based on MIKE11 model results. The average bankfull width is 76 m, and varies from 48 to 120 m.

Table 3.2. Channel width at selected cross-sections for various conditions.

Cross Section	Lower Bank	Channel Width (m)								
		December 1999 Edge of Water	April 2000 Edge of Water	Lower high water mark	Upper high water mark	Top of Left Bank	Top of Right Bank	Top of Bar	156 m <sup>3</sup> /s (simulated)	212 m <sup>3</sup> /s (simulated)
10	Right	42		61	72	129	75		70	73
13	Left	37	39	44		86	89	66	68	70
15	Right	53	54	59	73	78	75	66	63	71
18	Left	40	43	45	47	48	50		48	49
21	Left	33		73		92	105		81	95
23	Right	45	47	57		81	69		62	67
25	Left	31	46	65		98	109	97	92	99
28	Left	44	47	52		65			60	62
32	Left		55	62		62			60	62
37	Left		55			74			72	92
43	Left		57			82		79	81	82
50	Left		57			69		69	69	73
54	Right		53	57	78		85		64	78
57	Right		62	66		123	120	122	89	115
Average (m):		41	51	58	68	84	86	83	70	78

### 3.7 Meanders

A number of channel characteristic shape files were created in ArcView<sup>®</sup> in three temporal frames for the purpose of comparing meander characteristics. Historic characteristics are based on the 1893 / 1896 / 1911 cadastral survey of the meander corridor. Digitizing a line along the center of the meander corridor approximated the channel centerline. For 1947 / 1957 and 1992 data, the stream channel was digitized from geo-referenced aerial photography.

Meander characteristics of radius, amplitude, and length are determined and compared for the time periods of late 1890s / early 1900s, 1947, and 1992. These comparisons provide an insight to evolution of the main channel over the 100-year period. Channel alignment plots (Figures 3.11 to 3.13) indicate where the stream has frequent episodes of realignment and also where the channel alignment appears to be stable and less likely to avulse.

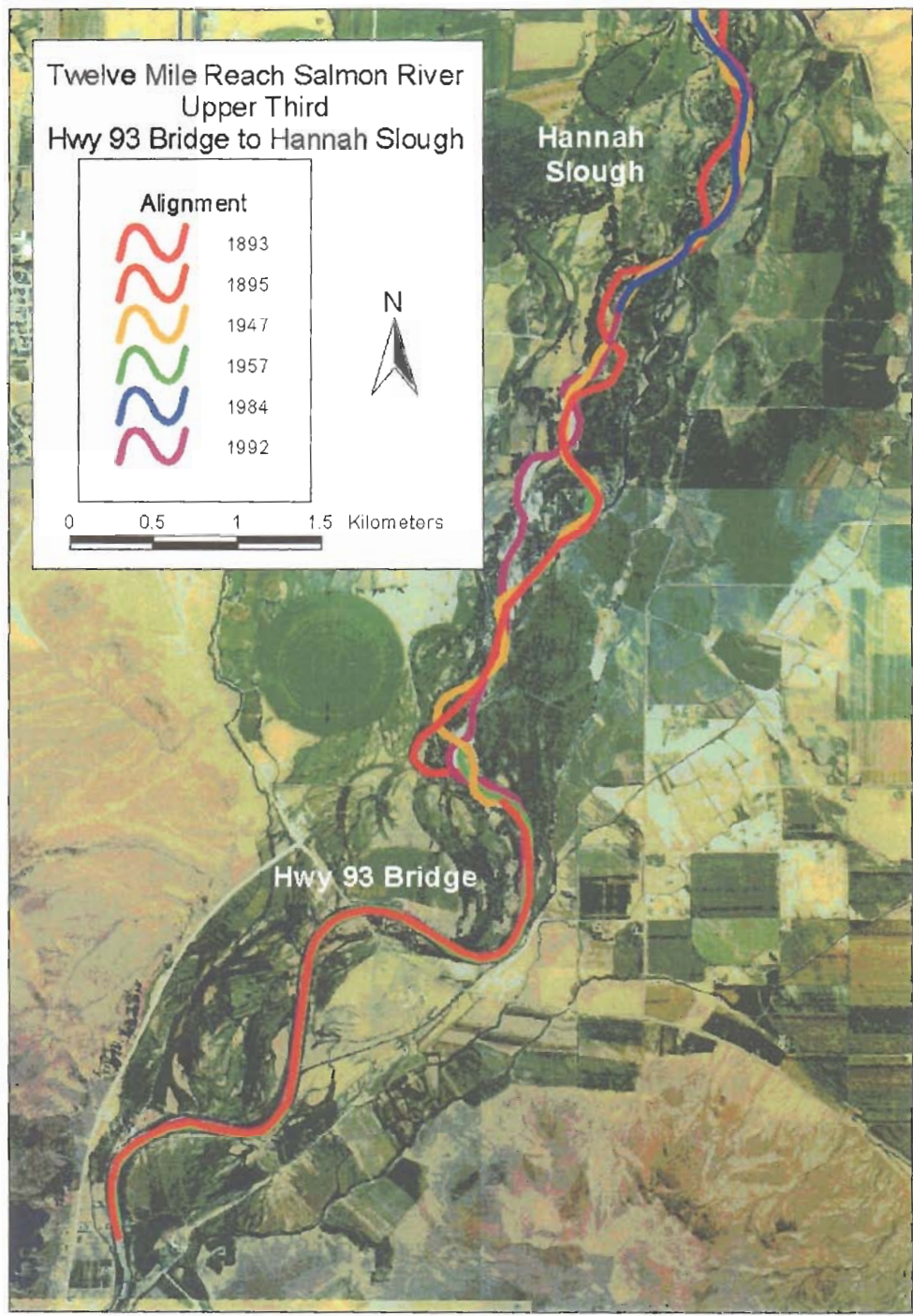


Figure 3.11. Channel alignments for upper third of the Twelve Mile Reach.

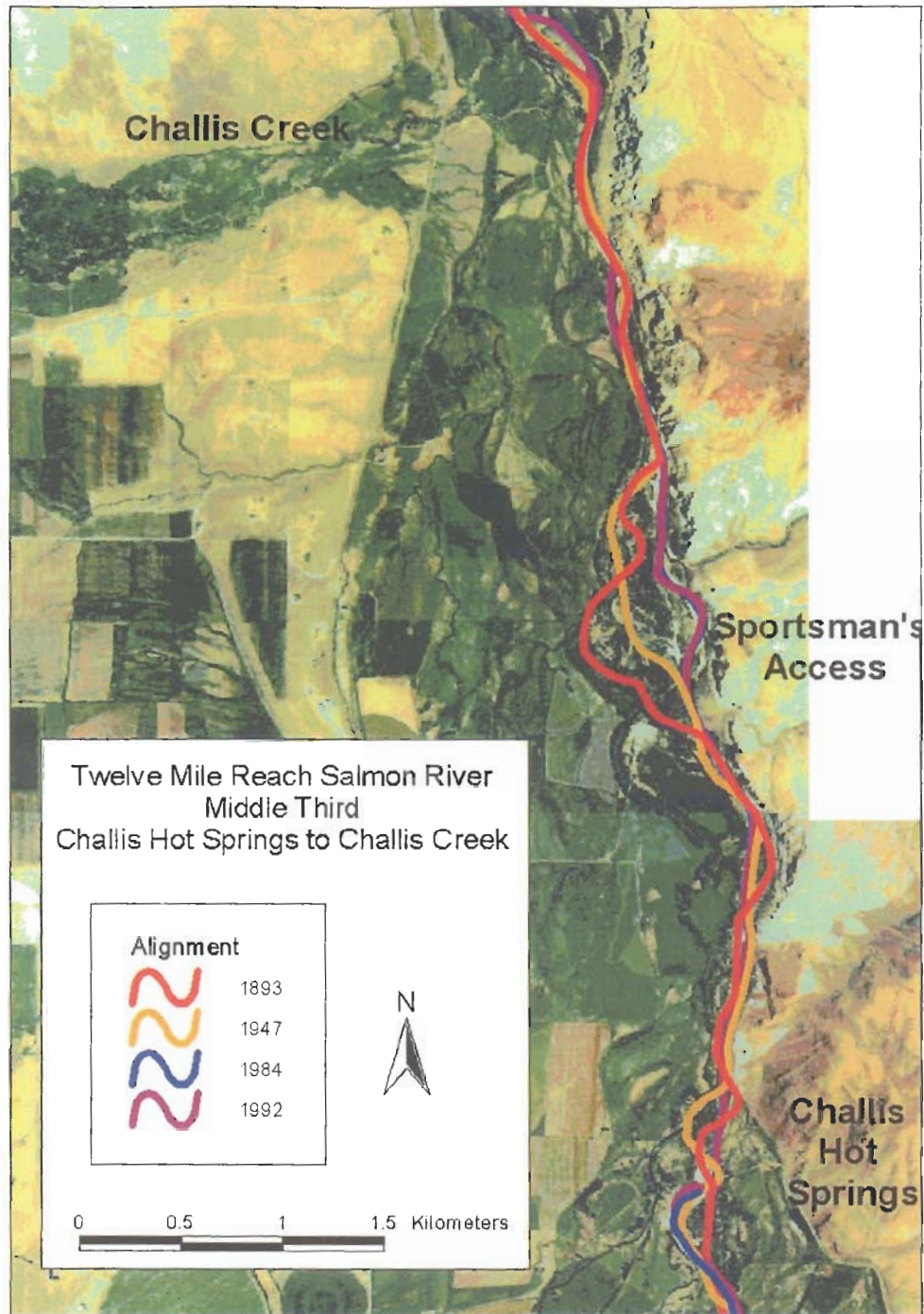


Figure 3.12. Channel alignments for middle third of the Twelve Mile Reach.

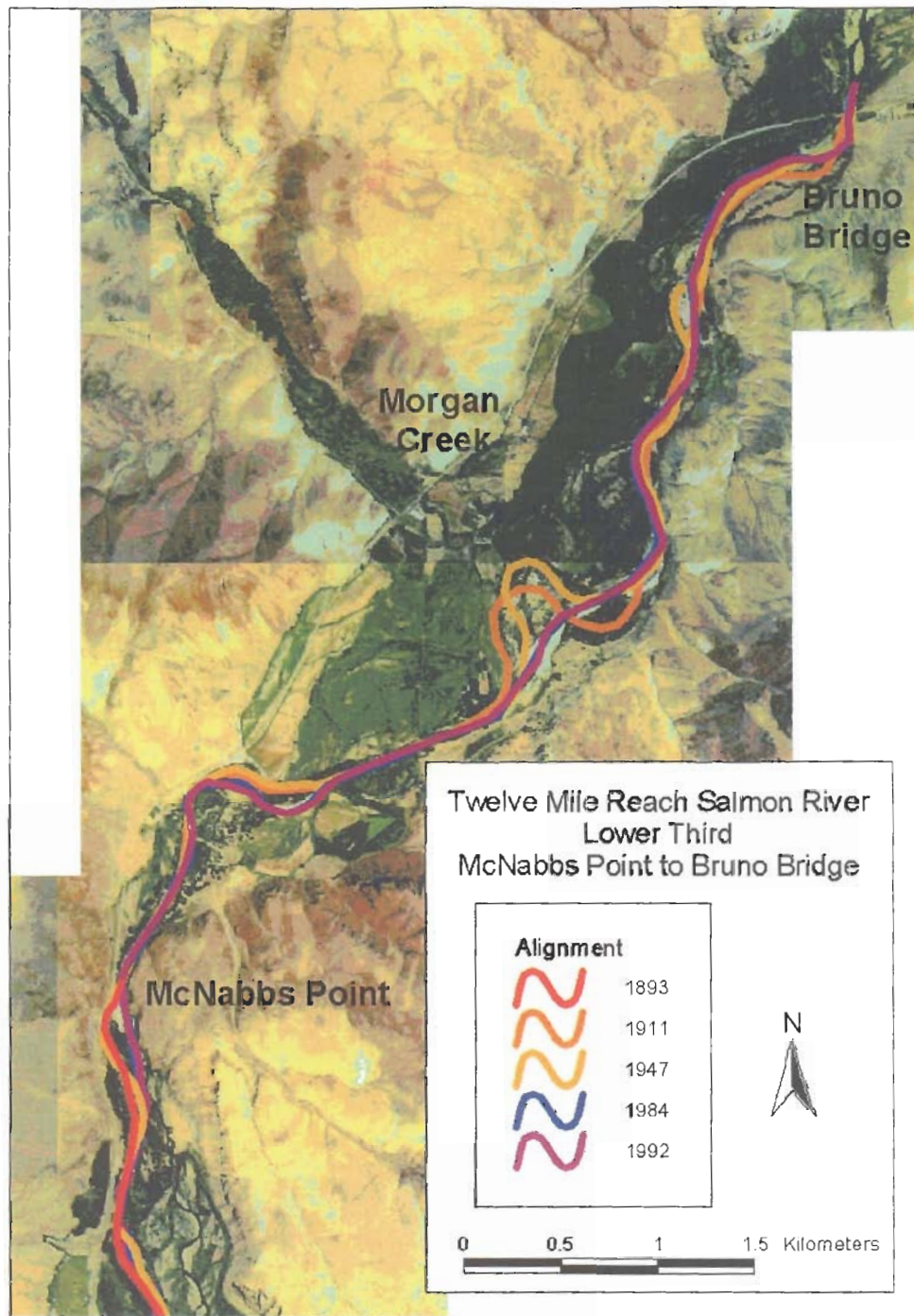


Figure 3.13. Channel alignments for lower third of the Twelve Mile Reach.

### 3.7.1 Methodology

The complete Twelve Mile Reach was split into seven sub-reaches for the purpose of geomorphic characteristic analysis and comparisons. Figure 3.14 depicts these sub-reaches against the historic channel alignment.

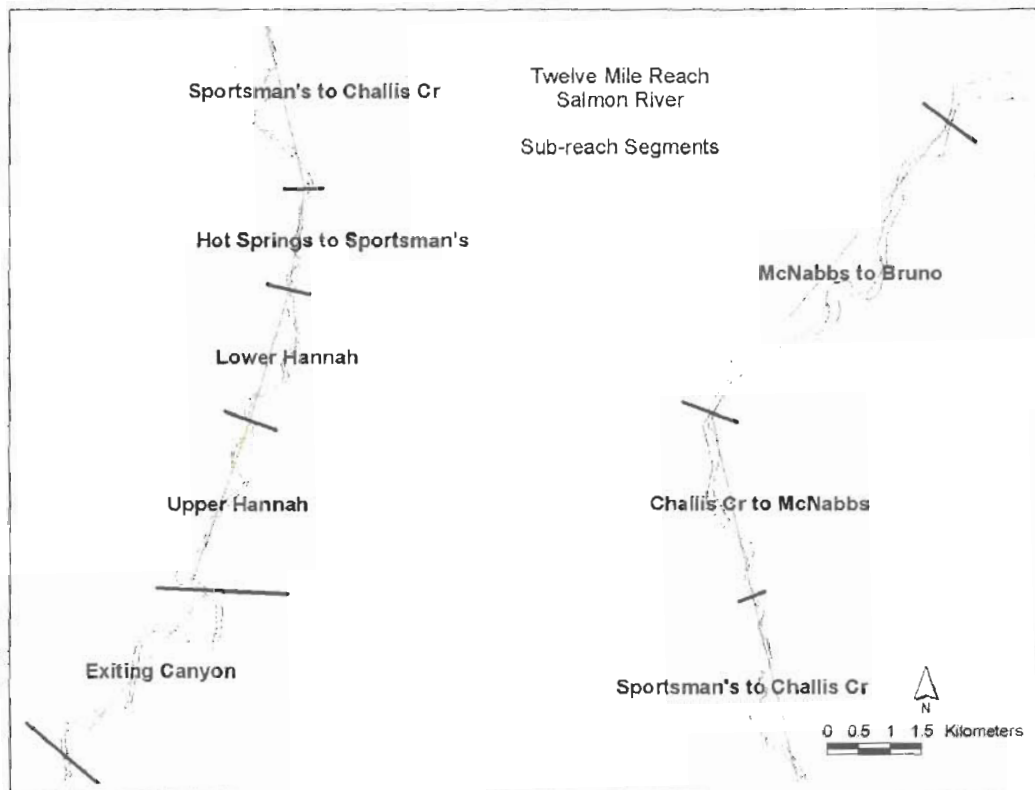


Figure 3.14. Sub-reach segments of the Twelve Mile Reach.

Characterization of meanders was accomplished in a GIS environment using U.S. government plat maps from 1893, 1896, and 1911, and aerial photography from 1947, 1957 and 1992 for base layers. The following shape files were created in ArcView<sup>®</sup> to assist in characterizing meanders:

- Channel Alignment based on digitized stream edges of water.
- Channel Centerline based on digitized center of channel.

- Meander Radius Circles drawn to approximate the meander radius of curvature ( $R_c$ ). Circles were generally created for meanders with angle of curvature exceeding 70 degrees.
- Meander Inflection Points depicting the inflection point between meanders.
- Meander Wavelength ( $L$ ), the distance between alternating meander inflection points.
- Wavelength Parallel lines drawn parallel to a given meander wavelength line and tangent to the upstream and downstream outside meander centerline and used for determining meander amplitude ( $M_a$ ).
- Meander Amplitude ( $M_a$ ), the distance separating wavelength parallels to approximate the meander amplitude ( $M_a$ ) defined as the distance from top to bottom of a wave. Note that this definition of wave amplitude differs from traditional wave mechanics amplitude, which is normally computed as  $\frac{1}{2}$  the distance from top to bottom of a wave. However, this definition is consistent with meander amplitude defined in other classic geomorphology textbooks (Leopold et al., 1964; Rosgen, 1996).

Geo-referenced aerial photography from 1992 and 1947 / 1957 was used for creation of channel centerline and channel alignment lines. Alignment lines were drawn based on the visible edge of water, and centerline along the center of the stream. As the most historic channel alignment is based on the government meander corridor survey and the alignment lines from aerial photography representing edge of water at moderate flow conditions, it is inappropriate to make comparisons between the apparent channel widths from these different sources. However, comparisons between meander radius of curvature, wavelength, and amplitude are appropriate and are thus presented.

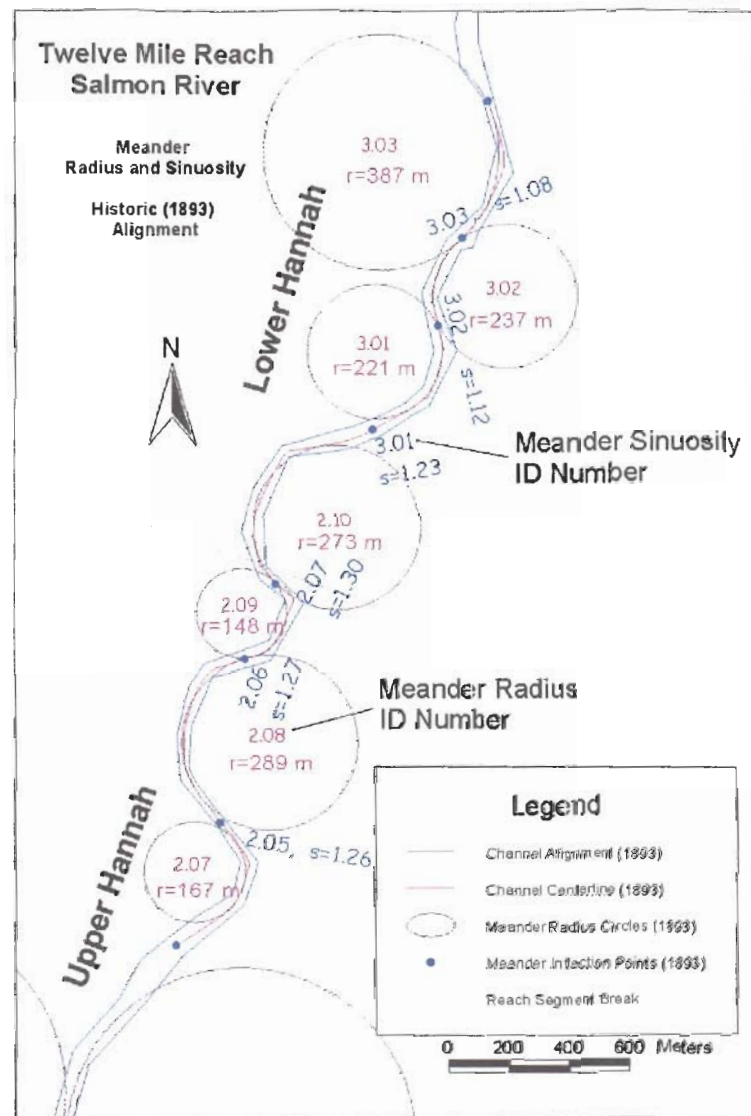


Figure 3.15. Meander radius and sinuosity for 1893 channel alignment.

Figure 3.15 presents meander radius circles and meander sinuosity lines for portions of two sub-reaches including the lower portion of the Upper Hannah sub-reach and the upper portion of the Lower Hannah sub-reach. Meander radius circles are identified by an assigned primary and secondary numbering system. The seven depicted radius circles are numbered 2.07, 2.08, 2.09, 2.10, 3.01, 3.02, and 3.03 and the radius of each circle is also presented in the figure. Secondly, a meander sinuosity number designates each meander sequence. For example, meander sinuosity line 2.05 with a sinuosity of 1.26 is based on the upstream and downstream meanders (meander radius characterized by circles 2.07 and 2.08 respectively).

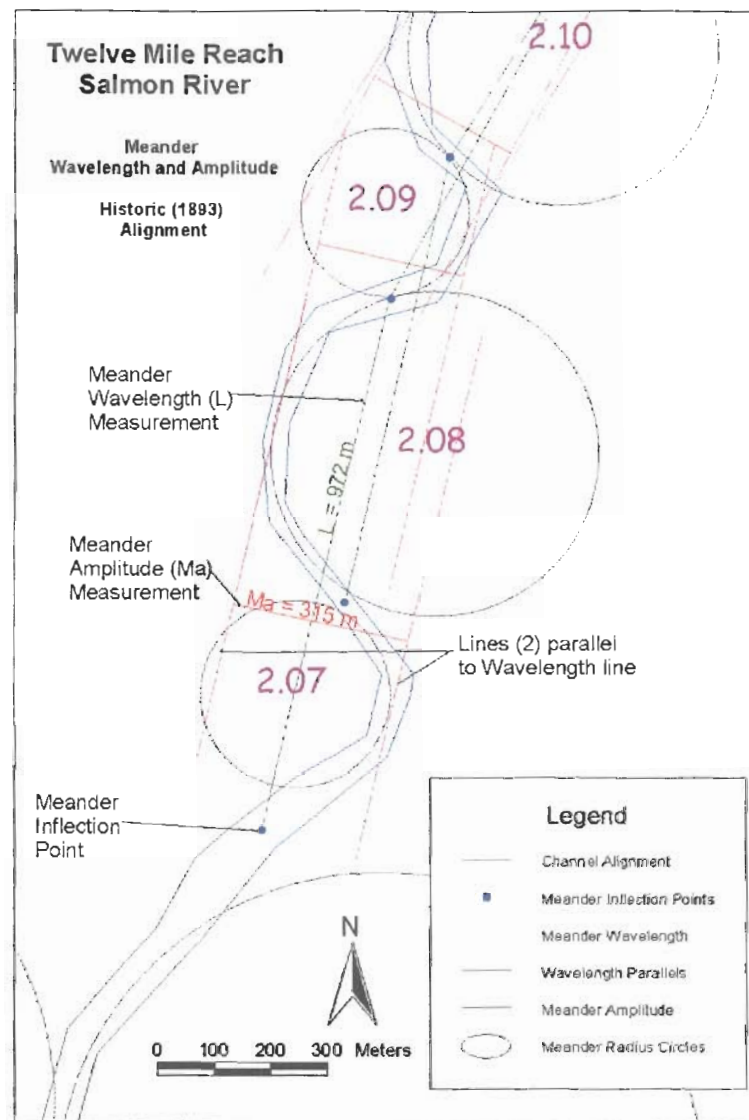


Figure 3.16. Meander inflection points, wavelength and amplitude.

Figure 3.16 presents meander wavelength and amplitude for one meander sequence in the Upper Hannah sub-reach. The meander wavelength line is drawn between the two meander inflection points defining the upstream and downstream ends of the meander sequence. The length of this meander wavelength is 972 meters. Two lines are drawn parallel to the meander wavelength line and tangent to the upstream and downstream meander centerlines. The distance between these two parallel lines provides the meander amplitude, in this case  $Ma = 315$  meters.

Likewise, meander 2.06 in Figure 3.16 with sinuosity of 1.27 is based on the adjacent upstream and downstream meanders, so that the meander represented by circle 2.08 is used to determine sinuosity for both meander 2.05 and 2.06. Not every meander is characterized; meander radius of curvature and sinuosity is generally determined only for meanders with angle of curvature exceeding 70 degrees. The length of the curved channel centerline between the same two inflection points is 1222 meters, and thus the sinuosity of this meander is  $1222 \div 972 = 1.26$ .

Table 3.3. Number of meander features including Wavelength (L), Meander Amplitude ( $M_a$ ), Sinuosity ( $M_s$ ), and Radius of Curvature ( $R_c$ ) determined by sub-reach.

	1	2	3	4	5	6	7
	Exiting Canyon	Upper Hannah	Lower Hannah	Hot Springs Sportsman's	Sportsman's Challis Cr	Challis Cr McNabbs	McNabbs Bruno
1893/1911 (L, $M_a$ , $M_s$ )	4	4	3	2	5	4	4
1893/1911 ( $R_c$ )	4	6	3	3	6	5	6
1947 (L, $M_a$ , $M_s$ )	photos not available	5	1	2	4	1	7
1947 ( $R_c$ )	photos not available	7	1	3	6	2	9
1992 (L, $M_a$ , $M_s$ )	4	5	1	0	2	4	9
1992 ( $R_c$ )	4	7	1	1	3	5	11

Table 3.3 provides a tabular listing of the number of meander features determined by sub-reaches of the Twelve Mile Reach. The 1893 / 1911 data set shows that in sub-reach 4 (Hot Springs to Sportsman's) the radius of curvature was determined for three meanders and wavelength, amplitude, and sinuosity was determined for two meander sets. The same number of each was determined for 1947 river conditions. However, in 1992, the radius of curvature was determined for only one meander, and no meander sets had wavelength, amplitude or sinuosity determined. In this case, the river was nearly straight through this sub-reach in 1992, and had lost several meanders from the earlier conditions. Likewise, in

sub-reach 3 (Lower Hannah), there were more meanders in the reach in 1893 than in 1947 and 1992. Note that 1947 photography was not available for most of sub-reach 1, and therefore nothing is presented in this sub-reach for 1947 conditions. 1957 photography was available for this sub-reach but was not included in this presentation, as the channel in this sub-reach appears to be nearly unchanged from 1893 through present.

### 3.7.2 Results

The following section presents a summary of meander characterization by sub-reach and year. Results of meander wavelength, amplitude, sinuosity, and radius of curvature analysis are provided in figures and tables. Alignment of sub-reach 1 remained relatively constant through the last hundred years. However, the remainder of the reach incurred significant adjustments in alignment and meander properties with a general trend to decreased wavelength, meander amplitude, radius of curvature, and sinuosity.

#### 3.7.2.1 Meander Wavelength

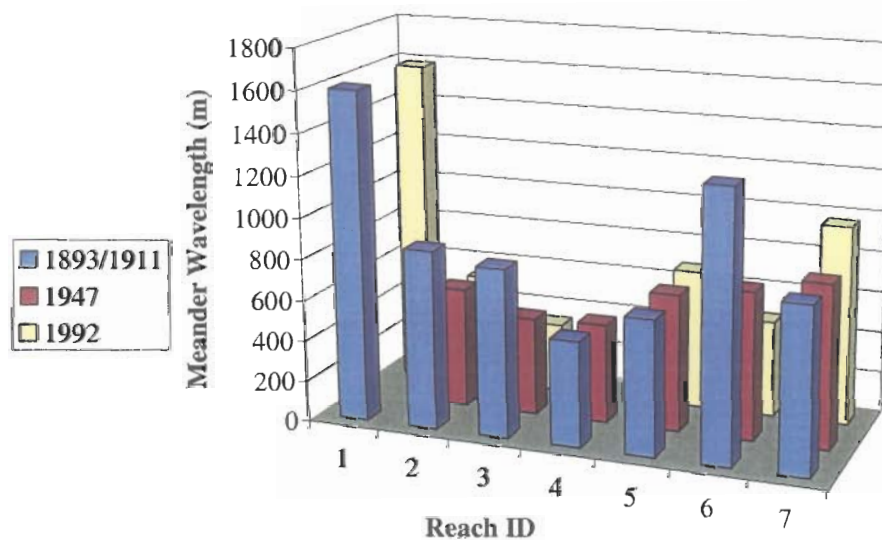


Figure 3.17. Meander wavelength by reach.

Meander wavelength is presented in Figure 3.17 and Table 3.4. The mean meander wavelength from sub-reaches 2 to 7 decreased from 830 to 600 m over the period of record.

Sub-reaches 3 and 6 had the most significant decreases in wavelength, while reach 7 had a modest increase.

Table 3.4. Meander wavelength by reach (m).

Reach ID	1893/1911	1947	1992
1	1601		1589
2	870	584	543
3	820	476	336
4	514	484	
5	658	670	680
6	1301	723	470
7	804	796	971

### 3.7.2.2 Meander Amplitude

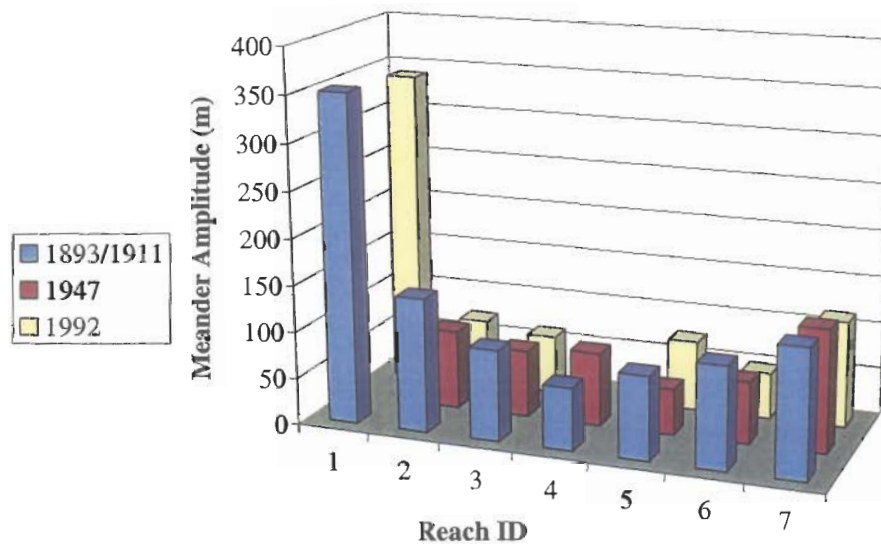


Figure 3.18. Meander amplitude by reach.

Figure 3.18 and Table 3.5 demonstrate the dramatic difference in meander characteristics between the upstream entrenched sub-reach and the remainder of the system. Meander amplitude decreased from an average of 107 to 74 m for all meanders in sub-reaches 2 to 7 over the period of record.

Table 3.5. Meander amplitude by reach (m).

Reach ID	1893/1911	1947	1992
1	352		340
2	143	84	72
3	97	71	62
4	67	78	
5	89	49	74
6	109	66	49
7	136	130	114

### 3.7.2.3 Meander Radius of Curvature

Meander radius of curvature decreased from an average of 294 to 199 m over the observed period for sub-reaches 2 to 7. Observations indicate that meanders with high radius of curvature tend to have lower angle of curvature than those with low radius of curvature.

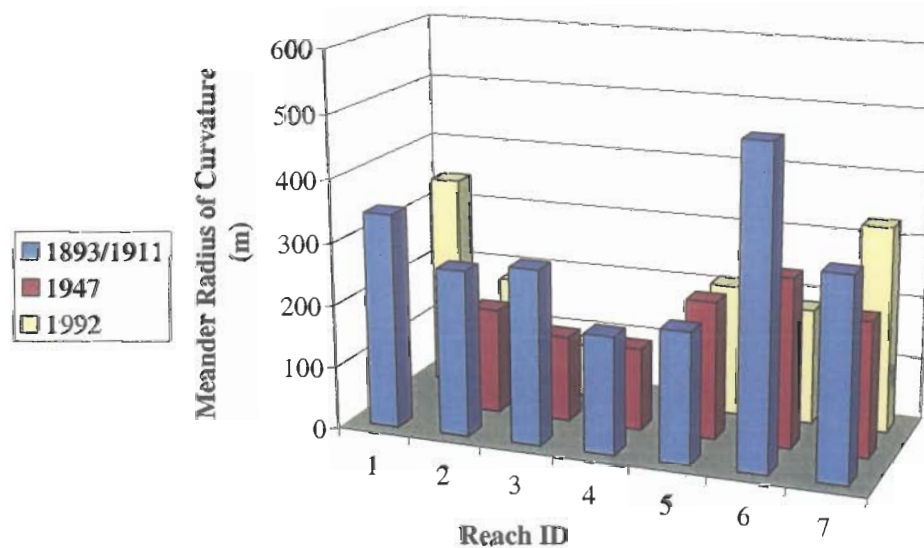


Figure 3.19. Meander radius of curvature by reach.

Table 3.6. Meander radius of curvature by reach (m).

Reach ID	1893/1911	1947	1992
1	344		343
2	265	169	184
3	280	137	86
4	188	131	
5	208	220	212
6	504	270	185
7	320	216	330

### 3.7.2.4 Meander Sinuosity

Meander sinuosity presented in Figure 3.20 and Table 3.7 is developed based on individual meanders, and is not reach-level sinuosity. Therefore, values presented here are generally higher than sinuosity in the following section as straight reaches are not included in this portion of the assessment. Meander sinuosity generally decreased from average values of 1.22 to 1.17. Although meanders in some sub-reaches decreases in sinuosity over time, others increased. In some of these reaches (e.g. 5 and 7), decreases in meander sinuosity can be attributed to localized stream straightening and levee construction.

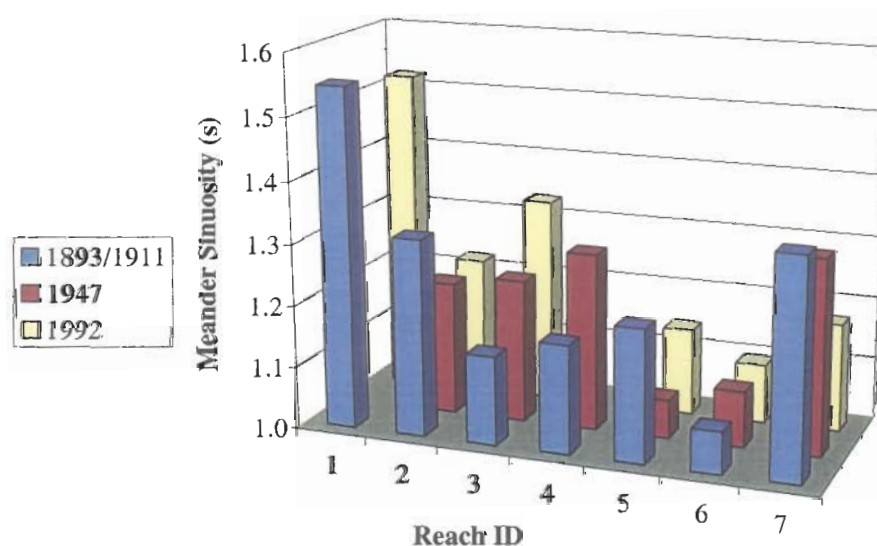


Figure 3.20. Meander sinuosity by reach.

Table 3.7. Meander sinuosity by reach.

Reach ID	1893/1911	1947	1992
1	1.55		1.52
2	1.32	1.21	1.22
3	1.14	1.23	1.33
4	1.18	1.29	
5	1.21	1.06	1.14
6	1.07	1.09	1.10
7	1.35	1.31	1.17

## 3.7.2.5 Sub-Reach Level Sinuosity

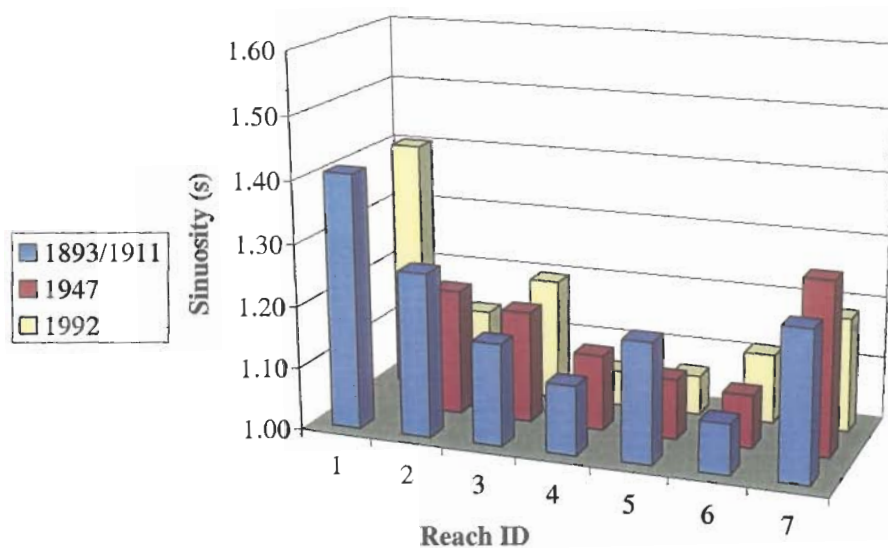


Figure 3.21. Reach-level sinuosity.

Table 3.8 and Figure 3.21 present reach-level sinuosity values determined by dividing channel centerline length by straight-line length between end points on a reach-wide basis. This is different from data presented in Table 3.7 and Figure 3.20. Figures 3.17 to 3.20 provide results of analyzing specific meanders within a reach, but straight sections of stream within the reach were not analyzed and are therefore not represented in these figures. Figure 3.21, on the other hand, represents the total stream length within the sub-reaches and is therefore a better indicator of overall conditions. Therefore, a reach with significant lengths

of straight alignment will have a low sinuosity in Table 3.8 and Figure 3.21, but the same reach may have one segment with a sinuous meander, thus indicating a high sinuosity in Figure 3.20.

Table 3.8. Reach-level sinuosity.

<b>Reach ID</b>	<b>1893/1911</b>	<b>1947</b>	<b>1992</b>
1	1.41		1.40
2	1.26	1.20	1.13
3	1.16	1.18	1.20
4	1.11	1.12	1.06
5	1.19	1.10	1.06
6	1.08	1.09	1.11
7	1.24	1.28	1.18

Table 3.8 and Figure 3.21 present the extent of total sinuosity variations over time. Reach 1, which has a very stable alignment over the past 100 years, indicates no significant change in sinuosity over this period. Reach 5, on the other hand, demonstrates a significant decrease in total sinuosity over the period of analysis. Sinuosity of reaches 2, 4, and 7 has also decreased, but to a lesser degree than reach 5. The average sinuosity of reaches 2 to 7 decreased from 1.18 to 1.12 over the observed period.

### 3.7.2.6 Stream Centerline Length

Table 3.9. Channel centerline length (m).

<b>Reach ID</b>	<b>1893/1911</b>	<b>1947</b>	<b>1992</b>
1	4913		4944
2	3458	3335	3102
3	2566	2345	2651
4	1671	1864	1747
5	4026	3605	3470
6	3251	3185	3259
7	7462	7697	7123
Total Stream Length	27347		26296

Table 3.9 presents channel centerline length for the various reaches in three different time frames. The chart quantifies the length of stream gained or lost as sinuosity fluctuates. Most notable, we see that reaches 2, 5, and 7 had significant decreases in total stream length of 360, 560, and 340 meters each respectively. In total, the 27.3 km reach has reduced to 26.3 km over the hundred-year period.

## 4 Hydrologic Conditions

---

### 4.1 Mean Daily Discharge

Stream discharge records for the Twelve Mile Reach are available from USGS gaging station number 13298500, Salmon River near Challis. This station operated from October 1, 1928 to October 5, 1972, providing a continuous record of average daily discharge with one break in data from December 8, 1971 to April 24, 1972. The station, shown in Figure 4.1, is located on the main stem Salmon River just downstream of Bayhorse Creek, about 13 km upstream of the Twelve Mile Reach. Figure 4.2 depicts observed daily average flows from this record with base flows near  $20 \text{ m}^3/\text{s}$  and peak discharges generally between 100 and  $400 \text{ m}^3/\text{s}$ . Daily readings from this station were discontinued after October 5, 1972, and peak annual discharge readings were discontinued in 1976.

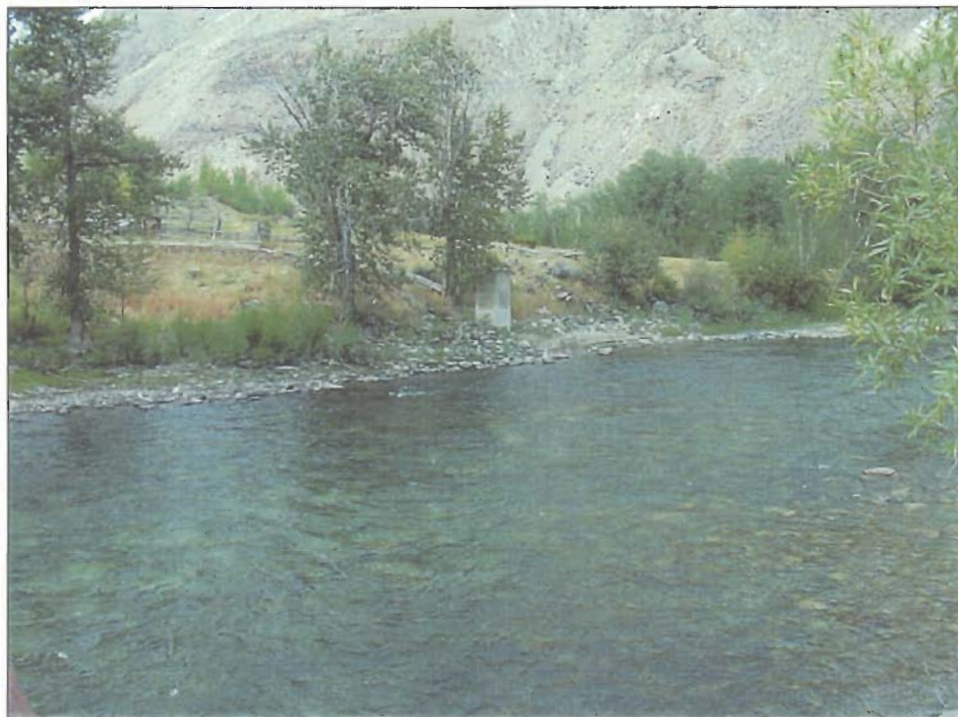


Figure 4.1. USGS gaging station 13298500, Salmon River near Challis, located below Bayhorse Creek, about 13 km upstream of the Twelve Mile Reach.

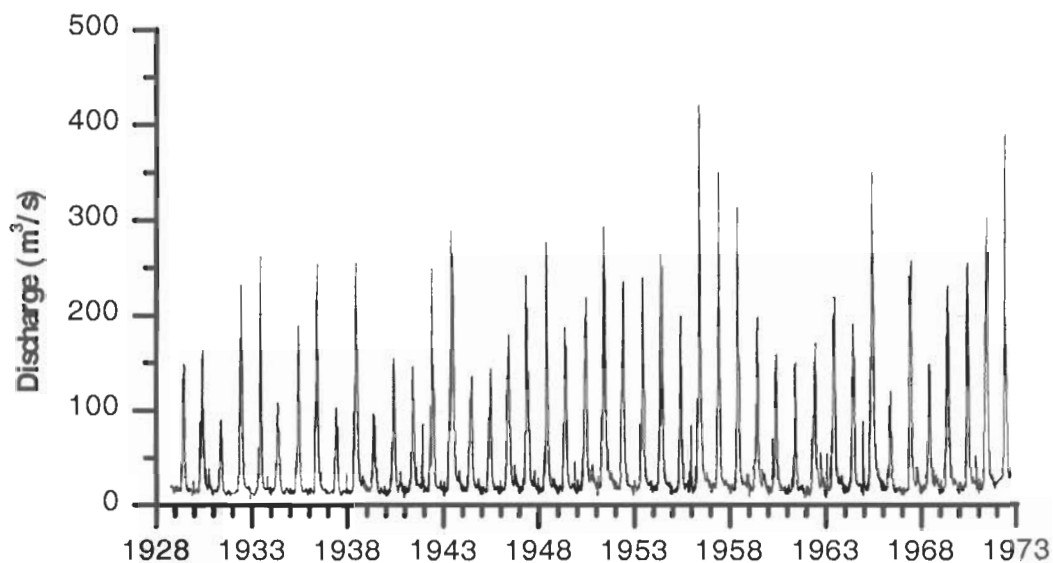


Figure 4.2. Salmon River near Challis, average daily discharge, 1928 – 1972.

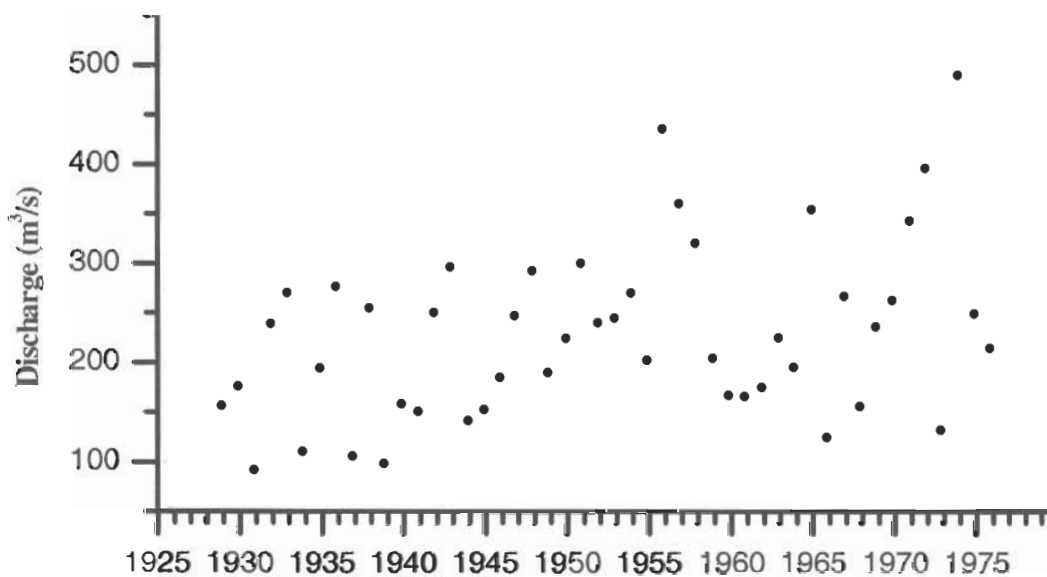


Figure 4.3. Salmon River near Challis, annual peak discharge, 1929 – 1976.

#### 4.2 Peak Annual Discharge

Peak annual flows are available from the same station for the period 1929 to 1976 providing 48 years of record (see Figure 4.3). The data appear to indicate that peak

discharges are increasing over time. However, the record is comparatively short and caution should be exercised in implying such a meaning.

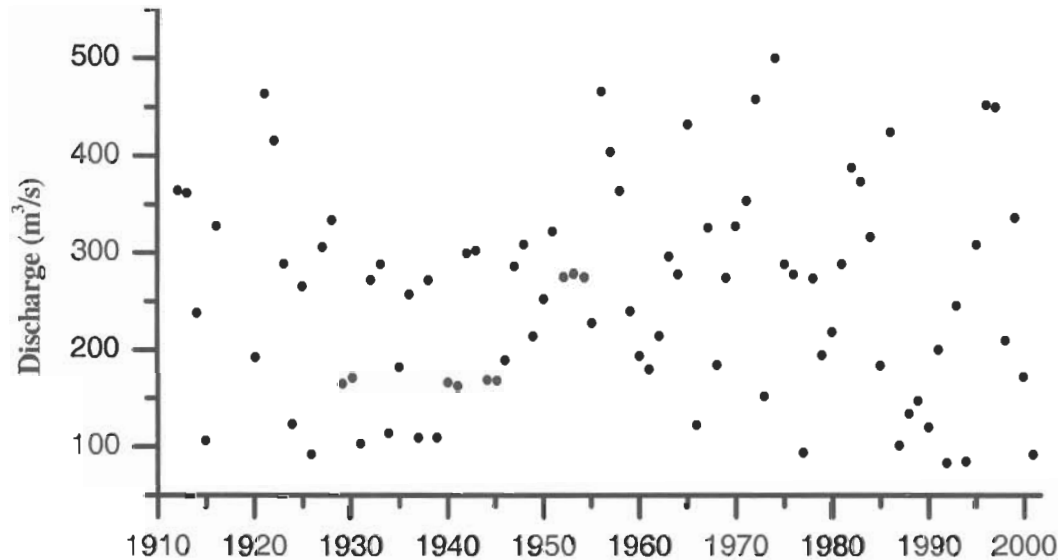


Figure 4.4. Salmon River at Salmon, annual peak discharge, 1912 – 2001.

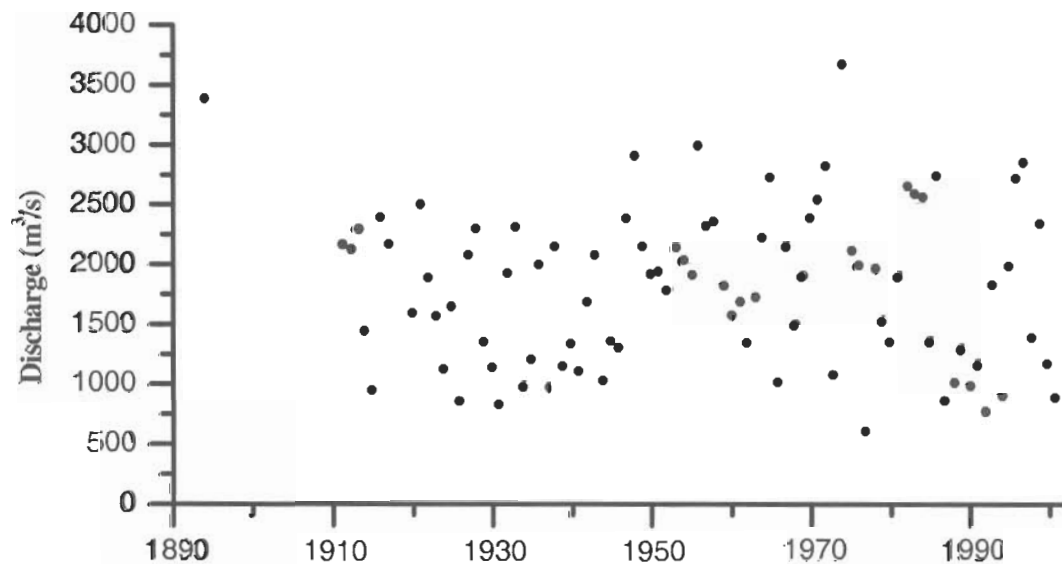


Figure 4.5. Salmon River at White Bird, annual peak discharge, 1894 – 2001.

Other main stem Salmon River gages providing longer periods of record do not support an increasing trend to annual peak flow, but rather show that the period from 1929 to

1955 was marked by rather moderate peak discharges. Salmon River at Salmon, an important gage for extending the near Challis record to recent years (see Figure 4.4), has recorded 86 years of annual peak flows from 1912 to 2000 (1917-19 missing). Farther downstream, the Salmon River at White Bird includes 89 years of annual peak flow with one estimated discharge point dating from 1894 and continuous data from 1911 to 2000 (1918-19 missing, see Figure 4.5).

Figure 4.6 provides a comparative perspective between peak discharges at Salmon and near Challis with the six highest peaks identified by year of occurrence. The peak flow at Salmon exceeds the peak near Challis except in the years 1930, 1935, 1936, and 1966. On average, the peak flow at Salmon is 10% greater than at Challis, but has ranged from 8% lower to 30% higher. Peak discharge generally occurs in May and June driven by snowmelt in the upper watershed. These peak discharge data have a positive correlation of 0.97.

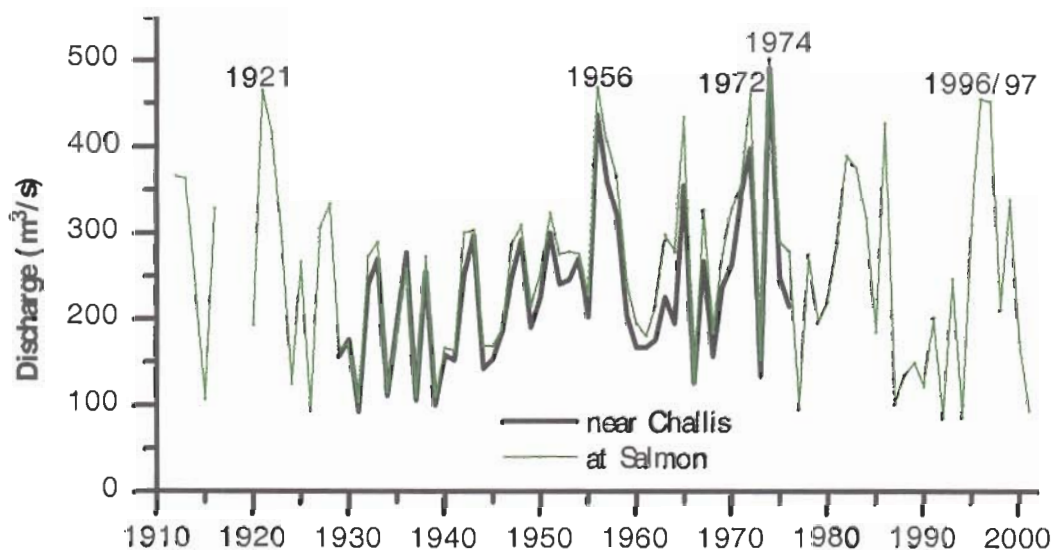


Figure 4.6. Salmon River peak annual discharge, 1912 – 2001. A comparison of peak discharges near Challis and at Salmon.

In order to provide estimates of recent peak discharges at Challis, flow records from two currently active downstream stations are used to develop a simple relationship for estimating peak discharge near Challis. One major tributary, the Pahsimeroi River, is gaged

and discharges between the upstream gage near Challis and the downstream gage at the City of Salmon. Peak discharges near Challis are approximated based on a best-fit equation where the peak discharges at the Challis and Salmon stations occurred within two days of each other (see equation 3.1). The relationship is based on thirty years of record where data exists for all three stations with two data points excluded because the peak discharges occurred more than two days apart. Figure 4.7 presents the basis for equation (4.1), a line fit to the peak discharge at Challis and corresponding peak discharge at Salmon less Pahsimeroi River discharge. Based on this relationship, peak discharges at Challis are approximated for recent years (see Table 4.1). Discharge records for the Pahsimeroi River are not always available, and therefore peak discharge at Challis can also be approximated with the peak discharge at Salmon (see equation 4.2). However, this relationship provides results slightly less accurate ( $R^2 = 0.95$ ) than equation (4.1).

$$Q_{Challis} [m^3 / s] \approx 0.91(Q_{Salmon} - Q_{Pahsimeroi}) + 7.59 \quad (4.1)$$

$$Q_{Challis} [m^3 / s] \approx 0.89(Q_{Salmon}) + 1.8 \quad (4.2)$$

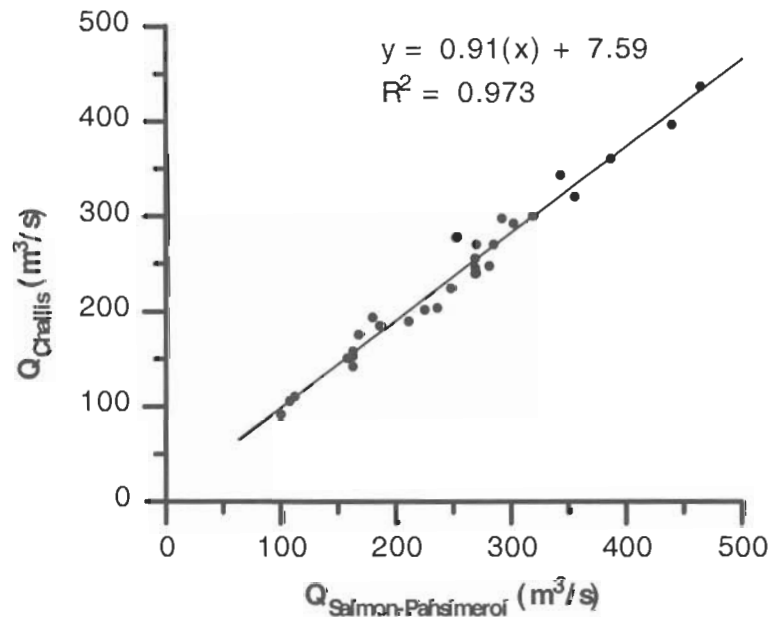


Figure 4.7. Relation between peak annual discharge of the Salmon River near Challis and the peak discharge at Salmon less Pahsimeroi River.

Table 4.1. Recent peak annual discharge at Salmon (measured) and near Challis (estimated).

Year	Measured Peak Discharge at Salmon (m <sup>3</sup> /s)	Estimated Peak Discharge near Challis (m <sup>3</sup> /s)
1995	309	281
1996	453	416
1997	450	406
1998	210	189
1999	337	303
2000	173	159
2001	93	90

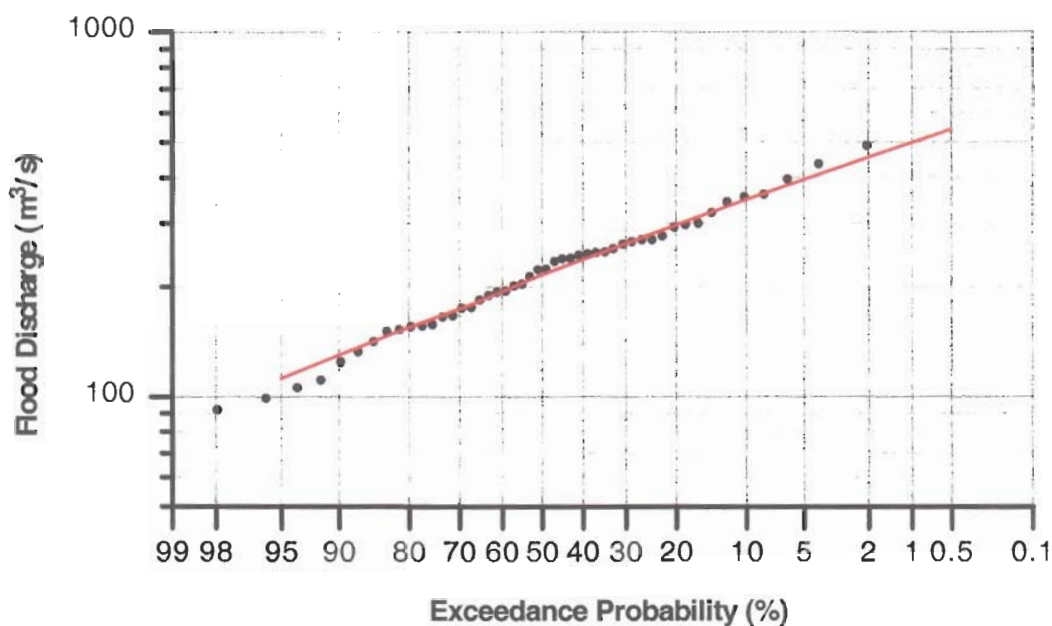


Figure 4.8. Salmon River near Challis, Log Pearson III fit.

### 4.3 Flood Frequency Analysis

Based on 48 years of record, application of the Log Pearson III method of flood frequency analysis for the Salmon River near Challis is presented in Figure 4.8. Figure 4.9 depicts the Log Pearson III analysis for the Salmon River at three locations. The lower curve in this figure represents the Salmon River below Yankee Fork, the upper curve is at Salmon, the two middle curves are near Challis with the dashed line based on the measured discharge record from the near Challis gage as in Figure 4.8, and the solid line is an adjustment to the near Challis data. At low flows, the Salmon curve drops below the Challis curve indicating

higher low peak flows at Challis than at the downstream Salmon gage, which is an unlikely condition. A series of recent lower peak flows, particularly during the drought years from 1987 to 1994, are not included in the near Challis gaging record. Using equations (4.1) and (4.2) to extend the near Challis record results in the adjusted flood frequency curve for this station.

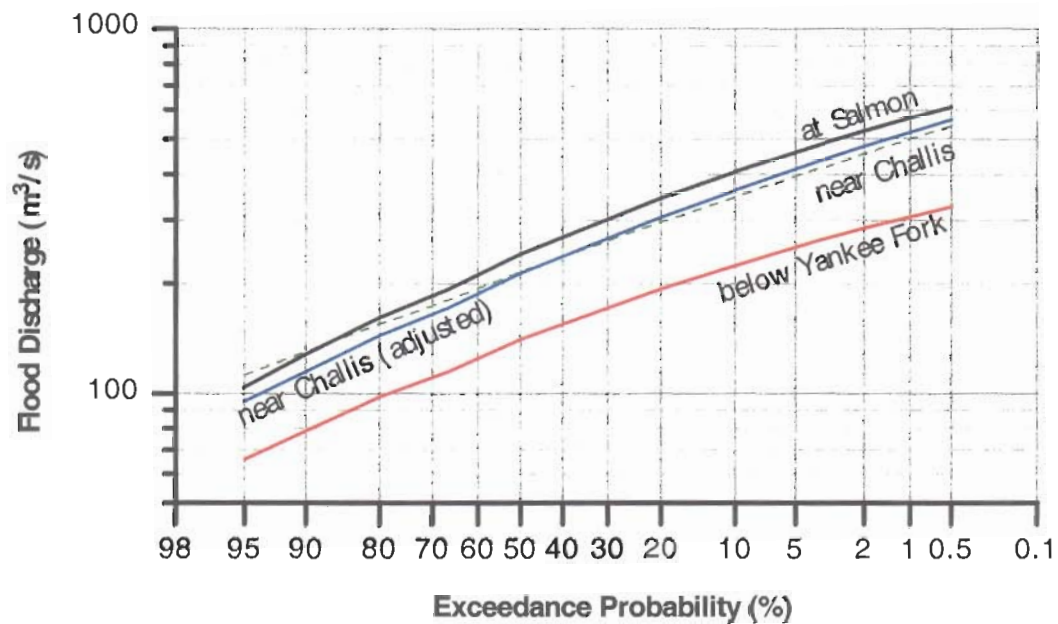


Figure 4.9. Salmon River Flood Frequency. Lower line is below Yankee Fork, middle solid line is adjusted near Challis, dashed line is unadjusted near Challis, and top line is at Salmon.

Table 4.2 provides exceedance probability ( $p$ ) and return interval ( $T$ ) for the Challis station, for stations at Salmon based on 86 years of record, and below the Yankee Fork based on 71 years of record. The table also provides an adjustment for the Challis data based on using equations (4.1) and (4.2) to extend the Challis data set. The adjusted values for Challis are recommended for design work.

Table 4.2. Exceedance Probability ( $P$ ) and Return Interval ( $T$ , years) for three Salmon River locations. Table includes an adjustment for the Challis station based on estimated peak discharges during periods without record.

---

Discharge ( $m^3/s$ )

P	T	below	near Challis		at Salmon
		Yankee Fk	near Challis	(adjusted)*	
0.95	1.05	66	112	95	104
0.90	1.11	79	130	115	128
0.80	1.25	98	155	144	161
0.67	1.50	115	180	172	193
0.50	2	141	216	214	241
0.20	5	194	296	305	344
0.10	10	225	347	362	405
0.04	25	261	409	429	476
0.02	50	285	454	476	525
0.01	100	307	498	520	570
0.005	200	327	542	563	612

\*near Challis (adjusted) data set includes estimates of peak discharge for 1912-1916, 1920-1928, 1977-2001.

#### 4.4 Bankfull Discharge

Bankfull discharge is defined as that water discharged when stream water just begins to overflow onto the active floodplain, and where the active floodplain is defined as a relatively flat area adjacent to the channel, constructed by the river, and overflowed by the river at a recurrence interval of about 2 years or a little less (Emmett, 1975; Wolman and Leopold, 1957). Furthermore, bankfull discharge is associated with the instantaneous maximum flow which, on the average, has a recurrence interval of 1.5 years as determined using a flood frequency analysis (Dunne and Leopold, 1978; Rosgen, 1996).

Emmett (1975) provides bankfull discharge values for 39 locations in the upper Salmon River area based on field surveys of channel geometry and utilization of stream-gaging data. The furthest downstream data site is the gaging station near Challis where bankfull discharge was estimated to be  $156 \text{ m}^3/\text{s}$  (5498 cfs). This discharge represents a 1.36-year return interval (see Table 4.2, near Challis adjusted). Emmett (1975) also includes values for the Salmon River above East Fork ( $145 \text{ m}^3/\text{s}$ , 5128 cfs) and below Yankee Fork ( $106 \text{ m}^3/\text{s}$ , 3740 cfs).

#### 4.4.1 Simulated Conditions

Water surface elevation and discharge were simulated using a MIKE11 model (see Chapter 6). Simulations were prepared to estimate stream discharge at several conditions including bankfull, top of bar, and observed water marks. Fourteen of the 67 surveyed cross-sections distributed throughout the reach were selected for detailed analysis because they were considered typical and representative of the reach and/or because water flow marks were identified and surveyed at the section. The water flow marks were identified by multiple characteristics including break in slope, change in sediment size (e.g. a seam between sand and gravel), and/or change in vegetation characteristics. A lower-elevation water mark was identified and surveyed at eleven sections, and a higher-elevation water mark was surveyed at four of these eleven sections.

Using U.S. Forest Service recommendations, bankfull stage and the active floodplain were determined based on field inspection described by Leopold (USDA Forest Service, 1995), and break in slope from survey data for the 11 sections with surveyed water marks. Cross-section profiles and photographs are provided in Appendix A. For the remaining three sections, bankfull is established based on break in slope from survey data alone. In addition, a gravel bar exists at five of the 14 sections and discharge is simulated for the top of bar condition. Results are presented in Table 4.3.

Modeled conditions indicate a bankfull discharge through the Twelve Mile Reach varying between 159 and 337 m<sup>3</sup>/s at individual cross-sections with an average value of 231 m<sup>3</sup>/s for the lower bank. These findings are based on the modeled discharge required to reach bank level at the 14 representative cross-sections.

In Table 4.3, the absence of an entry in the top of bank column indicates that the river is adjacent to a cliff or hill where a top of bank is either absent or could not be identified. Field inspections were not conducted for sections 37, 43, and 50 and therefore high water marks are not available and top of bank is based on cross-section break in slope only.

Table 4.3. Simulated discharge ( $\text{m}^3/\text{s}$ ) for selected cross-sections at various elevation conditions.

Cross-Section ID	Lower high water mark	Upper high water mark	Top of Bar	Top of Left Bank	Top of Right Bank	Top of Lower Bank
10	54	191		351	246	246
13	74		91	294	298	294
15	137	245	167	346	284	284
18	77	140		181	248	181
21	138			184	249	184
23	111			254	221	221
25	90		168	201	292	201
28	90			337		337
32	178			193		193
37				181		181
43			100	209		209
50			62	159		159
54	82	215			319	319
57	72		229	389	221	221
Average:	100	198	136	252	264	231

## 4.5 Sediment Transport

### 4.5.1 Sediment Transport Rate

Sediment transport, both bedload and suspended load, was measured by the USGS on the main stem Salmon River below Yankee Fork in 1999 and 2000. Slope at this station is 0.004 at low flow, and 0.0034 at higher discharges (Barry, 2002). Channel geometry at 144  $\text{m}^3/\text{s}$  includes a top width of 38 m and an area of 82  $\text{m}^2$ . At the low flow of 97.4  $\text{m}^3/\text{s}$ , top width is 35 m and area is 64  $\text{m}^2$ .

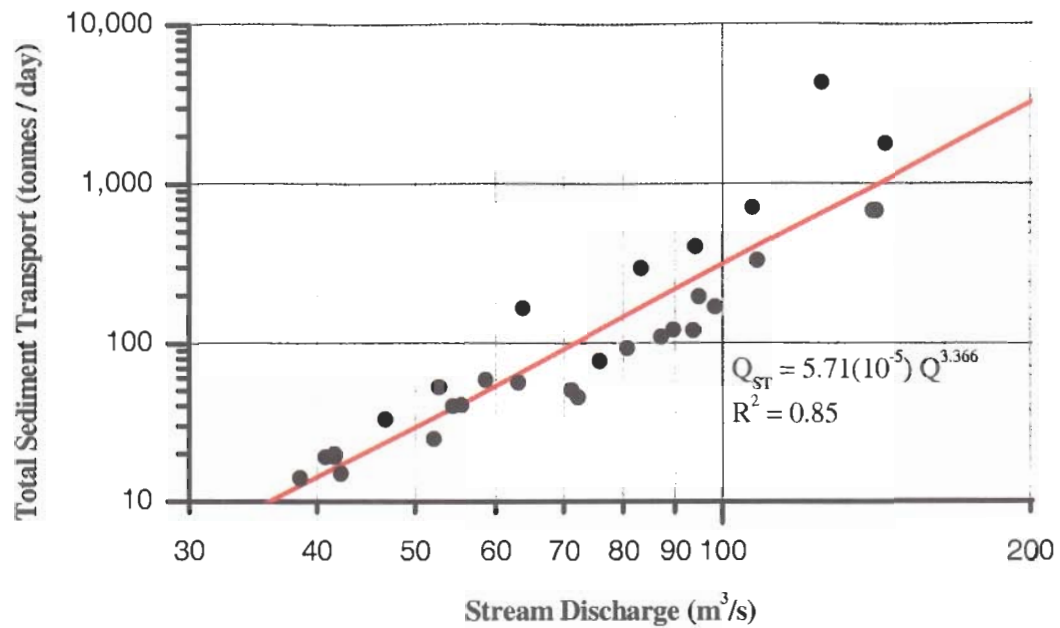


Figure 4.10. Total sediment transport ( $Q_{ST}$ ), Salmon River below Yankee Fork based on 1999 and 2000 measurements.

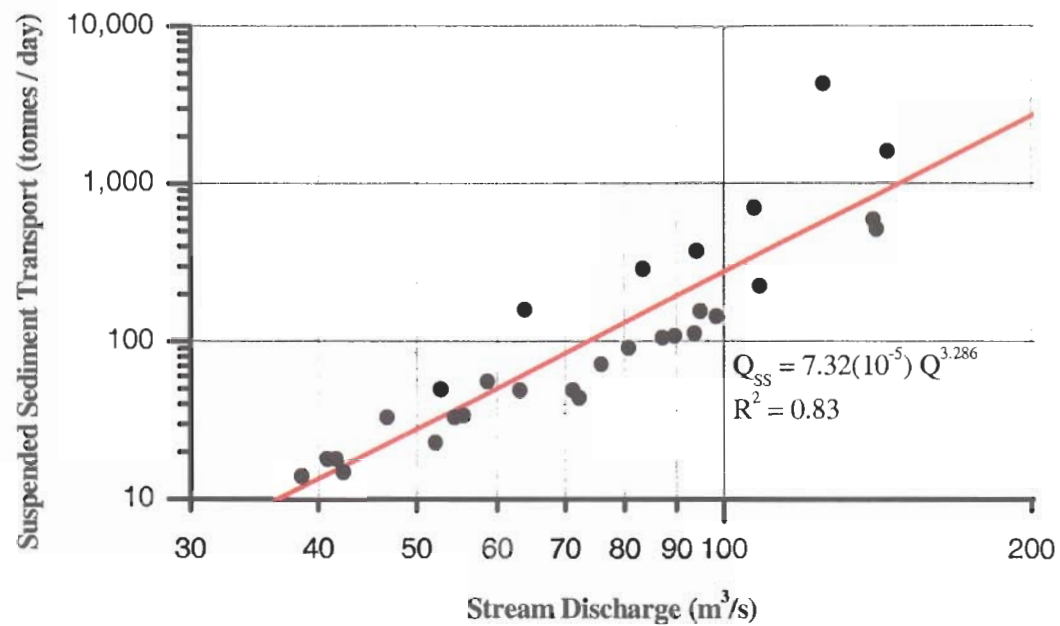


Figure 4.11. Suspended sediment transport ( $Q_{SS}$ ), Salmon River below Yankee Fork based on 1999 and 2000 measurements.

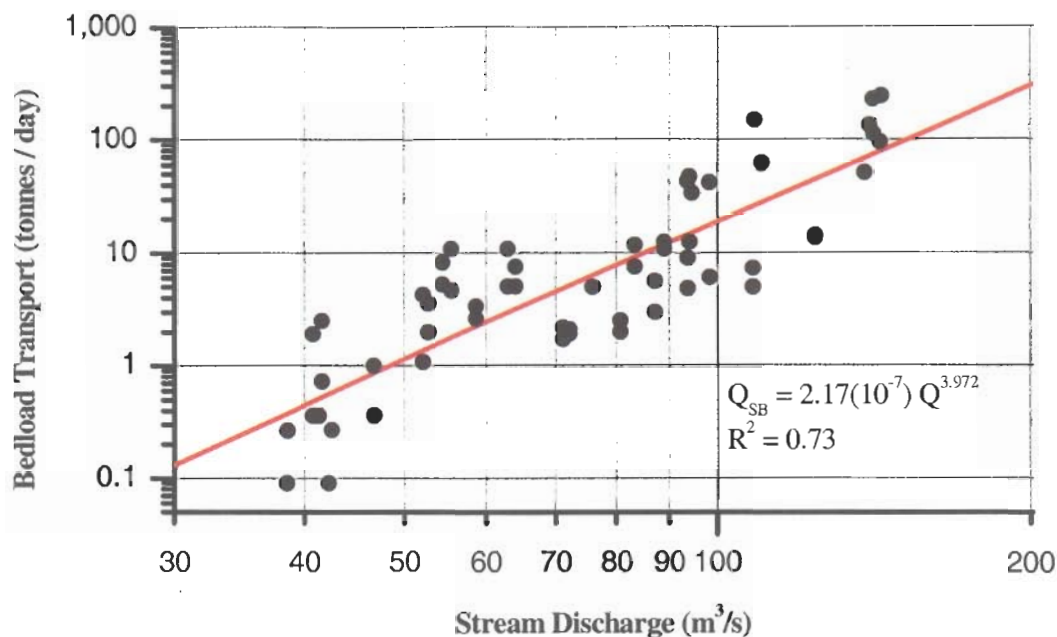


Figure 4.12. Bedload transport ( $Q_{SB}$ ), Salmon River below Yankee Fork based on 1999 and 2000 measurements.

Results of these sediment discharge measurements are presented in Figures 4.10, 4.11, and 4.12. A power-function of a type commonly used to describe the relationship between bedload transport and stream discharge (see equation 4.3) is fitted to data plotted in a log-log domain with the resulting equation and coefficient of determination ( $R^2$ ) presented in the figures. The computed transport rates for the Salmon River below Yankee Fork are applied to the Challis flow record for the purpose of approximating sediment transport into the Twelve Mile Reach .

It is assumed that sediment discharge below the Yankee Fork is a reasonable approximation of transport into the upper Twelve Mile Reach. The Salmon River flows through a constraining canyon environment from upstream of the Yankee Fork confluence to the upper Twelve Mile Reach. A state of equilibrium sediment transport between the Yankee Fork and the Twelve Mile Reach is assumed, an assumption that is supported by little evidence of changes to channel shape and alignment throughout the canyon. The vast

majority of the canyon reach is strongly entrenched and confined with little opportunity for out-of-channel sediment deposition and storage.

However, actual transport into the Twelve Mile Reach could be quite different due to different slopes and bed material composition, including armor. The location of sediment measurement is 74 km upstream of the Twelve Mile Reach's Highway 93 Bridge, and contributions to sediment supply from tributaries such as the East Fork Salmon River are not accounted for. Also, due to availability of an active floodplain and the braided nature of portions of the Twelve Mile Reach, it is likely that the rate of transport out of the reach is not equivalent to transport into the reach.

#### 4.5.2 Transport Capacity

Two sediment transport equations considered applicable to large gravel-bed rivers are presented for the purpose of estimating transport capacity and comparing to measured transport rates presented above. They are applied to the representative cross-section 10 in the Twelve Mile Reach for two particle sizes (10 and 45 mm), two discharge / width / depth conditions (100 and 250 m<sup>3</sup>/s, 66 and 76 m width, 1.02 and 1.63 m hydraulic depth, respectively), and a slope of 0.0032. The selected particle sizes are representative of those found in recent deposits at active portions of the reach. In addition, between 25 and 70 percent of measured bedload at higher discharges is in the 32 to 64 mm size class, and often 50 percent is greater than 10 mm. A bedload form of Bagnold (1966) is presented in equation (4.3). Results are presented in Table 4.4.

Bagnold (1966) bedload transport equation:

$$q_b = \frac{\lambda_s}{\lambda_s - \lambda} \cdot 0.1 \cdot \left( \frac{\omega - \omega_c}{0.5} \right)^{3/2} \cdot \left( \frac{D}{0.1} \right)^{-2/3} \cdot \left( \frac{d}{0.0011} \right)^{-1/2} \quad (4.3)$$

where

$$\omega = \rho \cdot g \cdot q \cdot S \quad (4.4)$$

$$\omega_c = 5.75 \cdot \left( \left( \frac{\rho_s}{\rho} - 1 \right) \cdot \rho \cdot 0.04 \right)^{3/2} \cdot \left( \frac{g}{\rho} \right)^{1/2} \cdot d^{3/2} \cdot \log \left( \frac{12D}{d} \right) \quad (4.5)$$

Table 4.4. Bedload transport capacity at cross-section 10 based on Bagnold (1966) equation for two discharges, two representative bedload particle sizes, and slope = 0.0032.

Q (m <sup>3</sup> /s)	Width (m)	Depth (m)	d (mm)	$\omega$ (kg/s <sup>3</sup> )	$\omega_c$ (kg/s <sup>3</sup> )	$q_b$ (m <sup>3</sup> /s/m)	$Q_{SB}$ (m <sup>3</sup> /s)	$Q_{SB}$ (tonnes/day)
100	66	1.02	10	48	0.94	0.0039	0.25	58,000
250	76	1.63	10	103	1.00	0.0091	0.70	160,000
100	66	1.02	45	48	7.10	0.0015	0.097	22,000
250	76	1.63	45	103	7.69	0.0039	0.30	68,000

The second bedload transport equation is Bathurst's (1987) modification of the Schoklitsch equation presented in equation (4.6). Table 4.5 presents results for the same discharge and particle size conditions as Table 4.4. The computed transport capacity is much less than determined by Bagnold's equation, and for low discharge with large particle size, zero transport is computed due to the threshold condition ( $q_c$ ).

Bathurst (1987) modified Schoklitsch bedload transport equation:

$$q_b = \frac{2.5}{\frac{\rho_s}{\rho}} \cdot S^{3/2} \cdot (q - q_c) \quad (4.6)$$

where

$$q_c = \frac{0.15}{S^{1.12}} \cdot \sqrt{g} \cdot (d_{50})^{3/2} \quad (4.7)$$

Table 4.5. Bedload transport capacity at cross-section 10 based on Bathurst (1987) modified Schoklitsch equation for two discharges, two representative bedload particle sizes and slope = 0.0032.

Q (m <sup>3</sup> /s)	Width (m)	d (mm)	$q_c$ (m <sup>2</sup> /s)	$q_b$ (m <sup>3</sup> /s/m)	$Q_{SB}$ (m <sup>3</sup> /s)	$Q_{SB}$ (tonnes/day)
100	66	10	0.29	2.1E-4	0.014	3200
250	76	10	0.29	5.1E-4	0.039	8900
100	66	45	2.8	0	0	0
250	76	45	2.8	8.5E-5	0.0065	1500

Except for the Bathurst results for 45 mm particles in low flow, both sets of equations indicate that the measured bedload transport from 1999 and 2000 (Figure 4.12) was less than capacity. This is not surprising as measurements were made during years of below normal discharge and at less than bankfull flow.

#### 4.6 Effective Discharge

A self-formed alluvial channel develops a channel size that reflects the quantity of water and the size and characteristics of sediment delivered to it from the drainage basin (Emmett and Wolman, 2001). This concept of an effective discharge that forms the channel size was initially developed for and applied to sand-bed streams where sediment is transported at nearly all discharges. Effective discharge is defined as the discharge that, over a long period of time, transports the greatest quantity of sediment. Application of the method was primarily based on measurements of suspended sediment load. Due to greater measuring difficulties, bedload transport was frequently neglected.

In sand-bed systems, the sand-sized materials transported in suspension are usually the same materials comprising the bed and banks so that transportable material is readily available. Therefore, the rate of sediment transport is frequently at or near capacity. In contrast, the effective discharge for gravel-bed streams is defined as the water discharge that over a long period of time transports the most *bedload* (Andrews, 1980; Emmett and Wolman, 2001). In these systems, bed and banks are typically comprised of sand, gravel and cobble material generally similar in size to that material transported as bedload. Channel size is determined by the higher discharges that can mobilize the larger particles and actually cause a change in channel dimensions.

Gravel-bed streams frequently form a layer of larger material that covers the bed and hides smaller underlying sand-sized particles, preventing their transport. The bed and banks are comprised of larger materials that are relatively immobile at lower discharges. The river may have capacity for transporting some sediment. However, much of the transportable material is hidden beneath the armor layer and not available, resulting in *supply limited* transport conditions. Moderate discharges may transport some material, but since most of the armor layer is often not mobilized at these flows, the underlying material remains unavailable for transport and therefore the actual rate of sediment transport is often below that computed from applicable equations. Only when flows are great enough to break up the armor layer and expose the underlying material can the rate of sediment transport approach theoretical capacity.

Due to this armoring, gravel-bed rivers often exhibit a threshold flow condition that must be met in order to initiate general bedload movement. Shear stress applied to the bed must exceed a critical value. This threshold condition can be observed in Figure 4.12 where bedload transport appears to initiate near 40 m<sup>3</sup>/s. In the Twelve Mile Reach, hydraulic depth is used to approximate hydraulic radius at bankfull conditions in order to compute applied shear stress using equation (4.8).

$$\tau = \rho \cdot g \cdot R \cdot S \quad (4.8)$$

The critical particle diameter is based on equation (4.9). Table 4.6 provides shear stress and critical particle sizes for bankfull conditions at selected cross-sections based on two values of critical dimensionless shear stress ( $\theta_c$ ). Bankfull discharge appears capable of mobilizing particles in the 60 to 100 mm range.

$$d_c = \frac{\tau}{\theta_c \cdot g \cdot (\rho_s - \rho)} \quad (4.9)$$

Table 4.6. Shear stress and critical particle size at bankfull flow ( $Q=231$  m<sup>3</sup>/s) for two critical dimensionless shear stresses, slope = 0.0032.

Cross-Section	Hydraulic Depth ( $D_h$ , m)	Shear Stress (Pa) $\tau \approx \rho g D_h S$	Critical Particle Size ( $d_c$ , mm)	
			$\theta = 0.030$	$\theta = 0.045$
10	1.58	49.6	102	68
13	1.70	53.3	110	73
15	1.39	43.7	90	60
18	1.72	54.0	111	74
21	1.15	36.2	75	50
23	1.48	46.5	96	64
25	1.07	33.7	69	46
28	1.84	57.7	119	79
32	1.85	58.1	120	80
37	1.21	37.9	78	52
43	1.52	47.8	98	66
50	1.63	51.2	106	70
54	1.65	51.9	107	71
57	1.05	33.1	68	45
Average:	1.49	46.8	96	64

Although the size of material comprising the bed through the Twelve Mile Reach has not been comprehensively characterized, some information is available. Pebble counts have been made on several bars indicating a median grain size in the range of 100-150 mm (Greenwald, 2002). Visual observations of the bed indicate a range of characteristic particle sizes through the reach. The bed in most segments appears to be comprised of large cobbles with many particles sized from 200 to 300 mm. Medium sized gravels and small cobbles (about 50 to 100 mm) are locally found through the One Mile Island segment (cross-sections 15-21) and at several other localized areas where channel braiding is pronounced.

#### 4.6.1 Effective Discharge as the Product of Flow Frequency and Instantaneous Transport Rate

In Figure 4.13, dimensionless values of flow frequency, instantaneous bedload transport, and total bedload transport are plotted as a function of stream discharge. Instantaneous bedload transport rate,  $Q_{BL}$ , increases to nearly the fourth power of stream discharge based on equation (4.10) and Figure 4.12:

$$Q_{BL} = \alpha Q^{\beta} \quad (4.10)$$

where  $Q$  is stream discharge ( $m^3/s$ ), the coefficients  $\alpha = 2.17 \times 10^{-7}$  and  $\beta = 3.97$  are based on bedload transport measurements made at an upstream location as described in section 4.5.1, and  $Q_{BL}$  is in tonnes per day. Generation of Figure 4.13 required extrapolation where (4.10) was applied to a range of discharges beyond that observed during measurements. Frequency occurrence of discharge is plotted as a function of discharge based on 44 years of mean daily discharge records from the USGS gaging station near Challis. The product of the two curves yields an approximation of total bedload transport for the 44 years of stream flow record (equation 4.11). A third order polynomial curve is fitted to the total bedload transport data (equation 4.12). Effective discharge is identified by the peak of the total bedload transport curve determined by differentiating equation 4.12 and occurs at a discharge of  $224 m^3/s$ . Based on Table 4.2, this discharge has a recurrence interval of 2.4 years.

$$Q_{BT} = \alpha Q^{\beta} \cdot \text{occurrence frequency}(Q) \quad (4.11)$$

$$Q_{BT} = -1.65 \times 10^{-7} Q^3 + 6.16 \times 10^{-5} Q^2 - 2.76 \times 10^{-3} Q \quad (4.12)$$

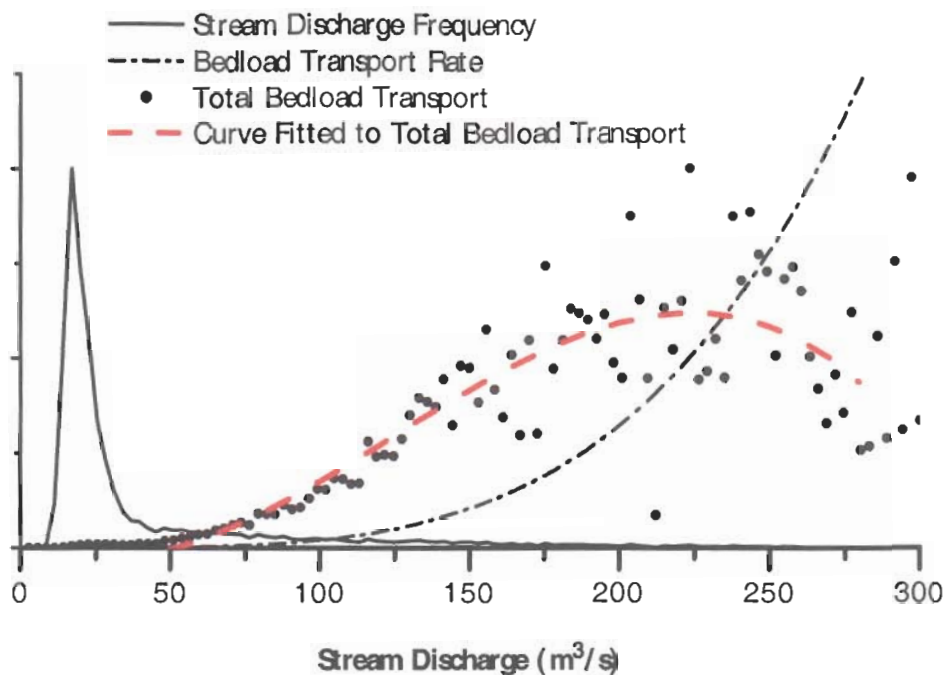


Figure 4.13. Instantaneous bedload transport rate, flow frequency, total bedload transport, and a curve fitted to the total bedload transport data points for the Salmon River at Challis.

#### 4.6.2 Effective Discharge as the Maximum Slope of the Cumulative Sediment Discharge Curve

A recent **modification** to the method of determining effective discharge is presented by Emmett and Wolman (2001). Effective discharge is determined by the maximum slope value from the cumulative bedload curve. This is the same principle as differentiation of the total bedload curve. However, it does not require fitting a curve to the total bedload transport data points and therefore **may be an improvement** when curve fitting is difficult.

The daily mean streamflows for the Challis gage were arranged in ascending order and the bedload discharge for each value of daily mean streamflow was computed using the bedload rating presented in equation (4.10). Figure 4.14 presents the cumulative percentage of bedload discharge as a function of stream discharge.

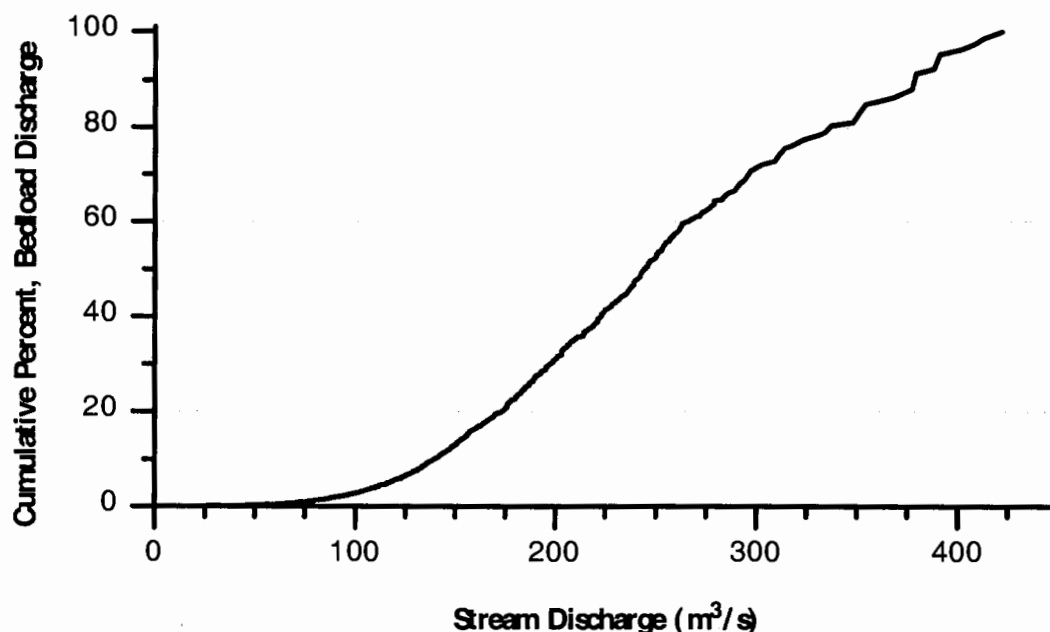


Figure 4.14. Cumulative percentage of bedload discharge as a function of stream discharge.

For each value of mean daily discharge, the slope of the cumulative bedload curve was determined as the slope of the straight-line segment extending over  $1/18^{\text{th}}$  of the range in streamflow. The slope of the cumulative bedload curve is graphed as a function of stream discharge. Effective discharge is the stream discharge at the peak value of the slope of the cumulative bedload curve. *Even with this graphing procedure, determination of effective discharge (water discharge at the peak value of the slope of the cumulative bedload curve) requires some judgment to determine the centroid of the peak value* (Emmett and Wolman, 2001). In this case the centroid of the peak value is approximately  $250 \text{ m}^3/\text{s}$  (3.2-yr return interval).

#### 4.6.3 Analysis

Based on the above approaches, effective discharge is in the  $225\text{-}250 \text{ m}^3/\text{s}$  range. In comparison, bankfull discharge is  $231 \text{ m}^3/\text{s}$ . The classic approach suggested by Leopold, Wolman and Miller (1964) implies that when a river is in equilibrium, the effective discharge will approximate bankfull stage. It follows that a river not in equilibrium will have an effective discharge greater or less than bankfull for an aggrading or incising (respectively)

system. Since bankfull and effective discharges are roughly equivalent, it appears that this reach is at or near equilibrium.

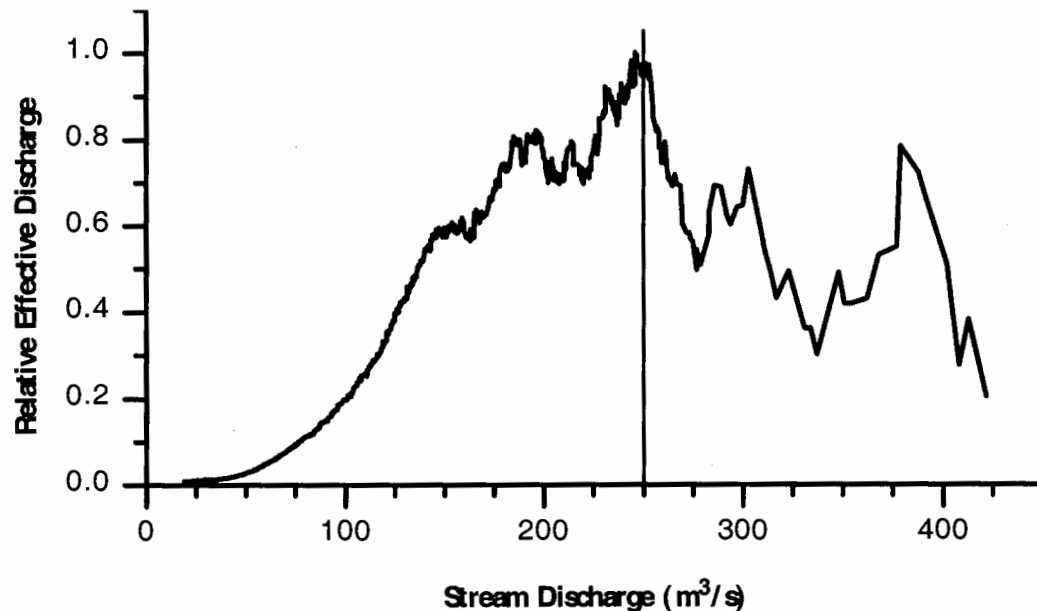


Figure 4.15. Slope of the cumulative sediment discharge curve as a function of stream discharge showing the relative magnitude of effective discharge.

The bankfull discharge of  $231 \text{ m}^3/\text{s}$  has a recurrence interval of 2.6 years, a value that is high compared with other rivers in the western United States. This may be due to incorrect identification of bankfull, or to differences in incipient motion conditions for the Salmon River compared to other rivers. Perhaps the riverbed is more heavily armored and/or the armor material is larger in size, which requires greater discharges in order to mobilize bed material. Typical bankfull recurrence intervals for four similar Idaho rivers ranges from 1.5 to 1.7 years with an average of 1.6 years (Emmett and Wolman, 2001).

In this system, effective discharge appears to be capable of mobilizing 100 mm particles (refer to Table 4.6), a size that is near the  $d_{50}$  of the armor layer. General breakup of the armor layer typically requires a discharge capable of mobilizing at least the  $d_{84}$  size. There is uncertainty that a discharge incapable of mobilizing the armor layer can cause enough of an adjustment to be considered the key indicator of channel geometry.

Recent work (Emmett and Wolman, 2001) on similar Idaho gravel-bed rivers indicates a tendency for effective discharge ( $Q_e$ ) to exceed bankfull flow ( $Q_b$ ). Five observed rivers were found to have a  $Q_e/Q_b$  ratio ranging from 1.0 to 1.3 with higher ratios corresponding with larger-sized bed materials and higher exponents of the bedload rating curve as described in equations (4.13) and (4.14):

$$\beta = 1.5612 + 2.11 \times 10^{-02} \text{ Bed Surface } d_{50} \quad (4.13)$$

$$Q_e / Q_b = 0.723 + 1.11 \times 10^{-01} \beta \quad (4.14)$$

Using the bedload rating curve exponent of 3.97 per Figure 4.12 and equation (4.13) results in a median size for the bed surface of 114 mm, a value in close agreement with the measured range of 100 to 150 mm (Greenwald, 2002). Also using the same exponent and equation (4.14), the expected  $Q_e/Q_b$  ratio is 1.16.

For this gravel-bed reach, effective discharge somewhat exceeds bankfull discharge. The  $Q_e/Q_b$  ratio of 1.08 ( $250 \text{ m}^3/\text{s} + 231 \text{ m}^3/\text{s}$ ) agrees with recent data suggesting that effective discharge exceeds bankfull for gravel-bed streams (Emmett and Wolman, 2001). However, the Twelve Mile Reach bankfull discharge recurrence interval of 2.6-years is higher than expected for streams in the western United States. It is possible that bankfull was over-estimated so that the recurrence interval is less than 2.6-years and the actual  $Q_e/Q_b$  ratio exceeds 1.08. It is also possible that due to larger particle sizes and higher incipient motion conditions, this reach has an abnormally high bankfull recurrence interval. Furthermore, the determination of effective discharge is based upon sediment transport equations developed for an upstream site and extrapolated to flows beyond the range of measured data, and therefore may not be representative of transport into the Twelve Mile Reach.

When considering stream restoration or other river engineering projects, hydraulic geometry for channel design should be based on effective discharge with application of a reasonable  $Q_e/Q_b$  ratio. A project designed to increase the frequency of floodplain inundation will have a bankfull discharge somewhat less than effective discharge.

## 5 Chinook Salmon

---

The Twelve Mile Reach offers a variety of aquatic habitat features that are important and beneficial to anadromous fisheries. Tributary sloughs maintain very high juvenile fish densities, and Chinook salmon spawning activity was recently observed throughout the reach. This section is included to document recent findings and provide support for this investigation.

### 5.1 Spawning

Idaho Department of Fish and Game (IDFG) staff provided Chinook redd count and parr monitoring data (Brimmer and Curet, 2002). Data includes Chinook redd counts in the upper Salmon River basin from 1989 to 2001, and parr monitoring in the Twelve Mile Reach from 1999 to 2001. Redds are counted by visual identification from helicopter during the period from late August into early September. Redd counts have been very low in the vicinity of the Twelve Mile Reach. Some have questioned if the reach was historically used for nesting. Local residents claim salmon did spawn here, but that there has been very little activity since 1987.

Table 5.1. Idaho Department of Fish and Game aerial count of Chinook redds, 1989 – 2001.

Year	Transect		
	NS-21	NS-22	NS-23
1989	5	3	0
1990	5	1	0
1991	3	0	0
1992	1	0	0
1993	0	0	0
1994	0	0	0
1995	2	N/C	N/C
1996	1	N/C	N/C
1997	1	N/C	N/C
1998	0	N/C	N/C
1999	0	1	1
2000	0	0	0
2001	1	0	0

The Chinook salmon return of 2001 in the upper Salmon River basin was very high. During the period when IDFG was counting redds, spawning was actively occurring at Indian Riffles and other upstream locations. However, no redds were spotted in the Twelve Mile Reach. Table 5.1 lists redd count results for the main stem Salmon River from the East Fork Salmon River to the Pahsimeroi River (“N/C” indicates that no count was conducted). Transect NS-21 is upstream of the Twelve Mile Reach; Transect NS-22 is wholly within the Twelve Mile Reach; and Transect NS-23 includes the lower 4 km of the Twelve Mile Reach and below down to the Pahsimeroi River confluence.

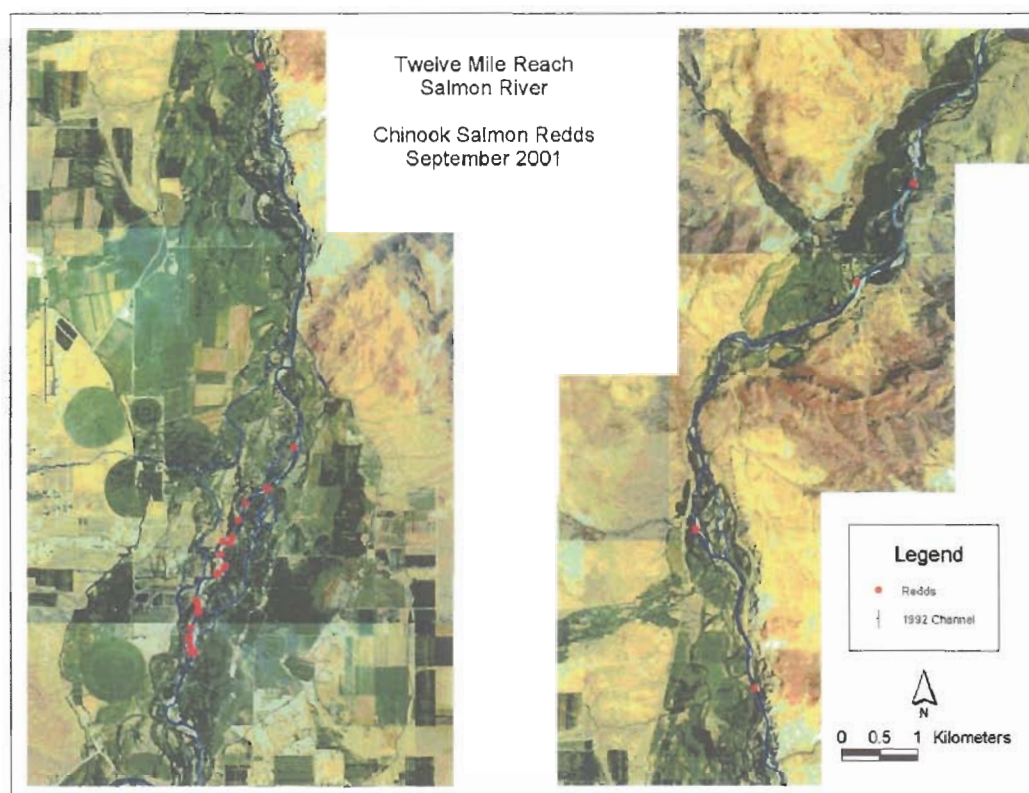


Figure 5.1. Chinook redd locations in the Twelve Mile Reach, September 2001.

During September 15 and 16, 2001, Tom Coates, a local river guide, and I floated the Twelve Mile Reach to survey staff gages and low-flow water surface elevations at numerous cross-sections. A total of 16 redds were counted between the head of One Mile Island and Challis Hot Springs. All had Chinook salmon on or nearby the beds and several appeared to

tributaries like the East Fork Salmon River, or in the main stem above the East Fork Salmon River confluence.

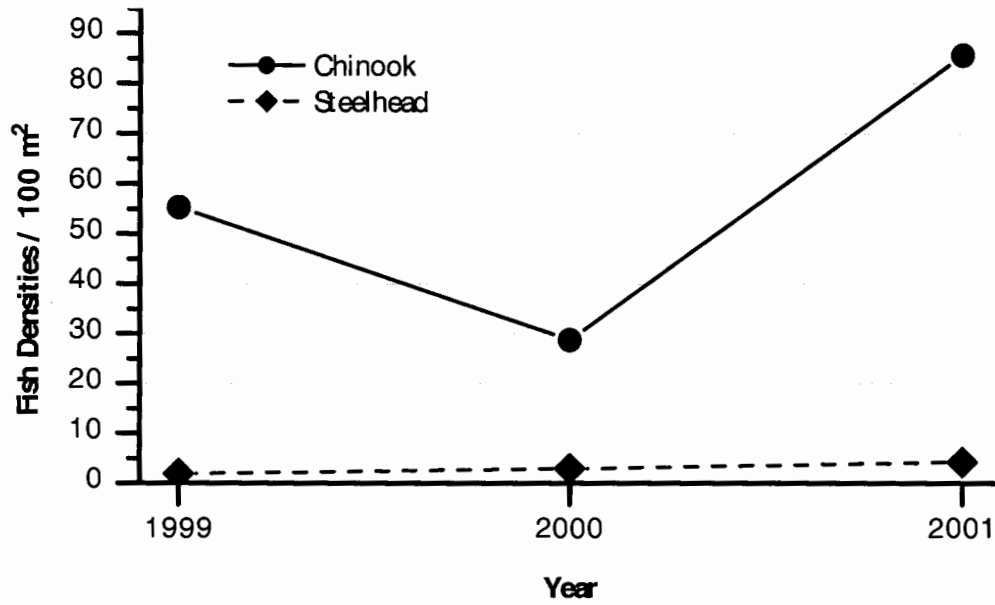


Figure 5.2. Chinook salmon and steelhead / rainbow trout densities in Hannah Slough.

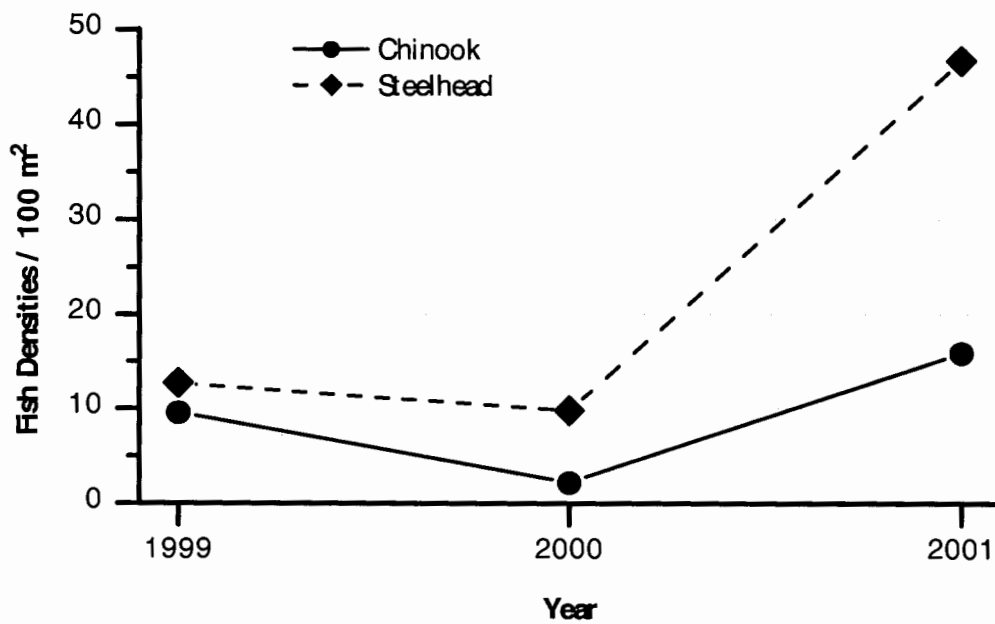


Figure 5.3. Chinook salmon and steelhead / rainbow trout densities in Philps Slough.



Figure 5.4. Features like Philps Slough on left and a spring near Challis Hot Springs on right provide important rearing habitat.

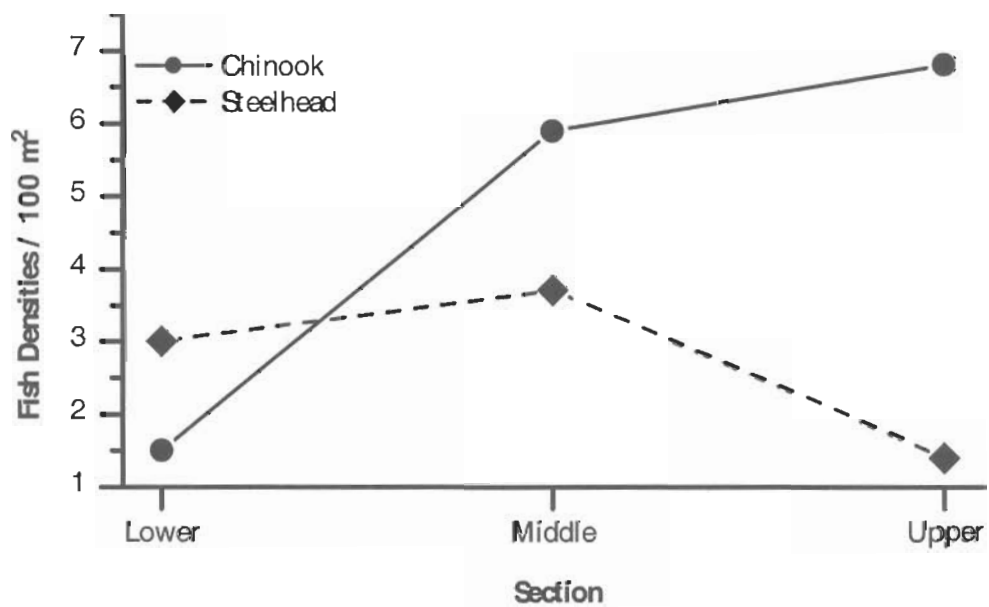


Figure 5.5. Chinook salmon and steelhead / rainbow trout densities in Challis Hot Springs Creek.

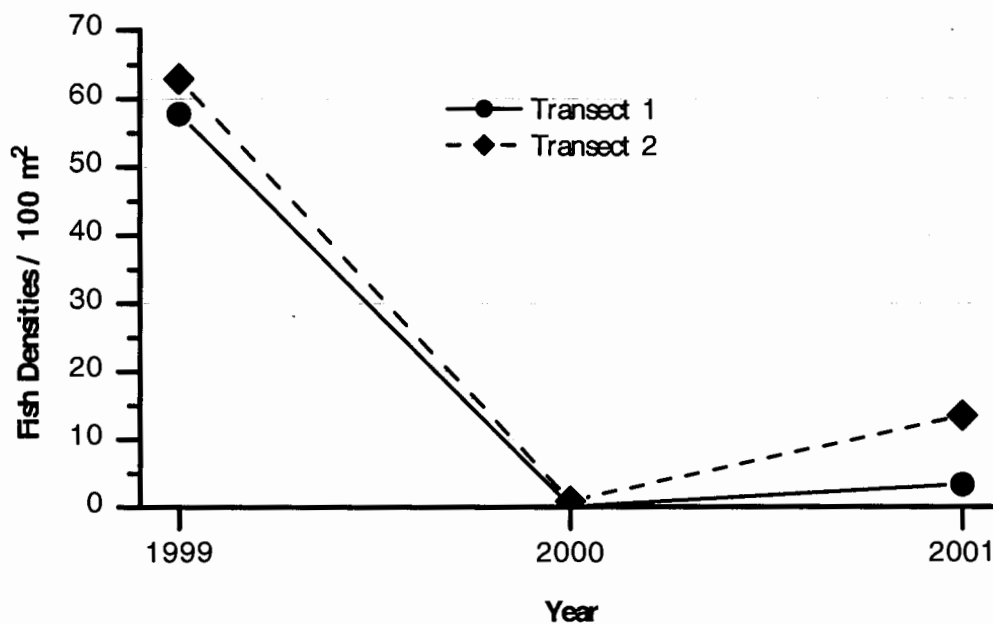


Figure 5.6. Chinook salmon densities in Capehorn Creek (no steelhead).

Although juvenile fish density in these systems is some of the highest in the upper Salmon River basin, there is potential for improvement. Tributary groundwater flows may be threatened by the conversion of irrigation systems from flood to sprinkler. Small dam structures pose migration problems in some tributaries. Farming and ranching practices have removed much of the riparian cover along these streams, and several oxbow channels have been blocked from the main channel. Also, irrigation return flows are introducing heavy silt loads that are changing the bed composition.

## 6 River Model

---

### 6.1 Description

A hydrodynamic model of the entire Twelve Mile Reach was set up using the MIKE11 software. MIKE11 is a modeling system for rivers and channels developed by the Danish Hydraulic Institute, and is further described in Appendix C.

Cross-sectional data were obtained from December 1999 and April 2000 surveys of the site. Flood plain topography at the 2-foot contour interval is based on aerial photogrammetry from May 2000. Roughness values are primarily based on the HEC2 model used for developing flood inundation maps presented in the FEMA flood study (FEMA, 1988; Kunz, 1999). The upstream boundary of the model, located 2.6 km upstream of the Highway 93 Bridge, consists of a flow boundary. The downstream boundary, located 1.2 km below the Bruno Bridge, is defined as a rating curve. The flow data for the upstream boundary are obtained from the USGS gaging station described in section 4.1. The downstream rating curve was established by calculating the conveyance of the measured cross-section at this location and assuming a bed slope in this location of 0.003, which is a typical channel slope value in the vicinity of this cross-section.

### 6.2 Calibration

After setting up the Twelve Mile Reach model in MIKE11, it was necessary to calibrate it to ensure that the calculated water levels and discharges were accurate. Calibration consists of comparing the output from the model to measurements of water level and discharge on the site and adjusting certain parameters in the model until the measured and calculated values coincide. The most significant parameter to be adjusted in the model is the Manning roughness coefficient. Due to a lack of historical discharge and water level measurements throughout the Twelve Mile Reach, it was quite difficult to calibrate the model for high discharges. The 1999 and 2000 survey of cross-sections provided calibration data for low flows.

Channel roughness is the primary calibration parameter for simulation of open-channel flow. Table 6.1 presents the Manning's roughness values used for model simulations and are applied from the indicated cross-section to the next identified section. For example, the Manning's  $n$  value of 0.037 is used for sections 1 through 8, and a value of 0.045 is used for sections 9 through 15 (refer to Figure 3.5 for cross-section locations).

Table 6.1. Roughness values used for simulated conditions.

Cross-Section ID	Chainage (m)	Manning's $n$
1	0	0.037
9	3522	0.045
16	6334	0.047
17	6883	0.050
18	7370	0.055
19	8132	0.045
22	9217	0.050
23	9827	0.045
68	27443	0.045

These roughness values are primarily based on the earlier HEC2 model developed for the detailed flood study conducted for the upper reach from the Highway 93 Bridge just above the Challis Creek confluence (FEMA, 1988; Kunz, 1999). A standard value of 0.045 was applied for the remainder of the reach below Challis Creek. Simulation results were in close agreement with measurements of water surface elevation during 1999 and 2000 surveys. Roughness values were not altered with stage, as data are insufficient to support such a relationship.

It is recognized that model verification at discharges substantially below bankfull does not necessarily reflect the model's ability to accurately determine bankfull discharge. All available water surface elevation measurements were used for model verification, but these measurements were made below bankfull stage. Verification data for higher discharges are not currently available and may be collected in the future as higher discharges occur.

### 6.3 Model

Figure 6.1 presents a description of the model network. The majority of the reach is simulated as a single channel with floodplain flows included in channel conveyance. In the One Mile Island and Hannah Slough areas, adding multiple flow channels to more accurately simulate actual conditions increases model complexity. Flow enters the East Branch from the Main Stem throughout the year and conveys approximately 1/4 total flow at bankfull discharge. The MIKE11 Weir function is used at the head of One Mile Island to balance flow entering the East Branch. Two link channels connecting the East Branch with the Main Stem allow flow to balance between the two channels at high discharge. The link channels are an approximation of the true physical behavior of this system; during very high flows, the East Branch captures more flow than it can carry and overland flow is conveyed back to the Main Stem in the area where the link channels are placed.

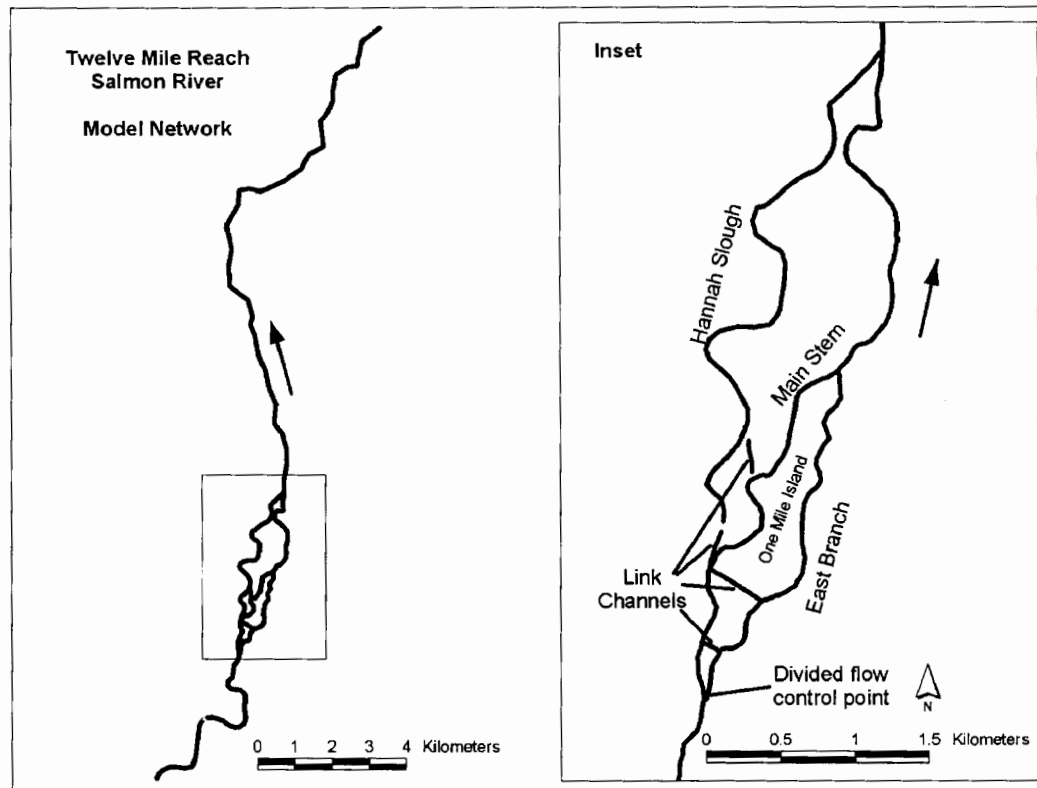


Figure 6.1. Model Network.

Hannah Slough only receives flow directly from the main stem during periods of high over-bank discharge. During periods of low flow, Hannah Slough receives water from Garden Creek, tributary groundwater flow, and irrigation return flow. Two link channels were established to simulate over-bank flow from the Main Stem into Hannah Slough.

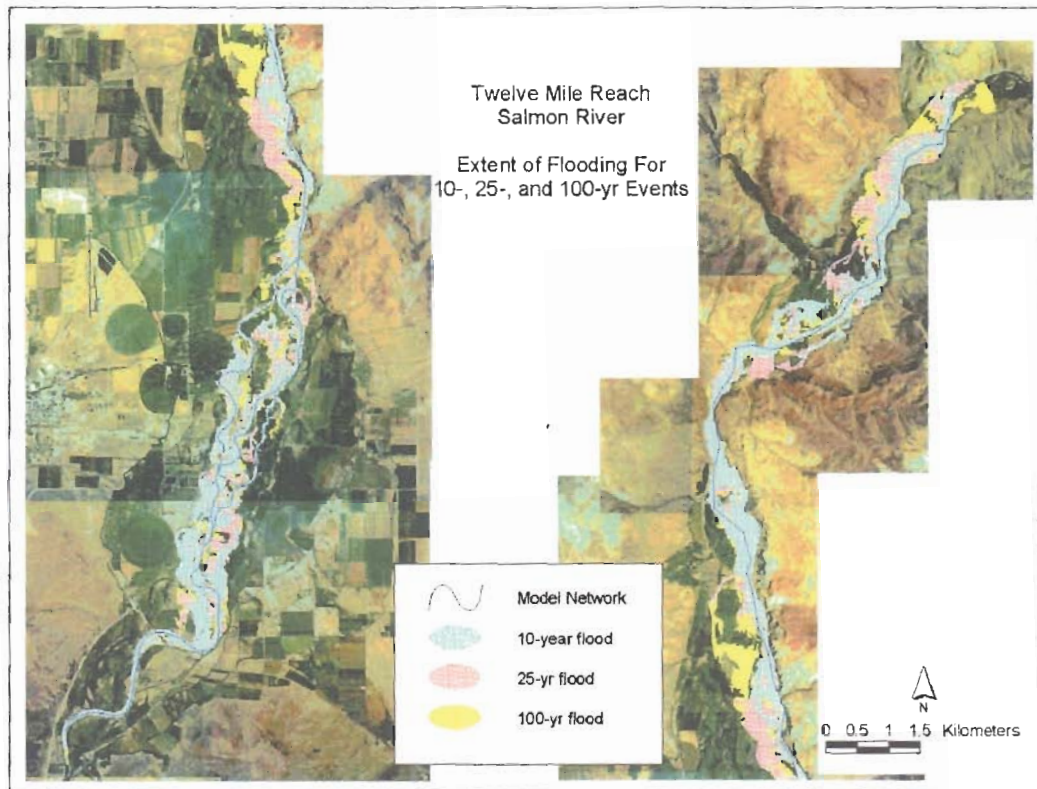


Figure 6.2. Extent of flooding for 10-, 25-, and 100-year flood flows.

#### 6.4 Results

Results from the Twelve Mile Reach model are presented in other sections of this paper. Width-to-depth ratio and width for selected cross-sections at two simulated discharges is presented in sections 3.5 and section 3.6, respectively. In section 4.4, simulated discharges for the high water marks, top of bank, and top of bar are presented.

Figure 6.1 presents the extent of flooding for 10-, 25-, and 100-year peak discharges based on model output where depth of inundation is 10 cm and greater. In this figure, all

areas inundated by the 10-year event will also be inundated by the 25- and 100-year events. Likewise, areas inundated by the 25-year event will be inundated by the 100-year event.

## 7 Conclusions and Recommendations

---

### 7.1 Conclusions

The Twelve Mile Reach of the Salmon River holds important and productive habitat for salmon and steelhead. The tributary sloughs and side channels have been found to have some of the highest juvenile fish densities in the upper Salmon River basin. Chinook salmon utilize the main stem for spawning, particularly in the One Mile Island sub-reach. However, these features are at risk due to encroachment from development, channelization, and the tendency of property owners to retard the river's development of new meanders, sloughs, and side channels.

The purpose of this study has been to provide background information on the physical process in the Twelve Mile Reach to aid future management actions.

Geomorphic analysis and review of historic photographs and cadastral survey notes indicates that the tendency of this system to braid is probably normal, but may be exacerbated by increased sediment loading from upstream land management practices and decreased bank stability due to grazing and removal of riparian vegetation. Some local sub-reaches have shown significant change, whereas others have been quite stable. Bed slope has also increased slightly through the reduction in stream length of 3.7 percent since the late 1800s. The nature of meanders in the reach has changed with an average 28 percent reduction in wavelength, 31 percent reduction in amplitude, and 32 percent reduction in radius of curvature. On a reach-wide level, sinuosity has decreased from 1.18 to 1.12.

Effective discharge slightly exceeds bankfull discharge, indicating that the channel is neither significantly incised nor aggraded and is likely near equilibrium. However, the return interval for bankfull discharge of 2.6 years is higher than expected with typical bankfull recurrence intervals for similar Idaho rivers between 1.5 and 1.7 years (Emmett and Wolman, 2001). This higher than normal return interval may be indicative of the large gravels and cobbles with higher incipient motion conditions found in and above the Twelve Mile Reach. In addition, effective discharge is based on a regression equation developed for bedload

transport measured below the Yankee Fork, an upstream location where conditions are not well characterized, and where bedload transport may not be representative of transport into and through the Twelve Mile Reach. Lower bedload transport rates will result in computation of lower effective discharge values, increasing the likelihood of an incised channel through the Twelve Mile Reach. The current channel capacity of 231 m<sup>3</sup>/s appears adequate and can be used as a design parameter for restoration plans.

## **7.2 Recommendations for Further Research**

### **7.2.1 Local Bedload Measurement**

The determination of effective discharge in this study is based on bedload measurements taken upstream near Yankee Fork. Tributary contributions of bedload from Yankee Fork to the Twelve Mile Reach are not accounted for. Local measurement of bedload discharge will allow a more thorough analysis of effective discharge, and it would be beneficial to have a better understanding about bedload movement into and out of the study area.

### **7.2.2 Model Calibration**

Development of the MIKE11 model used for simulating flows through the Twelve Mile Reach has required much effort and considerable expense. Throughout the time of this study, stream flows in the Salmon River have been only moderate and have not reached bankfull stage. When higher discharges occur in the future, stage and discharge measurements should be taken and used to calibrate the hydrodynamic model.

### **7.2.3 River Water Temperature Conditions**

Current water temperatures on the Salmon River are extreme for salmonids. Winter water temperatures may be sub-freezing. Summer water temperatures may exceed 21°C (70°F) frequently during the afternoon with daily fluctuations of 8°C (15°F) on a diurnal cycle. These water temperature extremes stress trout and salmon, certainly reducing growth potential and possibly causing direct mortality and/or thermal barriers.

A number of questions regarding water temperature have been posed and may warrant further research:

1. Are the high temperature problems due to conditions in the Twelve Mile Reach or is the primary problem associated with conditions further upstream?
2. The Idaho Department of Fish and Game has documented the critical importance of habitat and thermal refugia in the side channels and sloughs across the floodplain. What is the actual extent of these floodplain channels and what opportunities exist for enhancing or extending these areas?
3. What is the effect of the side channels and sloughs on the main river?
4. Winter mortality is known to be high. Has induced geomorphic changes in the channel contributed to this mortality by reducing the areal extent of viable winter habitat, increasing the in-channel area that freezes from the surface to the bed and reducing the percent of coarse gravel that might provide shelter for small fish during the winter?

Since extreme temperature conditions have been identified as a limiting factor by several agencies, further research into this problem may warrant additional investigation.

## References

---

- Andrews, E. D. (1980). "Effective and bankfull discharges of streams in the Yampa River basin, Colorado and Wyoming." *Journal of Hydrology*, 46, 311-330.
- Bagnold, R. A. (1966). "An Approach to the Sediment Transport Problem from General Physics." U.S. Geological Survey Professional Paper 422-J.
- Barry, J. J. (2002). Personal communication.
- Bathurst, J. C., Graf, W. H., and Cao, H. H. (1987). "Bed load discharge equations for steep mountain rivers." *Sediment Transport in Gravel-bed Rivers*, C. R. Thorne, J. C. Bathurst, and R. D. Hey, eds., John Wiley & Sons Ltd., 453-491.
- Brimmer, A., and Curet, T. (2002). Personal communication.
- Bryant, M. D., and Frenette, B. J. (1994). "Sloughs, Side Channels, and Beaver Ponds: Links between Land and Water." *The Ecology and Management of Aquatic-Terrestrial Ecotones, Proceedings of the International Workshop on*, University of Washington, Seattle USA, 144.
- Dunne, T., and Leopold, L. B. (1978). *Water in Environmental Planning*, W. H. Freeman and Company, San Francisco.
- Emmett, W. W. (1975). "The Channels and Waters of the Upper Salmon River Area, Idaho." 870-A, U.S. Geological Survey.
- Emmett, W. W., and Wolman, M. G. (2001). "Effective Discharge and Gravel-Bed Rivers." *Earth Surface Processes and Landforms*, 26, 1369-1380.
- Federal Emergency Management Agency (1988). "Flood Insurance Study, Custer County, Idaho and Incorporated Areas."
- Greenwald, W. (2002). "Salmon River at Challis, Aquatic Ecosystem Restoration Project, Geomorphology Study." (unpublished)
- Knighton, D. (1998). *Fluvial Forms and Processes, A New Perspective*, Oxford University Press Inc.
- Kunz, P. (1999). Personal communication.

- Larkin, M., and Curet, T. (2001). Personal communication.
- Leopold, L. B., and Wolman, M. G. (1957). "River Channel Patterns: Braided, Meandering, and Straight."
- Leopold, L. B., Wolman, M. G., and Miller, J. P. (1964). *Fluvial Processes in Geomorphology*.
- Montgomery, D. R., and Buffington, J. M. (1997). "Channel-reach morphology in mountain drainage basins." *Geological Society of American Bulletin*, 109(5), 596-611.
- Rosgen, D. (1996). *Applied River Morphology*, Printed Media Companies, Minneapolis, Minnesota.
- U. S. Army Corps of Engineers (1994). "Channel Stability Assessment for Flood Control Projects." *EM 1110-2-1418*.
- U.S. Department of Agriculture. "Digital Soil Database." U.S. Department of Agriculture Natural Resources Conservation Service.
- USDA Forest Service, Rocky Mountain Forest and Range Experiment Station, Stream Systems Technology Center. (1995). "A Guide for Field Identification of Bankfull Stage in Western United States." Fort Collins, CO.
- Wohl, E. (2000). *Mountain Rivers*, American Geophysical Union, Washington DC.
- Wolman, M. G., and Leopold, L. B. (1957). "River Flood Plains: Some Observations On Their Formation." 282-C, U.S. Geological Survey.
- Wolman, M. G., and Miller, J. P. (1960). "Magnitude and Frequency of Forces in Geomorphic Processes." *Journal of Geology*, 68, 54-74.

### List of Symbols

---

$d$	Particle diameter
$d_c$	Critical value of $d$
$g$	Gravitational constant, $9.81 \text{ m/s}^2$
$q_b$	Unit bedload discharge, $\text{m}^3/\text{s}/\text{m}$
$w$	Channel width, $\text{m}$
$\lambda$	Specific weight of water, $\text{N}/\text{m}^3$
$\lambda_s$	Specific weight of sediment, $\text{N}/\text{m}^3$
$\rho$	Density of water, $\text{kg}/\text{m}^3$
$\rho_s$	Density of sediment, $\text{kg}/\text{m}^3$
$\theta$	Dimensionless shear stress
$\tau$	Shear stress, $\text{Pa}$
$\omega$	Unit stream power, $\text{kg}/\text{s}^3$
$\omega_c$	Critical unit stream power, $\text{kg}/\text{s}^3$
$D$	Depth, $\text{m}$
$D_h$	Hydraulic depth, $\text{m}$
$L$	Meander wavelength, $\text{m}$
$M_a$	Meander amplitude, $\text{m}$
$M_s$	Meander sinuosity
$Q$	Stream discharge, $\text{m}^3/\text{s}$
$Q_b$	Bankfull discharge, $\text{m}^3/\text{s}$
$Q_e$	Effective discharge, $\text{m}^3/\text{s}$
$Q_{ST}$	Total Sediment discharge, tonnes/day
$Q_{SS}$	Suspended Sediment discharge, tonnes/day
$Q_{BL}$	Bedload discharge, tonnes/day
$R$	Hydraulic radius, $\text{m}$
$R_c$	Radius of curvature, $\text{m}$
$S$	Slope, $\text{m}/\text{m}$

**Metric to English Units Conversion Chart**

---

---

To convert from	to	multiply by
m, meter	ft, foot	3.28
km, kilometer	mi, mile	0.6214
kg, kilogram	lb, pound	2.205
tonne (metric ton)	ton (long)	0.9842
m <sup>3</sup> , cubic meter	ft <sup>3</sup> , cubic foot	35.31
N, Newton	lbf, pound force	0.2248
Pa, Pascal	lb/ft <sup>2</sup> , pound per square foot	0.0209

---

## **Appendix A. Profiles and Photographs of Selected Cross-Sections**

---

In this Appendix, photographs and profiles for 14 selected cross-sections are presented. For most of these sections, field-identified water marks were located on one bank. The section diagrams indicate the measured water surface elevation and the approximate discharge at the time of measurement. Simulated discharge, based on MIKE11 model results, is presented for other features including the lower and upper water marks, top of bar, and top of banks. All section diagrams are at the same scale with 300 meters on the x-axis and 10 meters on the y-axis. Therefore, the y-axis is exaggerated. For the surveyed sections that were longer than 300 m, a full section profile is presented in Figures A.30 to A.39, located at the end of this Appendix. Photographs of the sections are also presented, many of which depict surveying the location of the lower and upper water marks.

## Cross-Section 10

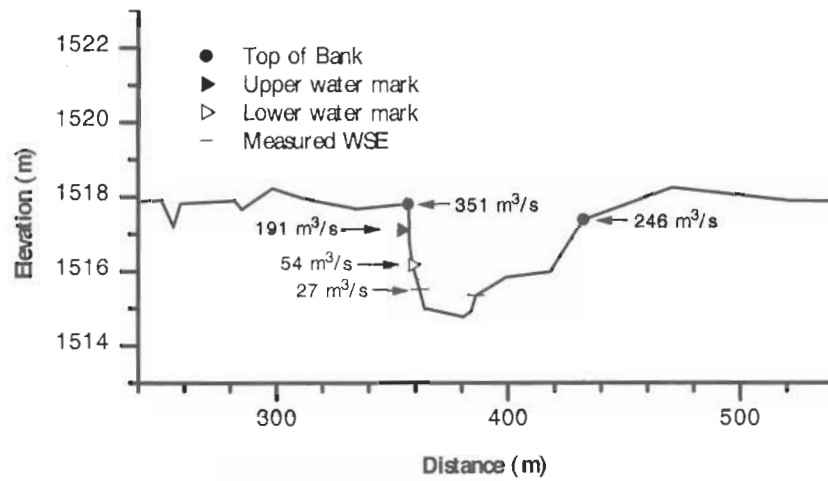


Figure A.1. Profile of cross-section 10.

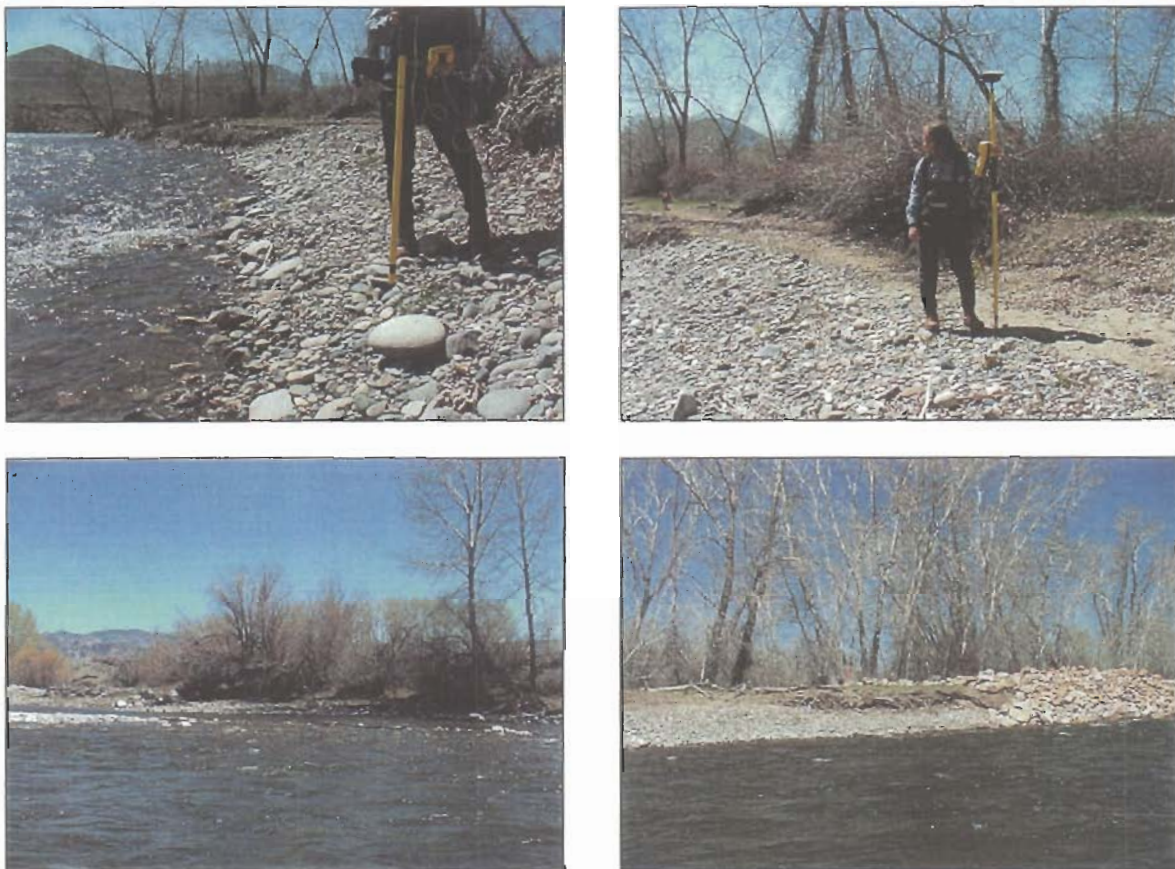


Figure A.2. Photographs of cross-section 10. Lower water mark (1) and upper water mark (2) surveyed on left bank facing upstream; right bank (3); and left bank downstream from surveyed points (4).

## Cross-Section 13

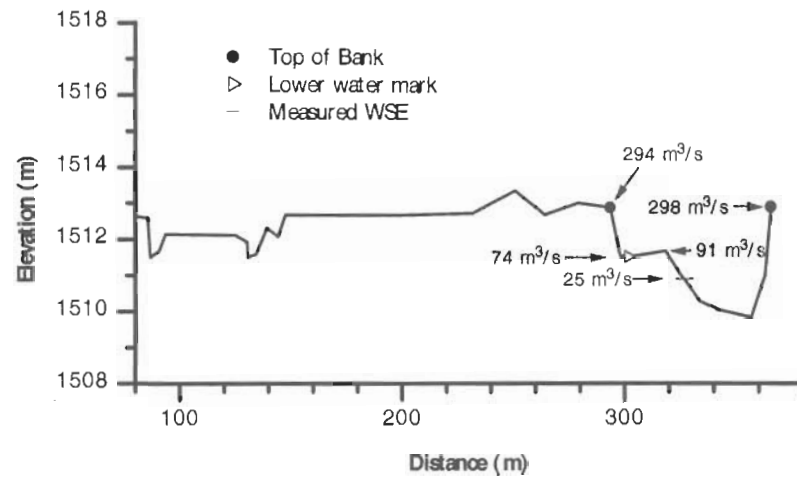


Figure A.3. Profile of cross-section 13.

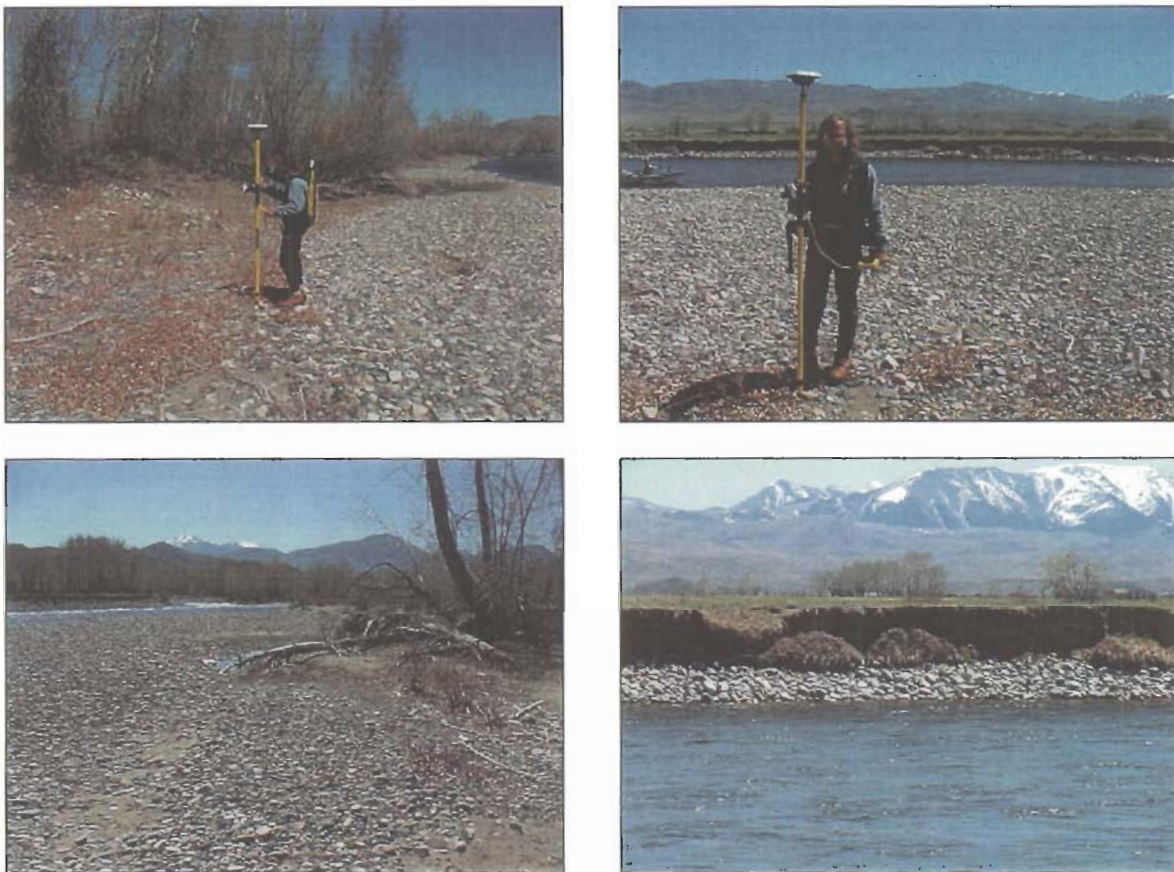


Figure A.4. Survey of lower water mark on left bank of cross-section 13 facing downstream (1); facing right bank (2); facing upstream (3); and close-up of right bank (4).

## Cross-Section 15

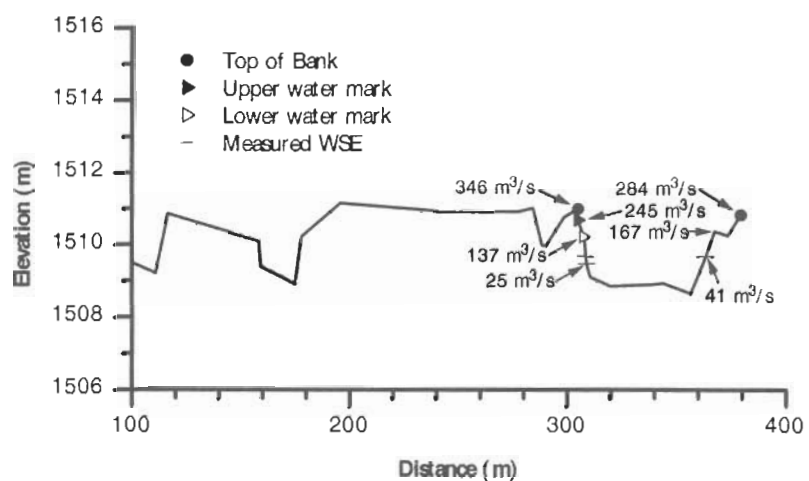


Figure A.5. Profile of cross-section 15.



Figure A.6. Lower water mark on left bank of cross-section 15 indicated by dashed marks in (1) and (2); higher water mark indicated by debris (3); and right bank (4).

## Cross-Section 18

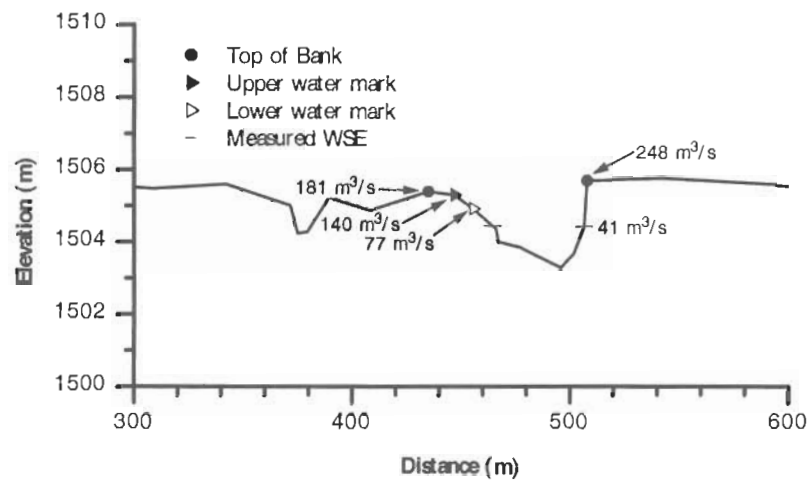


Figure A.7. Profile of cross-section 18.

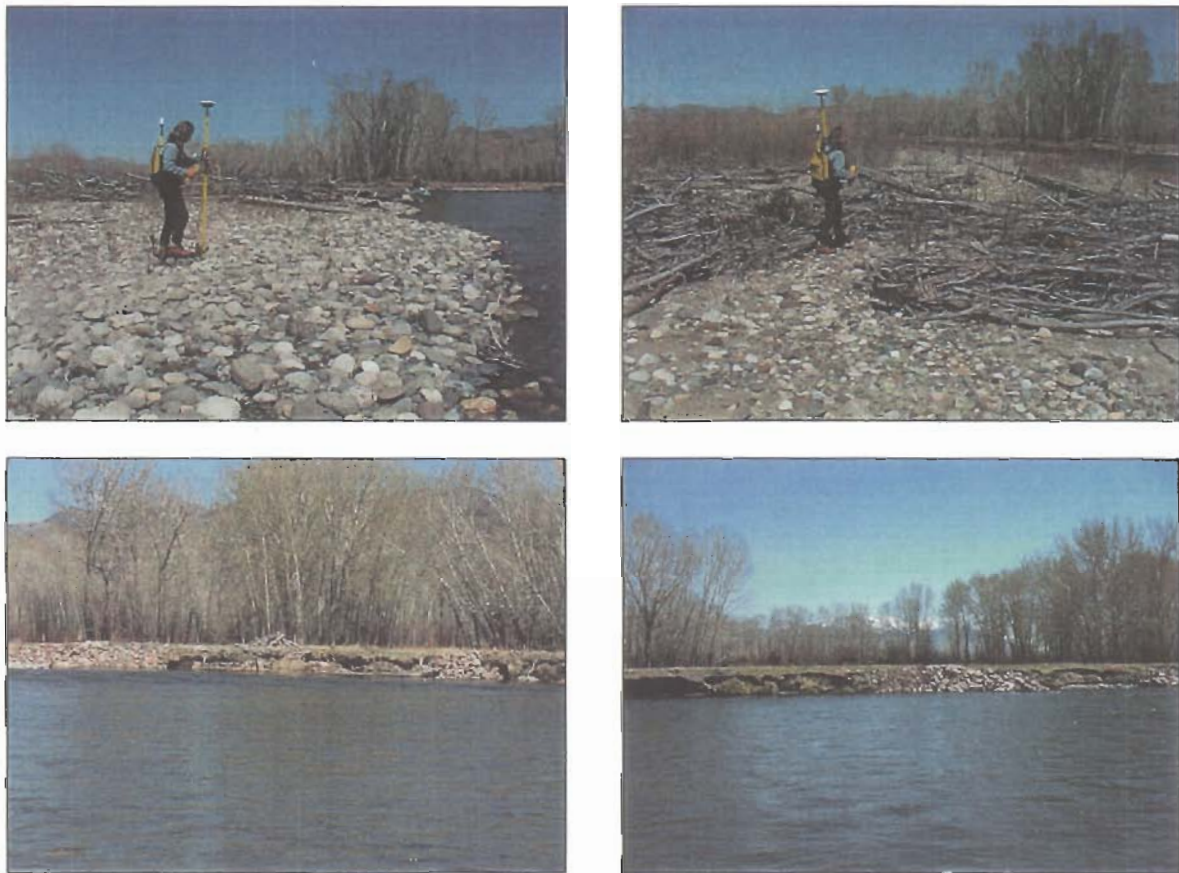


Figure A.8. Survey of lower water mark on left bank of cross-section 18 (1); upper water mark (2); right bank (3) and (4).

## Cross-Section 21

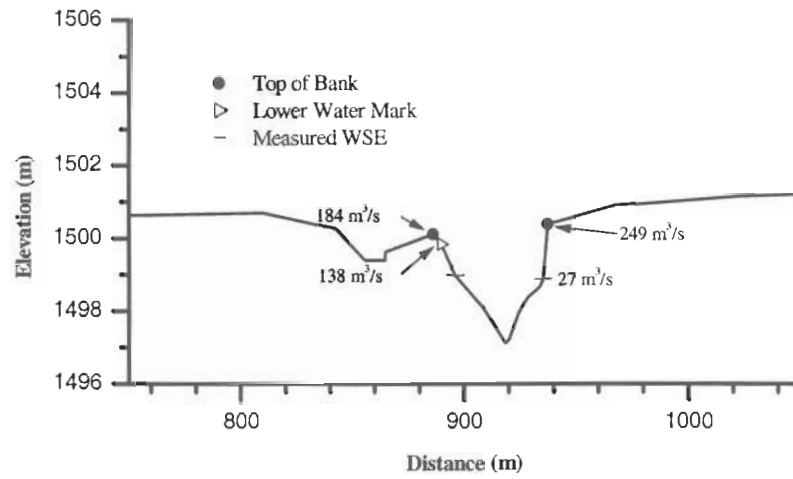
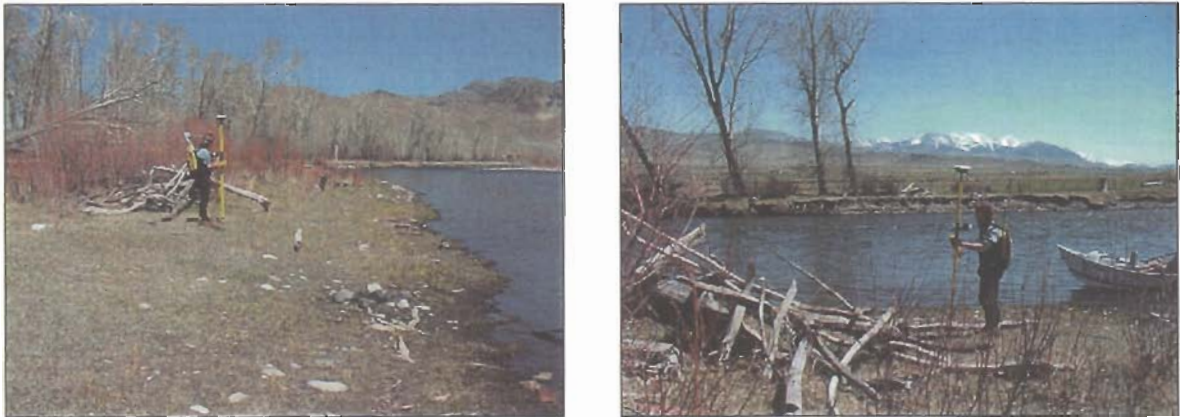


Figure A.9. Profile of cross-section 21.

Figure A.10. Lower water mark **survey on left bank** of cross-section 21 **facing downstream** (1); and facing right bank (2).

## Cross-Section 23

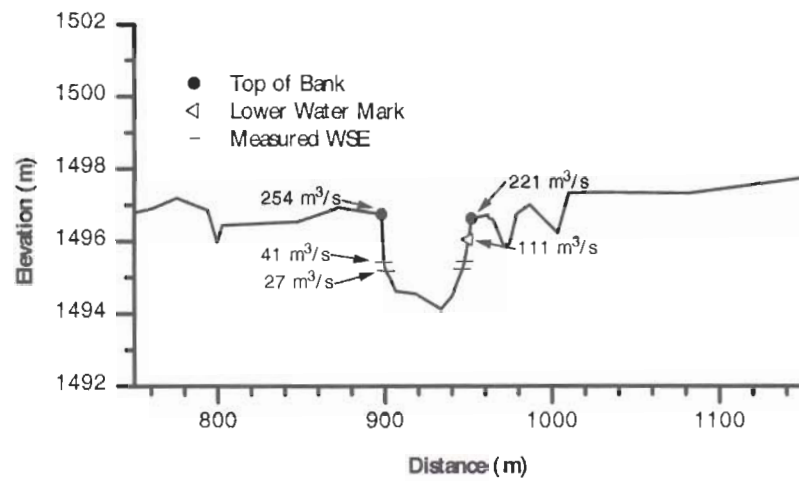


Figure A.11. Profile of cross-section 23.



Figure A.12. Lower water mark survey on right bank of cross-section 23 facing downstream (1); facing upstream (2); and facing across to left bank (3).

## Cross-Section 25

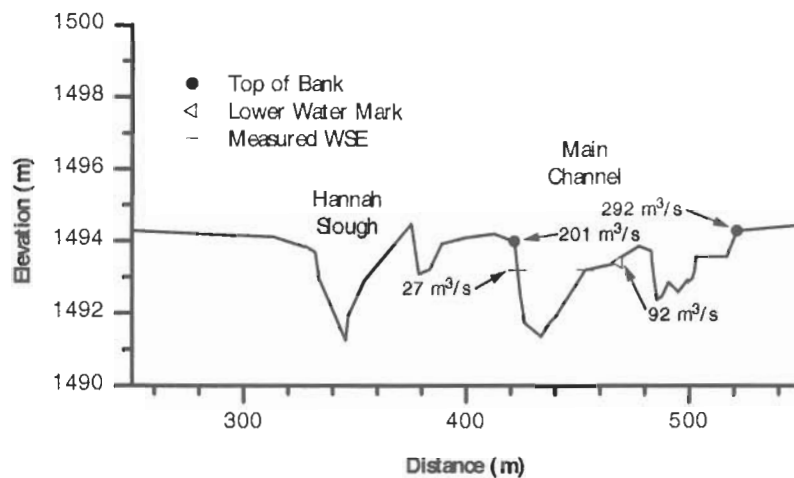


Figure A.13. Profile of cross-section 25.

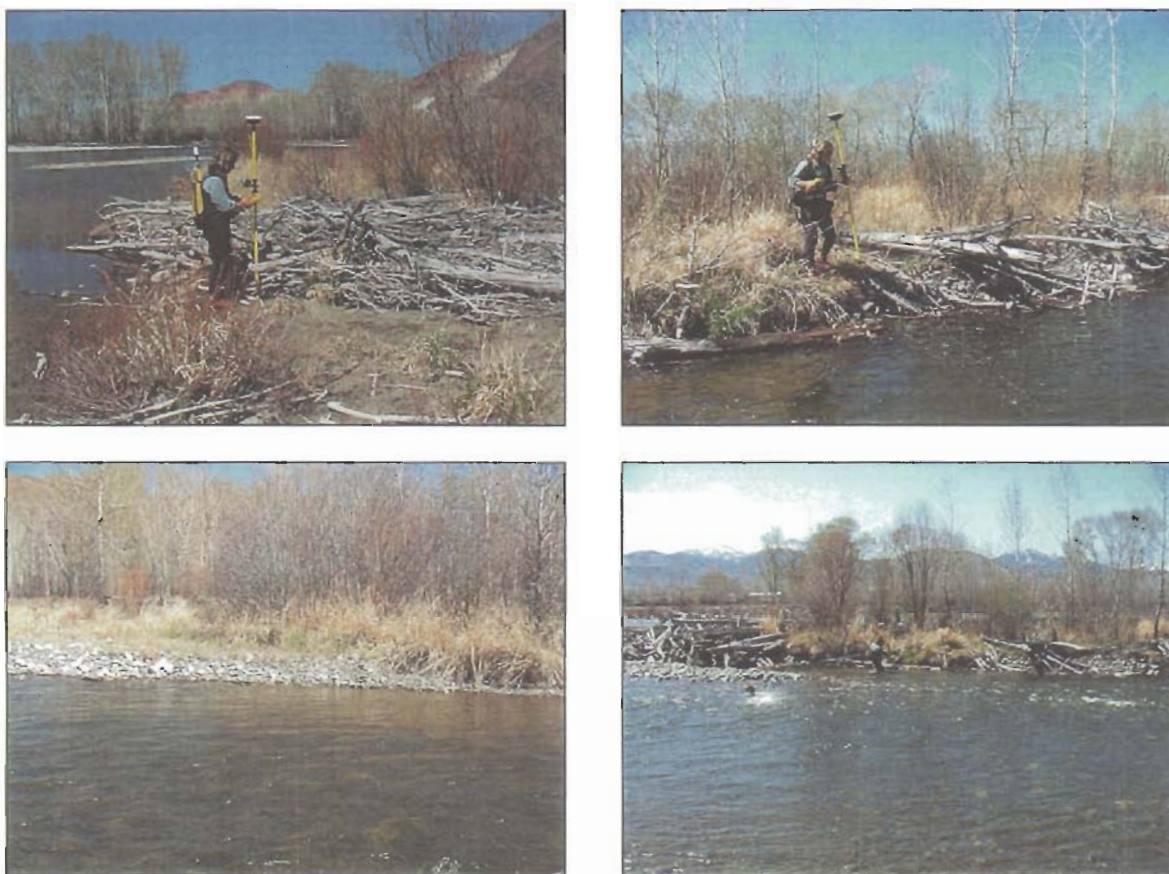


Figure A.14. Lower water mark survey on left bank of bar at cross-section 25 facing downstream (1); right bank of bar (2); far right bank (3); and bar from right bank (4).

## Cross-Section 28

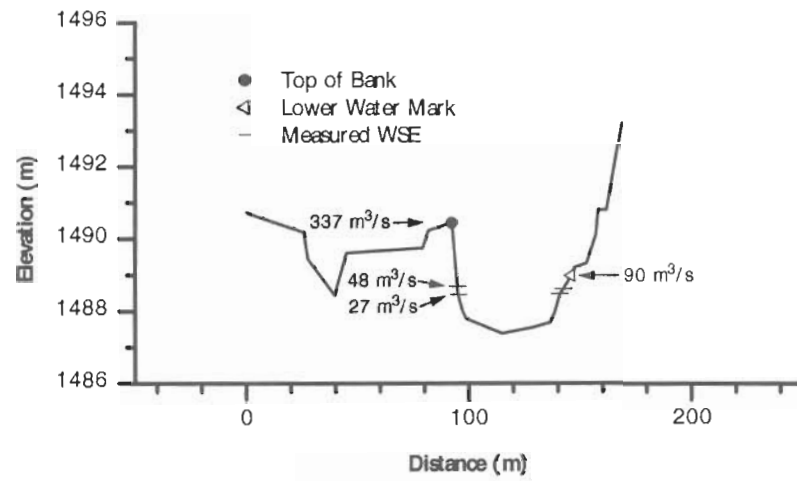


Figure A.15. Profile of cross-section 28.

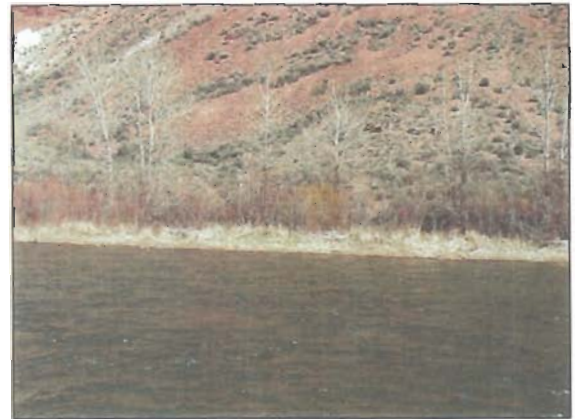


Figure A.16. Cross-section 28 left bank (1); and right bank (2).

## Cross-Section 32

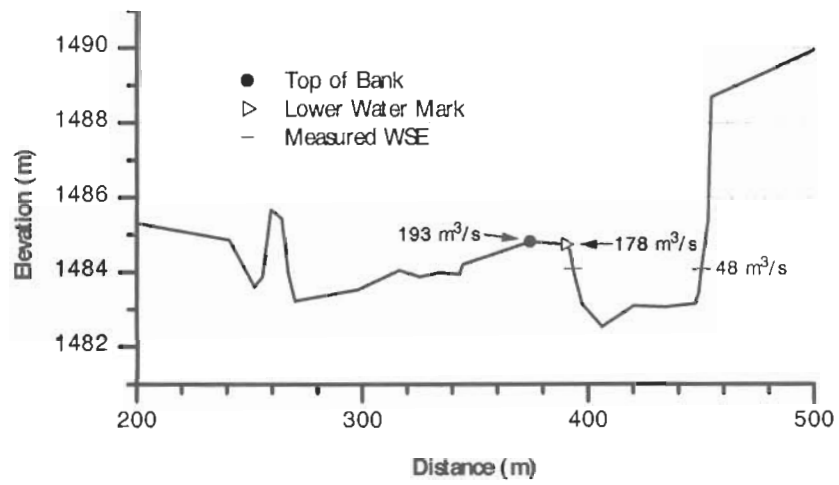


Figure A.17. Profile of cross-section 32.



Figure A.18. Lower water mark on left bank of cross-section 32 (1); and alluvial fan on right bank (2).

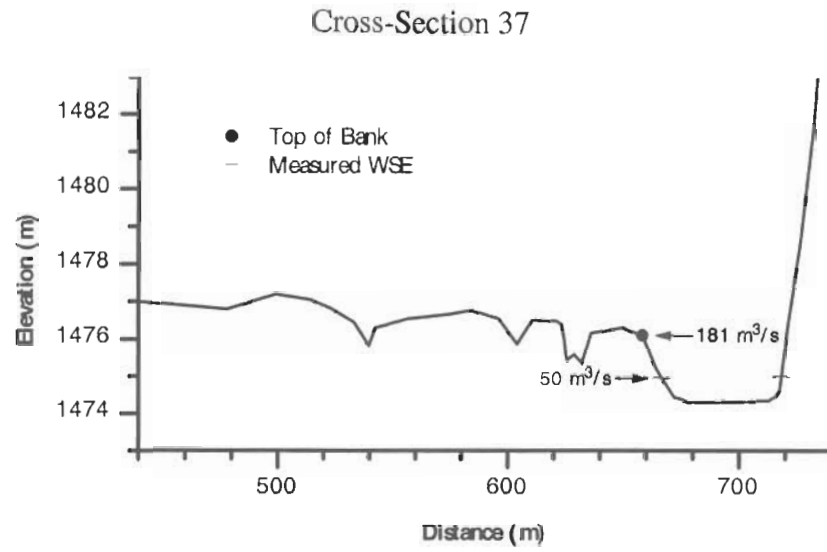


Figure A.19. Profile of cross-section 37.



Figure A.20. Cross-section 37 right bank (1); and left bank (2).

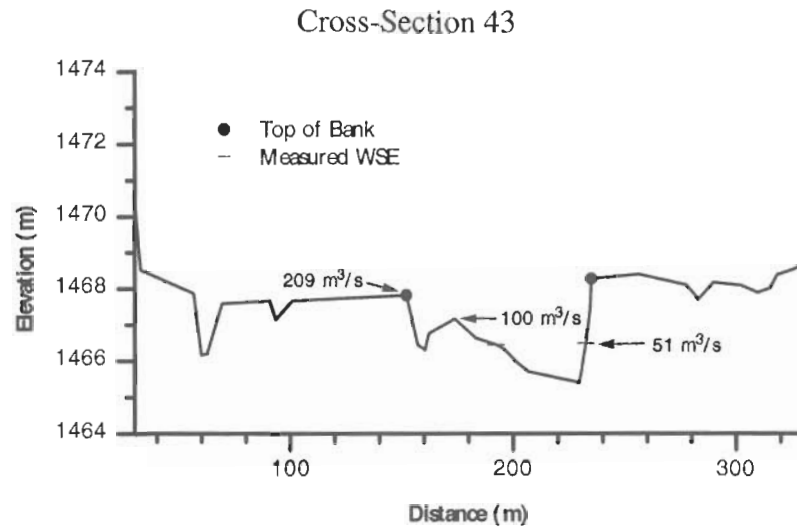


Figure A.21. Profile of cross-section 43.

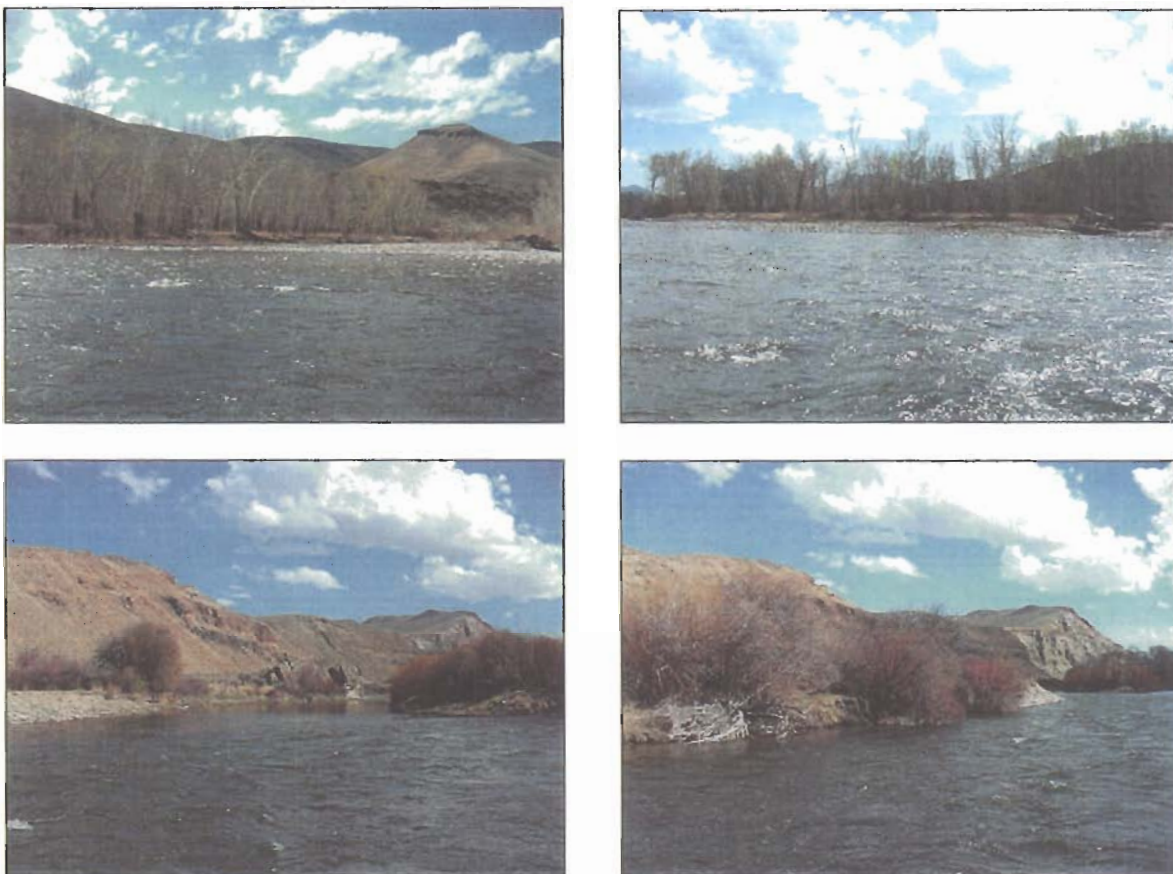


Figure A.22. Left bank of cross-section 43 facing slightly downstream (1); and upstream (2); right bank facing upstream into Henderson slough with main channel to right of image (3); and facing upstream at right bank (4).

## Cross-Section 50

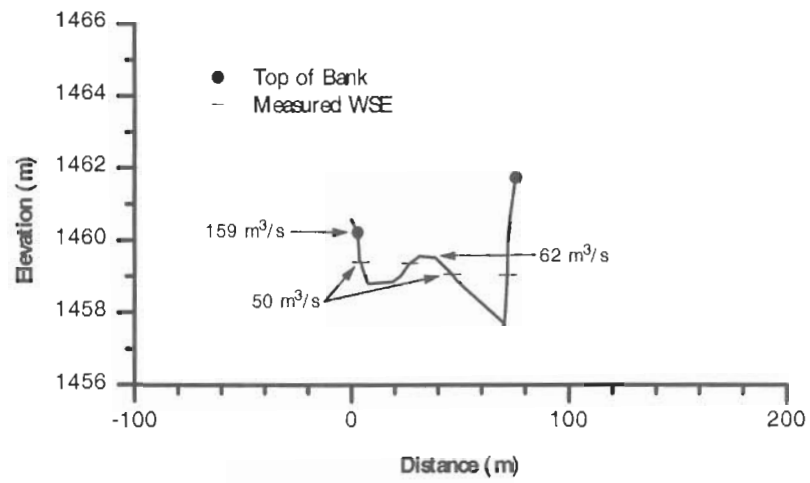


Figure A.23. Profile of cross-section 50.

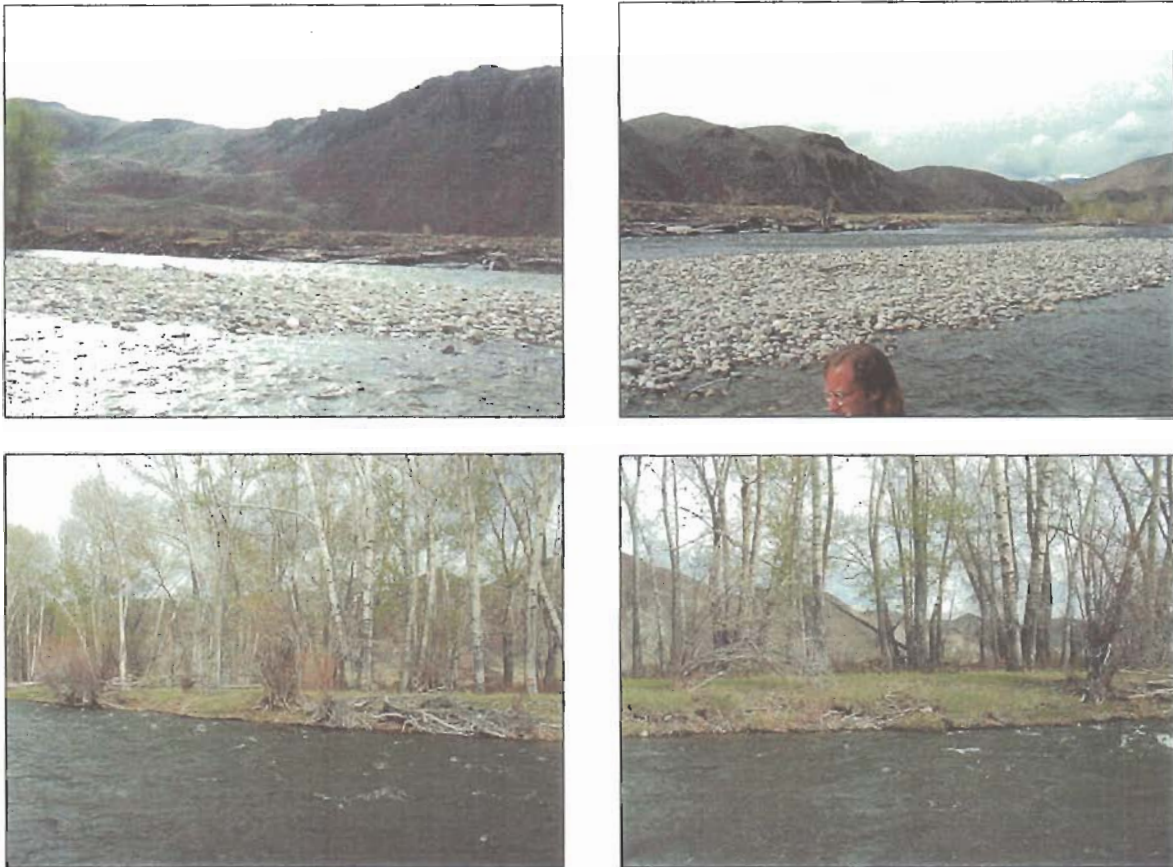


Figure A.24. Right bank of cross-section 50 (1) and (2); left bank (3) and (4).

Cross-Section 54

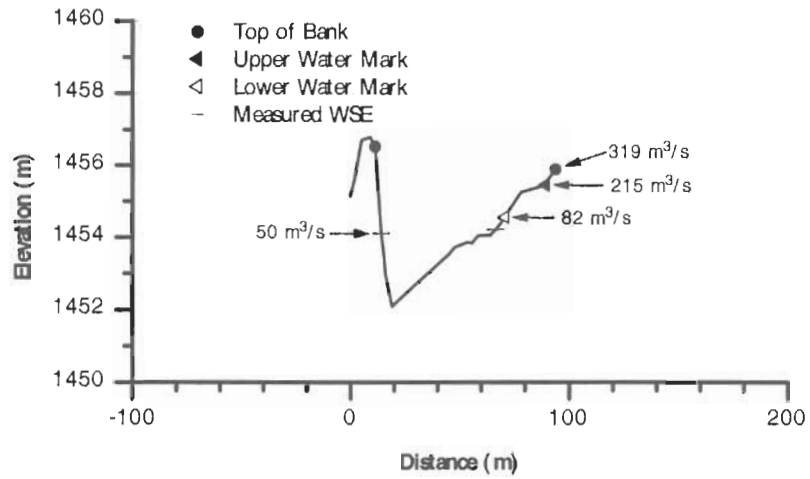


Figure A.25. Profile of cross-section 54.



Figure A.26. Right bank of cross-section 54 facing upstream (1) and (2); facing downstream at lower water mark (3); and upper water mark (4).

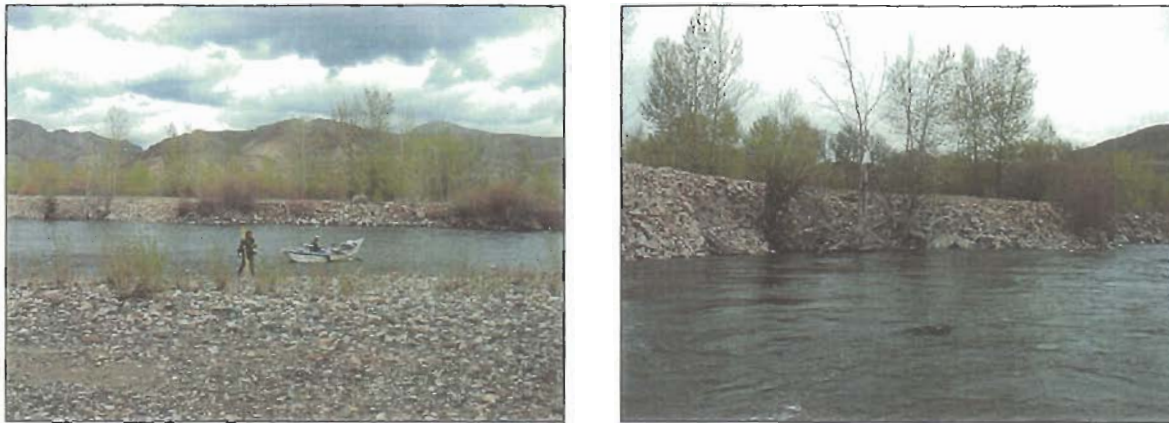


Figure A.27. Facing across channel to left bank of cross-section 54 (1); and levee forming left bank (2).

## Cross-Section 57

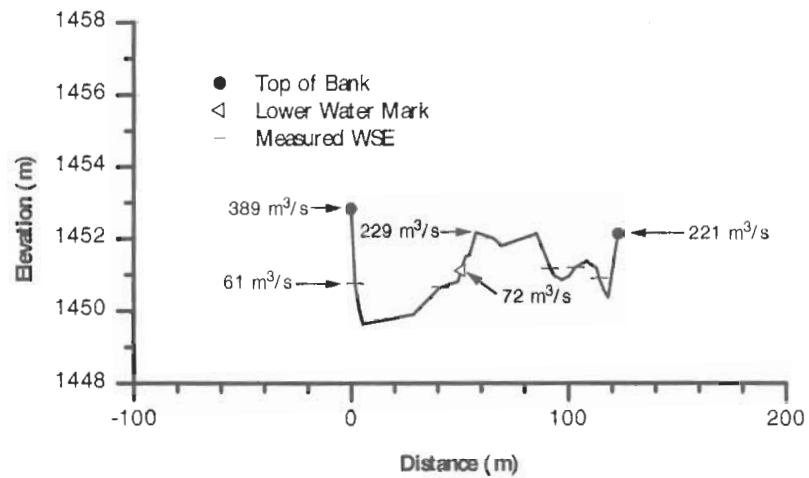


Figure A.28. Profile of cross-section 57.

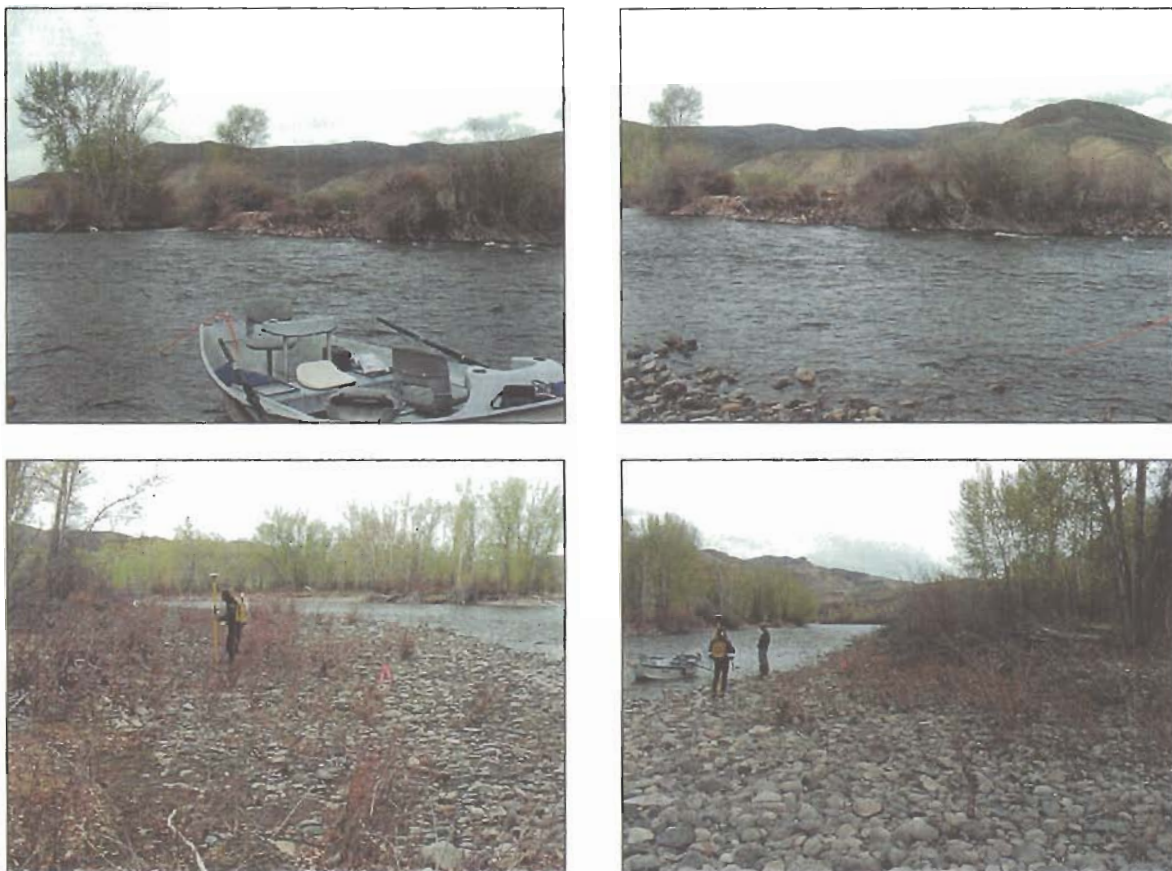


Figure A.29. Cross-section 57 facing upstream to slough on left side (1); left bank (2); survey of lower water mark on right bank (3); and facing downstream (4).

Following are full surveyed profiles of cross-sections that exceeded 300m in width.

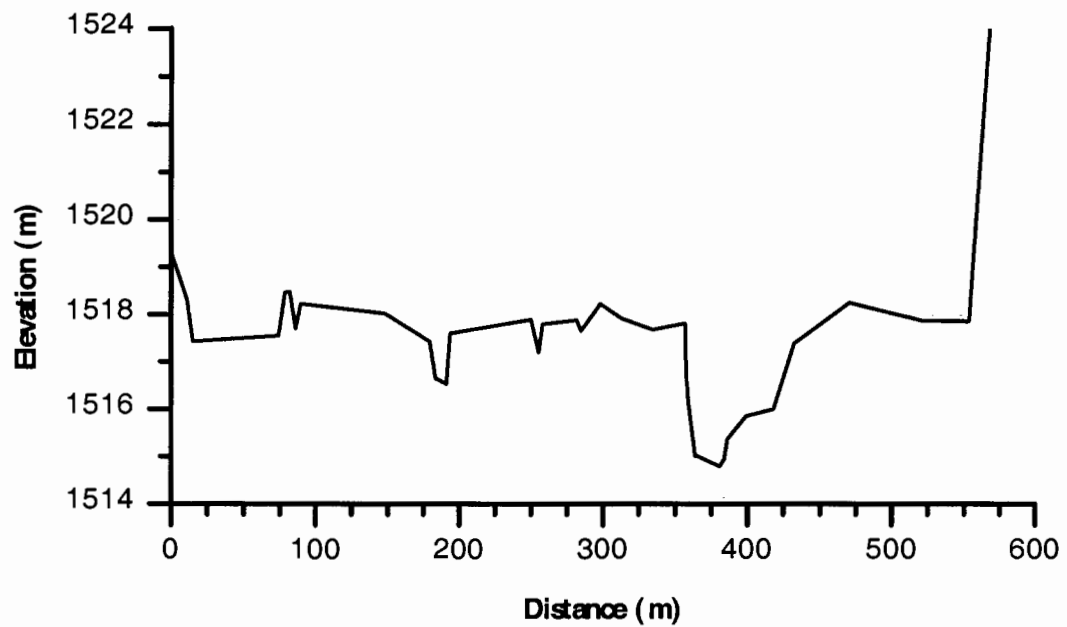


Figure A.30. Full profile of cross-section 10.

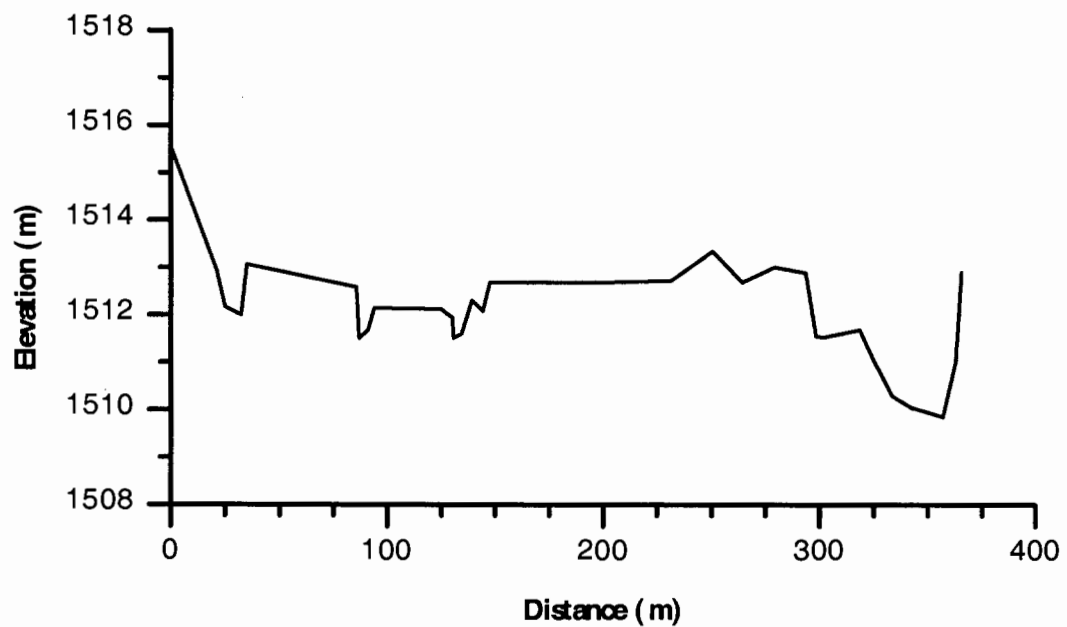


Figure A.31. Full profile of cross-section 13.

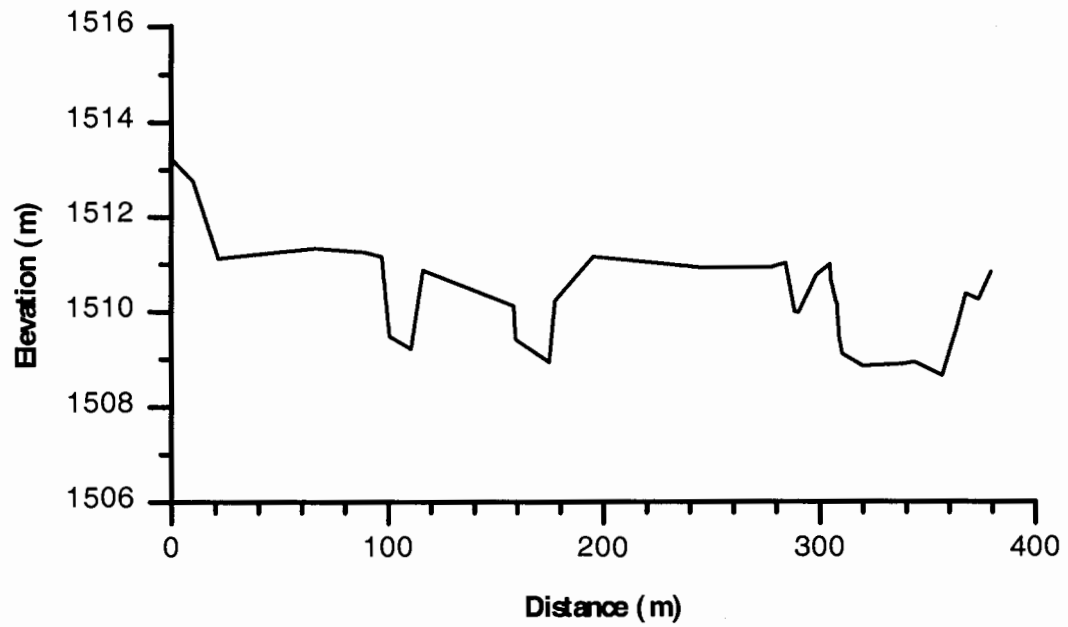


Figure A.32. Full profile of cross-section 15.

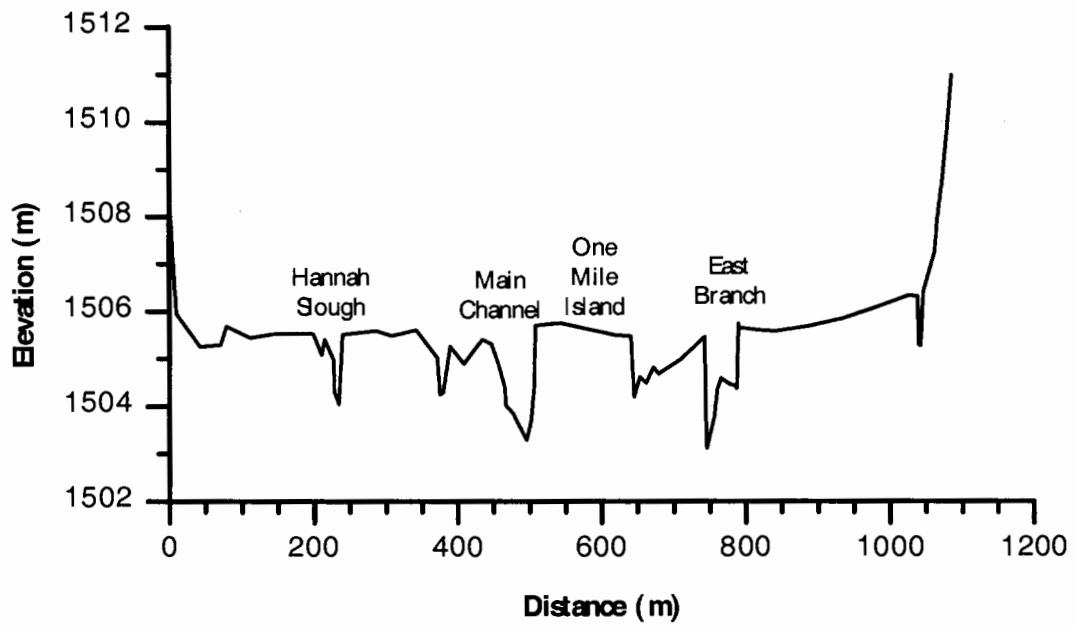


Figure A.33. Full profile of cross-section 18.

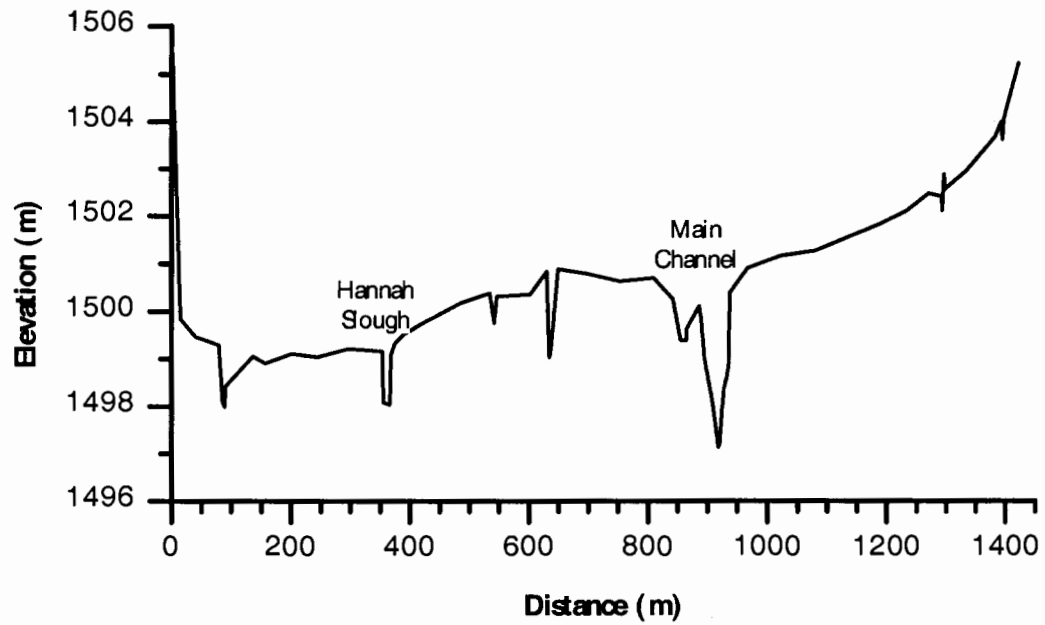


Figure A.34. Full profile of cross-section 21.

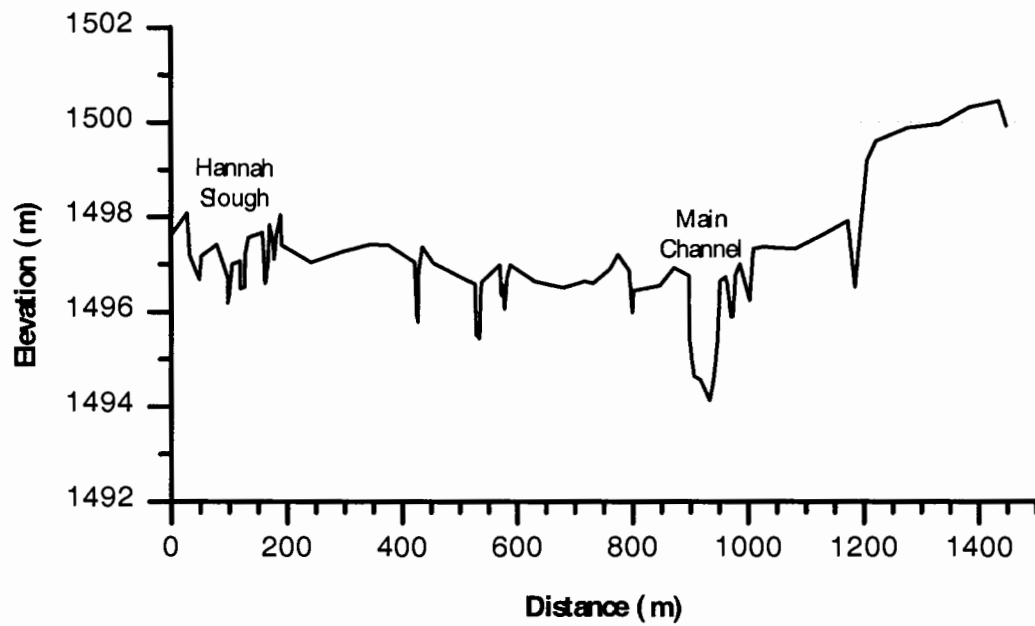


Figure A.35. Full profile of cross-section 23.

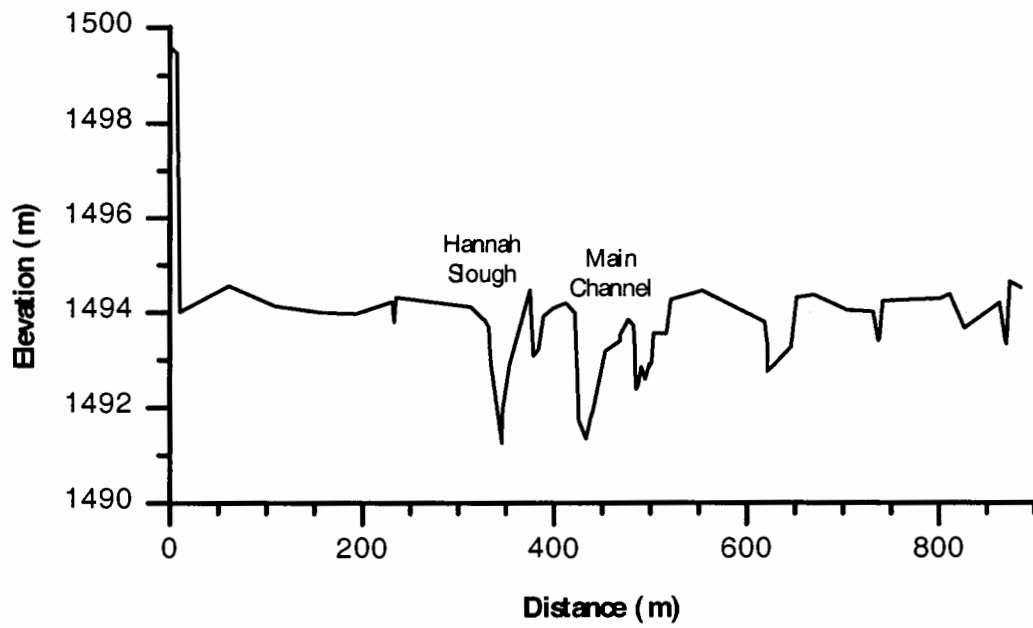


Figure A.36. Full profile of cross-section 25.

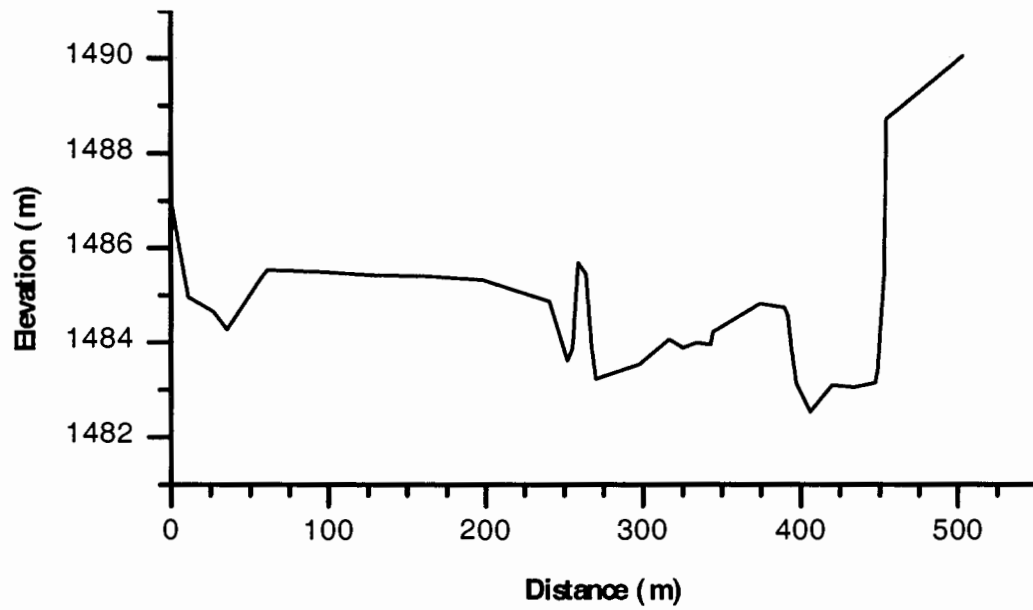


Figure A.37. Full profile of cross-section 32.

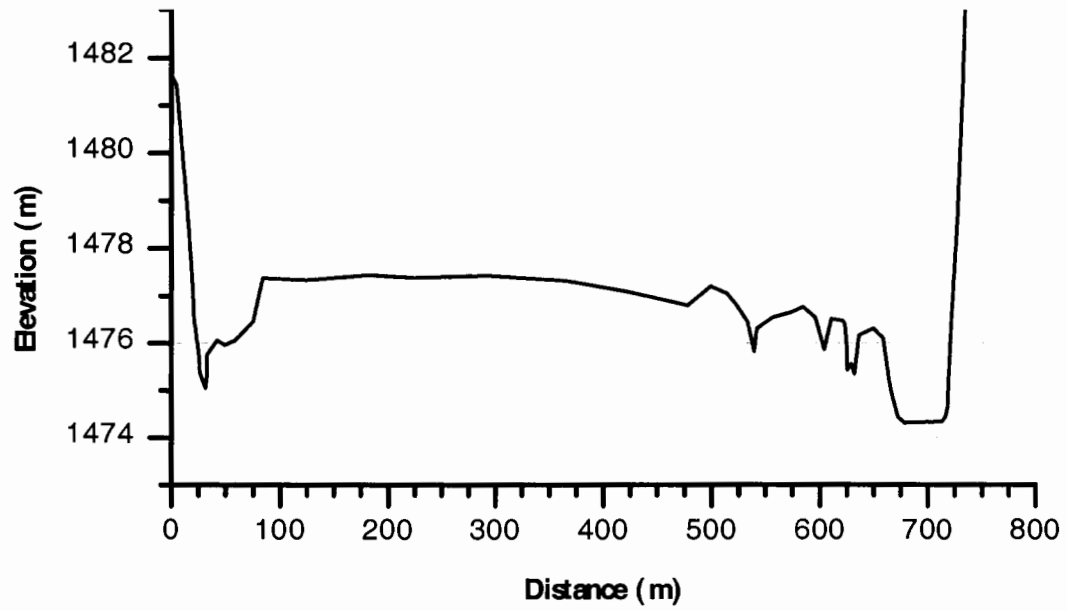


Figure A.38. Full profile of cross-section 37.

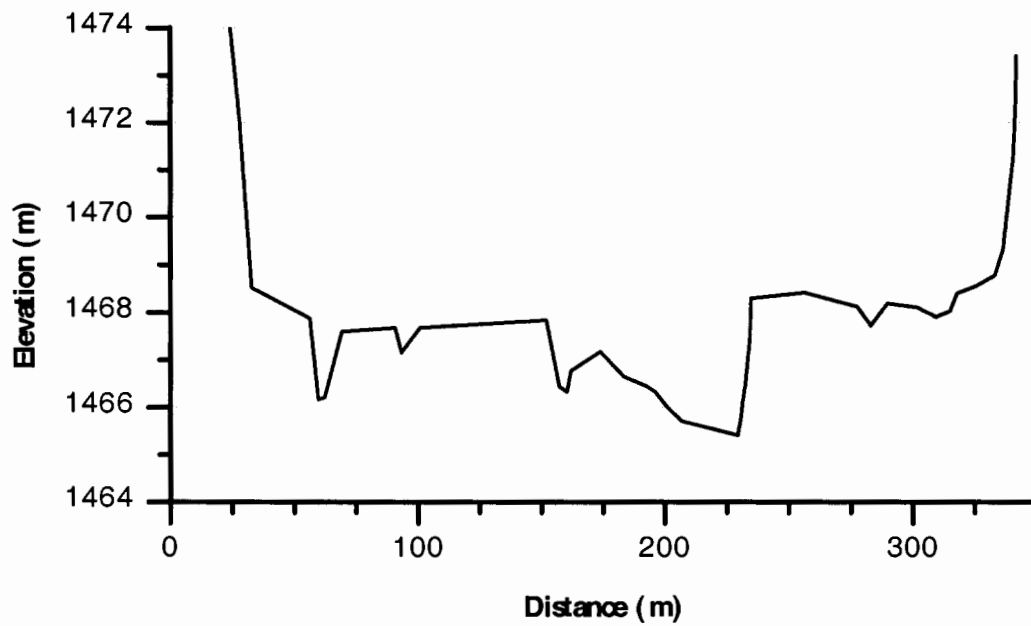


Figure A.39. Full profile of cross-section 43.

## Appendix B. Survey Descriptors

---

In Table B.1. are common descriptors found in the Cadastral Survey meander corridor survey notes. The 1883 & 1885 surveys were notably more descriptive than the 1911 notes regarding land, water, and vegetation features. Subdivision survey notes document significant land use characteristics including homes, fences, fields, canals, and roads. The meander corridor notes summarized here list far fewer of these land use features as the survey concentrates on the riverbanks and riparian corridor.

Table B.1. Cadastral survey descriptors and number of times each was noted per survey.

Descriptor	13N 19E, 1895		14N 19E, 1893		15N 19E, 1911	
	Right Bank	Left Bank	Right Bank	Left Bank	Right Bank	Left Bank
undergrowth	5	4			7	10
dense undergrowth	12	11			3	8
scattering undergrowth					1	
willow			6	6	5	9
dense willow undergrowth	8	10	32	27		
rose / dense rose brush			4	4		
sage			2	1		
dense sage			3	1		
brush			6	13		
grass land			1	3		
field			1			
timber	4	5		2	4	6
heavy timber						1
scattering / scattered timber	1	4		1	4	6
alder		1				
aspen	2	7				
cottonwood	1			2	8	13
pine	2					
no timber	6	5	6	6	1	3
old river bed	2					
creek, creek bed	1	1	1			1
slough			15	9		
bar, gravel bar			11	8		
sand bar		2				
bluff	2		4			
high bluff	2					
banks 2-4 ft	3	2	2	3		
banks 5-9 ft	2	1				
banks 10-19 ft	4	1				
banks 20+ ft	3	4		1		
land level	4	5	6	6	5	16
land rolling	5	5			1	
land broken rolling	1					
soil 1st rate			6	6		
soil 2nd rate	6	5			5	9
soil 3rd rate	3					
soil 4th rate		4	2			
irrigation canal	2	2				
headgate	1	1				
drain		1				
fence	3	3	2	3		
house		2			2	
stable		1				
road	1	1	1	2		
bridge	1	1				

### Appendix C. The Hydrodynamic Model

MIKE11 is a professional engineering software package for the modeling of rivers, channels and irrigation systems, including rainfall-runoff, advection-dispersion, morphological and water quality modules. The main computational engine is a hydrodynamic modeling system that solves the fully dynamic, one-dimensional, free-surface flow equations. The software package is developed and maintained by the DHI Water and Environment (formerly the Danish Hydraulic Institute). The package has been used successfully and reliably by DHI for more than 15 years, and is now installed in hundreds of engineering offices worldwide.

For channels of irregular topographies, the unsteady flow phenomenon can be described by the de Saint Venant equations:

$$\frac{\partial Q}{\partial x} + b_s \frac{\partial h}{\partial t} = 0 \quad \text{continuity}$$

$$\frac{\partial Q}{\partial t} + \frac{\partial}{\partial x} \left( \beta \frac{Q^2}{A} \right) + g A \frac{\partial}{\partial x} (h + H) + g A \frac{|Q|Q}{K^2} = 0 \quad \text{momentum}$$

where:

$$Q = \text{discharge} \quad (\text{m}^3/\text{s})$$

$$h = \text{water depth} \quad (\text{m})$$

$$b_s = \text{storage width} \quad (\text{m})$$

$$A = \text{cross-sectional area} \quad (\text{m}^2)$$

$$K = \text{conveyance} = CA\sqrt{R} = \frac{1}{n} AR^{2/3} \quad (\text{m}^3/\text{s})$$

$$C = \text{Chezy resistance coefficient} \quad (\text{m}^{1/2}/\text{s})$$

$$n = \text{Manning roughness coefficient} \quad (\text{s}/\text{m}^{1/3})$$

$$R = \text{hydraulic radius} \quad (\text{m})$$

$$\beta = \text{Boussinesq coefficient}$$

$$H = \text{bottom elevation} \quad (\text{m})$$

$$g = \text{acceleration due to gravity} \quad (\text{m}/\text{s}^2)$$

These equations are solved in MIKE11 using an implicit finite difference approximation of the Abbott-Ionescu type on a staggered grid. Between two successive gridpoints both the continuity and the momentum equations are applied. Together with the boundary conditions, a sufficient number of equations are obtained to solve for  $Q$  and  $h$ . This numerical scheme is very accurate and unconditionally stable.

The core of the MIKE11 system consists of the hydrodynamic (HD) module, which is capable of simulating unsteady flows in a network of open channels. The results of an HD simulation consist of time series of water levels and discharges. Advection-dispersion (AD), water quality (WQ), and non-cohesive sediment transport (NST) calculations can be carried out from special modules that utilize the results of an HD computation. In addition, the NST module can be run in tandem with the HD module as a morphological module.